The Dissertation Committee for Byung-Soon Min
certifies that this is the approved version of the following dissertation:

Analysis of the Fuel Economy Potential of a Direct Injection Spark Ignition Engine and a CVT in an HEV and a Conventional Vehicle Based on In-Situ Measurements

Committee:

Ronald Matthews, Supervisor

Matthew Hall

Janet Ellzey

Ofodike Ezekoye

Robert Larsen

Analysis of the Fuel Economy Potential of a Direct Injection Spark Ignition Engine and a CVT in an HEV and a Conventional Vehicle Based on In-Situ Measurements

by

Byung-Soon Min, B.S., M.S.

Dissertation

Presented to the Faculty of the Graduate School of
The University of Texas at Austin
in Partial Fulfillment
of the Requirements
for the Degree of

Doctor of Philosophy

The University of Texas at Austin
August 2004

Dedication

To my mother, Pyungja Shim and to my father, Kwanshik Min,
who love, encourage and support me.

and

Eunjin, Jiyoon and Dayoon

Acknowledgements

I owe an eternal debt of gratitude to Dr. Matthews for helping me with kindness and patience. He is the best mentor I have ever had and I am very fortunate to have the opportunity to work with him.

Thanks to the whole Argonne National Laboratory for its great welcoming and its wonderful working environment. The contacts I made were really enriching both for the work and human relationships: Bob Larsen, John Anderson, Mike Duoba, Justin Kern, Henry Ng, Dave Shimcoski.

I would like to thank Cynthia Webb at the Department of Emissions Research of SwRI for granting me a chance to use their facility.

Thanks to the rest of the members of my dissertation committee for helping send me on my way a better person than I was when I got here:
Dr. Ezekoye, Dr. Ellzey, Dr. Matt Hall.

I thank my office partners: Myoungjin, Shinhyuk and Myoungjun. It was a great pleasure to work with them. Additionally, I appreciate support received from colleagues: Dohyung, Daejong and Younghoon.

Thanks to my wife Eunjin and kids Jiyoon and Dayoon, for love and life.

Analysis of the Fuel Economy Potential of a Direct Injection Spark Ignition Engine and a CVT in an HEV and a Conventional Vehicle Based on In-Situ Measurements

Publication No._____

Byung-Soon Min, Ph.D.
The University of Texas at Austin, 2004

Supervisor: Ronald Matthews

A Toyota OPA was selected as a test vehicle as it has the components of interest: a Direct Injection Spark Ignition (DISI) engine and a Continuously Variable Transmission (CVT). In order to estimate the benefit of the DISI engine and CVT, a 2001MY Toyota OPA was tested to collect the engine and CVT maps using in-situ measurement techniques. Two torque sensors were installed into the powertrain in the vehicle for that purpose; one is between the engine and transmission and the other one is installed on the driveshaft. The overall efficiency of the engine and transmission was estimated using the measured torques and speeds during Phase 3 of the FTP cycle The overall efficiencies of the engine at different operating modes including the lean and stoichiometric combustion modes were compared to each other. The overall efficiencies of the CVT are analyzed similarly. Finally, the measured steady state efficiency maps and emissions maps were used to predict the fuel economy and emissions of an HEV with the DISI engine and CVT.

The FTP test for the test vehicle shows that Toyota has made a remarkable improvement of tailpipe HC and NOx emissions with their second generation DISI engine. The reduction of HC emissions is attributed to the improvement in the combustion system using a slit nozzle injector. The dominant factor for NOx reduction

turns out to be the catalyst efficiency. Due to the increase in the catalyst capacity, the average catalyst efficiency for NOx is improved from 67.5% to 89.9%.

The steady state characteristics of the DISI engine and CVT were collected successfully using the in-situ mapping technique. The operating range of the lean combustion was revealed. The maximum engine load for lean operation was 6 bar BMEP and the maximum engine speed was 2750 rpm. The improvement in steady state fuel consumption is about 20% at low speed and around 3 bar BMEP. The engine-out HC emissions are 2~3 times more and the engine-out NOx emissions are one-half to one-sixth of that in stoichiometric combustion mode.

The energy losses were calculated from the measured power flows. The engine, the largest energy sink, consumes 62.3% of total energy loss during power mode and additionally consumes 11.8% more during idling and braking. The CVT consumes 5.6% and the vehicle consumes 20.2%. The overall efficiency of the engine, which is 29.3% during the Hot 505 cycle, is improved to 32.7% with the change in combustion mode to lean combustion. The resulting fuel economy improvement was measured as 5.7%. Therefore, it can be concluded that the fuel economy benefit of the second generation Toyota DISI engine over a PFI engine during Phase 3 of the FTP cycle is 5.7% which is due to the 3.4% improvement in the overall engine efficiency.

The benefit of a DISI engine over a conventional SI engine in an HEV application is found to be 4.2% in terms of composite fuel economy and 3.9% for the Hot 505 cycle, which is less than that of 5.7% for a DISI engine in a conventional vehicle. The overall engine efficiency improvement of a DISI engine in an HEV application is 0.5 percentage points which is also less than that for a DISI engine in a conventional vehicle application. This is because the engine is working in the high load region due to the down-sized engine. This DISI engine operates primarily in homogeneous charge mode for high load, and thus does not offer a large fuel economy benefit. The HC emissions of both types of engines are similar to each other and the NOx emissions of HEV with a DISI engine is 26% higher than that with an SI engine.

TABLE OF CONTENTS

LIST OF FIGURES

LIST OF TABLES

CHAPTER 1: INTRODUCTION

The Partnership for a New Generation of Vehicles (PNGV) identified the Hybrid Electric Vehicle (HEV) as a key configuration to achieve significant fuel economy improvements [3]. The FreedomCAR Partnership, the successor to the PNGV, continues to support the electric propulsion systems applicable to both fuel cell and internal combustion/electric hybrid vehicles. The benefit by hybridization depends on the balance between improvements in hybrid designs and improvements of powertrain components. The engine in the HEV is the least efficient component in the powertrain so the development of an efficient engine is more effective than improvements to the other components of an HEV drivetrain. Therefore, the use of an efficient engine and transmission is also important in HEVs as well as in conventional vehicles.

In the present Ph. D. research, the fuel economy benefit of DISI engine over the Port Fuel Injection engine is investigated in both a conventional and a hybrid electric vehicle. The benefit of a Continuously Variable Transmission (CVT) is also researched. For that purpose, the 2001 MY Toyota OPA was selected to be tested as a vehicle with the state-of-the-art DISI engine and CVT. To overcome the difficulty of benchmarking tests, an in-situ measurement technique was developed and used. The following sections address the basic information for the important issues in this research.

1.1 BACKGROUND

1.1.1 Development of the Hybrid Electric Vehicle

As the hybrid system is regarded as a promising system that can reduce energy consumption and emissions regardless of using the different power plants such as the diesel engine and fuel cell, the development of the HEV system is a general trend of the automotive industry. As a first step, Toyota launched the Prius in 1997 and added two more models in 2001 – the Estima Hybrid minivan and Crown mild-hybrid. Honda has

two HEV models – Insight and Civic. The specifications of the mass produced HEVs are shown in Table 1.1.

Table 1.1 Specifications of mass produced HEVs as of November, 2003

Manufacturer	Vehicle	Configuration	Engine	Transmission
Toyota	Prius	Power split	SI	ECVT
	Estima	Parallel (2 motor 4WD)	SI	CVT
	Crown	Parallel	DISI	AT
Honda	Insight	Parallel	Lean burn	MT/CVT
	Civic	Parallel	Lean burn	MT/CVT

It is seen in this table that the parallel type is the majority of current HEVs. The potential for fuel economy gains due to vehicle hybridization can be estimated on the three elements [3]: the reduction of engine idling, the recovery of braking energy and the capability of high efficiency operation control. However, according to Toyota, the parallel type HEV is somewhat unfavorable for the high efficiency operation. A common misconception of how a hybrid works is the dated thermostat concept [31]. That is, a small engine is operating at a constant output power at its maximum efficiency point, providing the averaging energy with a battery acting as a load follower. One problem of this concept is that some trips need a higher than average load condition for a long time period. Therefore, the improvement of the efficiency of each powertrain component is essential for an efficient HEV.

1.1.2 Attractions and barriers of DISI engines

Current lean burn engines, both compression and spark ignition, have high potential efficiencies. The Direct Injection Compression Ignition (CIDI) engine has higher potential than the spark ignition engine. However, the Direct Injection Spark Ignition (DISI) engine is also attractive due to its emissions potential over the CIDI engine and fuel economy potential over the PFI gasoline engine. Thus, The important viewpoints for the adoption of the DISI engine are how much benefit can be obtained and if the DISI engine can meet the strict emissions regulations. Zhao and coworkers [41]

summarized the major factors contributing to the improved BSFC of the DISI engine over that of a conventional PFI engine as follows;

- Decreased pumping losses due to unthrottled part load operation using overall lean mixtures
- Increased knock limited compression ratio due to low end gas temperature
- Increased cooling of the intake charge due to in cylinder injection during induction
- Increased cycle efficiency due to the incrementally higher specific heat ratio of lean mixtures
- Decreased cylinder wall and combustion chamber heat loss due to stratified combustion

In the stage of decision making, it is necessary to evaluate the actual benefit that can be drawn from the adoption of a DISI engine. There are several arguments regarding this matter. Karl and coworkers [20] said that the stratified GDI engine can reduce the fuel consumption by 20~25% at part load with the optimized gas cycle, heat transfer and geometric configuration. A 25% increase in fuel economy potential is reported by Wojik and Fraidl[39]. The theoretical potential of fuel economy is reported as 20% at part load and 35% at idle by Fraidl and coworkers [14]. Regarding the fuel economy benefit in the vehicle, Kume and coworkers [25] said that the vehicle fuel economy can be improved by 35%. According to the recent publication by Alkidas and El Tahry [1], the potential of the DISI engine is overestimated and its advantage in the FTP cycle is only 15%. However, GM's Fritz Indra said in the report of Dan Carney that, in production, the engine lost 1% because of the wide range of operating conditions and margin of mass production. In addition, the condition around the spark plug is not ideal. Finally, the gain ends up with a 6~7% benefit for a stratified charge DISI engine [7]

A DISI engine has the barriers into the market as well as the attraction. The first barrier is a higher level of emissions. At a constant engine speed of 2000 rpm, Matthews and coworkers [29] found that the early injection mode (homogenous charge near stoichiometric) engine-out HC Emission Index (g/kg_{fuel}) was about twice as high as that

for a comparable PFI engine. The HC Emission index for late injection was higher by a factor of up to four. Brehob and coworkers [6] measured the brake specific HCs (BSHCs) to be ~25% higher in early homogeneous charge mode than those from a comparable PFI engine. For late injection, the brake specific HCs increase monotonically with increasing air/fuel ratio up to 3 times.

On the contrary, the NOx emissions in the stratified charge lean mode is reported as less than that of the homogeneous charge stoichiometric mode [34]. However, for the DISI designed to operate with lean combustion, the conventional three way catalyst can not be used effectively to remove the NOx. Therefore, other techniques for in-cylinder NOx reduction or after-treatment are necessary. As an in-cylinder NOx reduction technique, EGR is widely used. For a DISI engine using charge stratification, stable combustion is possible with a high level of EGR because the mixture near the spark plug is not affected by diluted exhaust gas. A comparison of the effect of EGR on the NOx reduction reported by Kuwahara and coworkers [26] shows that a larger NOx reduction can be realized for DISI than that for PFI.

A number of technologies are being explored for a NOx reduction catalyst for lean exhaust gas. Two catalyst concepts have entered into the market as follows [24].

- The continuously reducing Iridium catalyst using HC in lean burn phases as selective reductant for NOx
- The non-continuously reducing NOx storage catalyst which stores NOx in lean burn phases and reduces NOx to harmless N_2 in rich or stoichiometric operation mode

Only the NOx storage catalyst has the potential to meet the stringent U.S. emissions standards but it needs to develop not only the catalyst but also a sophisticated additional engine management. In addition, the fuel originated sulfur compounds are known to reduce the effectiveness of this catalyst. Therefore, the De-NOx catalyst with more potential for sulfur tolerance or sulfur free fuel is necessary.

1.1.3 Efficient transmission

Another feature of the OPA is its CVT. The Super CVT is Toyota's first steel push-belt and pulley continuously variable transmission, manufactured in-house and using a Dutch Van Doorne Transmissie belt. Toyota boasted that the newly introduced Super CVT realized both good fuel economy and high driving performance [30].

According to Kluger and Long [21], the overall efficiency of a belt type CVT is 84.6% which is less than the efficiency of manual and automatic. However, the major advantage of a CVT is that it allows the engine to operate in a more fuel efficient region. Thus the combination of a CVT and conventional engine can improve the typical powertrain's fuel economy by 5~10%.

1.1.4 In-situ measurement technique

Most automotive manufacturers have been doing benchmarking tests and comparing the performance and fuel economy of competing vehicles to devise countermeasures. However, the testing of other maker's engines or transmissions has become difficult because the control system of the engine is integrated with that of the transmission and vehicle. In addition to that, the engine control computer controls not only the injection and ignition but also VVT, EGR and so on. Especially for DISI engines, it controls the throttle valve and swirl valve. The recent ECU communicates even with the brake and ABS. As a result of that, even a little modification of the engine can induce a complete malfunction of engine control.

Therefore, the best way of benchmarking testing is doing that without any modification to the powertrain. To do that, it is necessary to install a torque sensor between the engine and transmission in a vehicle. There have been several attempts to put a torque sensor in such a position. Duoba and coworkers [12] attempted and succeeded in measuring engine-out torque to examine the powertrain of the Prius, the first HEV in the market. In another publication of them [13], an axle shaft torque sensor was installed on an Insight. The characteristics of two kinds of HEVs were assessed and

compared. Another example of in-situ measurements was published by Corsetti and coworkers [9]. They refined the torque measuring system in a vehicle to supplement the engine dynamometer development and validation of an ECM torque model.

1.2 OVERVIEW AND GOAL OF THIS PROJECT

In the present PhD research, the actual fuel economy benefit of a DISI engine and CVT was evaluated in terms of overall efficiency for a driving cycle and fuel economy as a result of that for both a conventional vehicle and an HEV. In the conventional vehicle, the efficiency of the DISI engine will be measured and compared with the same engine operating in stoichiometric mode in the same vehicle. The itemized factors on the fuel economy benefit of a DISI engine was reported by Kume and coworkers [25] and Alkidas and El Tahry [1] and tabulated in Table 1.2.

Table 1.2 Factors contributing to the fuel economy benefit of a DISI engine

	Factors	By [Kume and coworkers, 1996]	By [Alkidas and Tahry, 2003]
Positive	Reduced pumping loss	15%	10.2%
	Higher specific heat	5%	7.5%
	Reduced thermal dissociation	2%	
	Compression ratio	4%	3.1%
	Reduced heat loss	5%	2%
Negative	Lower combustion efficiency		-4%
	Higher friction		-3.9%
Total		30%	15%

By means of a scan tool, the DISI engine's operating mode was manipulated to operate in homogeneous stoichiometric mode. With the same engine hardware and different mixture preparation, we can examine the all the factors in Table 1.2 except for the compression ratio. Thus, according to Alkidas and El Tahry [1], the fuel economy benefit should be about 12%. The power flow through each powertrain component was measured and integrated to be the total energy flow. From this energy flow, the overall and average efficiencies of the engine and transmission will be obtained. The

comparison between the conventional gasoline engine and the DISI engine in the same vehicle was accomplished by controlling the second generation Toyota D-4 DISI engine to operate either i) in homogenous charge, throttled mode for all engine operating conditions or ii) as a DISI engine.

Through the vehicle testing, steady state efficiency and emissions maps were collected and used in an HEV simulation. For evaluation of the benefits of the DISI engine and CVT in an HEV, a simulation method was used because it is not possible to build a physical HEV as necessary to allow direct experimental measurement. As a simulation tool, ADVISOR (Advanced Vehicle Simulator) and PSAT (Powertrain System Analyst Toolkit) were used. The ADVISOR is one of the most well known tools for vehicle modeling, developed in the National Renewable Energy Laboratory (NREL) and programmed in MATLAB/Simulink. The PSAT is developed in Argonne National Laboratory (ANL) and programmed in MATLAB/Simulink, too.

In summary, three primary deliverables are expected from this dissertation:

- A comparison of the fuel economy of a conventional gasoline and a DISI engine in the same vehicle operating over a transient driving cycle.
- A comparison of engine/drivetrain/vehicle energy distributions for the same vehicle with a conventional gasoline engine and a DISI engine, as averaged for operation over a transient driving cycle.
- Prediction of fuel consumption and emissions for a DISI engine in an HEV.

CHAPTER 2: TEST VEHICLE DESCRIPTION AND PREPARATION

This chapter describes the test vehicle used in this study. The major reason to select the OPA as the test vehicle is that it has the 2nd generation D-4 engine of Toyota. The differences of the 2nd generation and the 1st generation D-4 engine are explained to help the understanding of the differences in measured emissions that will be mentioned in the later chapters.

2.1 THE 2ND GENERATION TOYOTA D-4 AND SUPER CVT

A 2001 model year Japanese market Toyota OPA is used as the test vehicle. The University of Texas previously tested a vehicle, a 1998 Corona Premio, equipped with the 1st generation D4 and automatic transmission. Stovell and coworkers [35] measured the fuel economy and emissions and compared with those of a 1999 Corolla with a PFI engine. In this previous collaboration between UT and Argonne National Labs, it was shown that high tailpipe emissions of NOx and, to a lesser extent, HCs were the biggest barriers to introduction of vehicles with DISI engines into the U.S. market. Furthermore, periodic regeneration of the lean NOx trap/catalyst and an extended period of homogenous stoichiometric operation to light-off this catalyst at the beginning of the FTP penalized fuel economy. Additionally, it was shown that tailpipe NOx emissions were high during acceleration and high speed cruises. It was postulated that use of a DISI in an HEV might overcome the emissions barriers while improving fuel economy.

Toyota has developed a new generation D-4 engine with an improved combustion system and launched several vehicles with it. Table 2.1 shows the difference of specifications between the vehicles with the 1st and 2nd generation D-4 engine. From this table we can see that the OPA shows better fuel economy and emissions due to improvement in the combustion system.

Table 2.1 Specifications of the OPA and Corona

		Corona Premio G	OPA 2.0a 2WD
Vehicle	Weight	1200 kg	1250 kg
	Total Weight	1475 kg	1525 kg
	Fuel consumption (10-15 mode)	17 km/L	17.8 km/L
	Emission rating	Japan 1978 regulation certified*	J-TLEV certified*
Engine	Name	3S-FSE	1AZ-FSE
	Displacement volume	1998 cc	←
	Valve train	VVT-i	VVT-i
	Fuel pressure	12 MPa	←
	Intake port	Helical + Straight	Straight
	Rated Power/Speed	107 kW/ 6000rpm	112 KW/6,000 rpm
	Max Torque/Speed	196 N-m/ 4400rpm	200 N-m/4,000 rpm
	EGR	Yes	Yes
Transmission	Type	ECT(4AT)	Super CVT

* 70% reduction in regulation

2.2 DIFFERENCES BETWEEN THE OLD AND NEW D-4 SYSTEM

The major differences between these two D-4 systems are shown in Table 2.2 and Figure 2.1.

The original D-4 relies on the incoming air's powerful swirl motion to create charge stratification, gathering a fuel-rich portion around the spark plug. Swirl is generated by closing the straight port letting air enter through the open helical port. The swirl control valve (SCV) and helical port are combined with a deep, asymmetrical heart shaped bowl in the piston to obtain charge stratification. The bent intake port and deep bowl designs impede efficient filling in the engine's high load, homogeneous charge operation, limiting maximum torque and power.

The new D-4 combustion system uses the mixture's inertial dynamics versus the original version's swirl flow. The key to the system is the new "slit" injector design.

From this novel design, fuel is injected in a solid, fan-like pattern versus the previous hollow cone "casting net" pattern.

Table 2.2 Difference in combustion system of new D-4 engine

		Old system	New system
Injector		Cone nozzle	Slit nozzle
Intake	Flow	Swirl	(Weak tumble)
	Port	Helical & straight port	2 straight ports
Piston bowl		Deep and asymmetrical heart shaped	Shallow and symmetrical shell (oval) shaped
Mixture preparation		By charge motion	By spray's own energy

Figure 2.1 shows a schematic of mixture preparation of the two combustion systems [18]. In the old system, a helical shaped swirl intake port is used to produce an optimum swirl in the cylinder by variable controlled swirl control valve. Pistons with a concave bowl and high pressure fuel injection system provide a fine fuel-air mixture in the combustion chamber. Compared to the previous spray, the new spray has large penetration and uniform fuel distribution [23].

Due to these improvements, the new D-4 system achieved stratified combustion over a larger range of operating conditions and higher output performance compared to the previous one [16]. In addition to the advantage in power and enlarged stratified combustion region, the engine-out THC and NOx are reduced by 20~30% [18] and the robustness of engine control is improved. The catalyst of the OPA is also improved. The new one has 1.5 times the NOx storage capacity of the previous type and its sulfur resistance has been increased. The amount of tailpipe NOx after durability testing is about one-third of that with the conventional catalyst [15]. The combined improvement in combustion system and catalyst system results in far better emissions rating. The previous Corona was certified for 1978 Japanese regulation[1] whereas the OPA was certified for J-TLEV[2] which is only 30% of 1978's regulation.

[1] HC: 0.25 g/km, CO: 2.1g/km, NOx: 0.25g/km

[2] HC: 0.06 g/km, CO: 0.67g/km, NOx: 0.06g/km

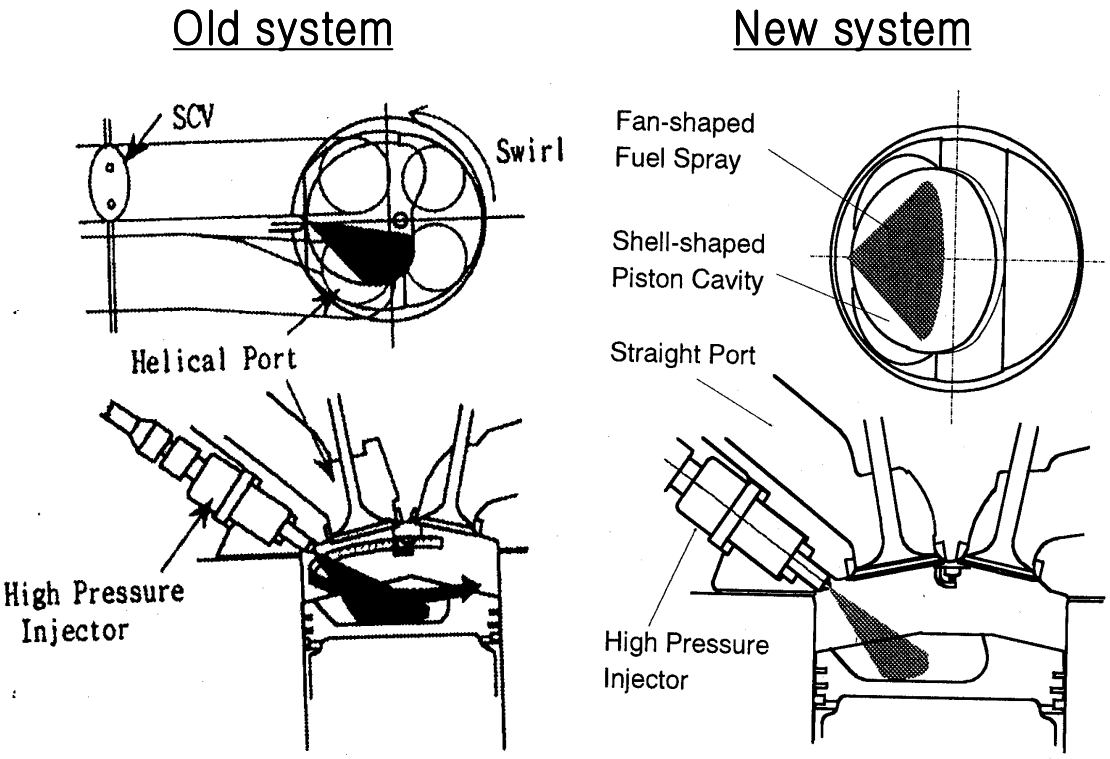

Figure 2.1 Comparison of two D-4 combustion systems

2.3 D-4 COMBUSTION AND EMISSIONS CONTROL SYSTEM

The engine control computer determines the optimum combustion scheme based on the engine operating point determined from various sensors as shown in Figure 2.2. It switches the control scheme by controlling injection timing and quantity, throttle position and EGR valve opening.

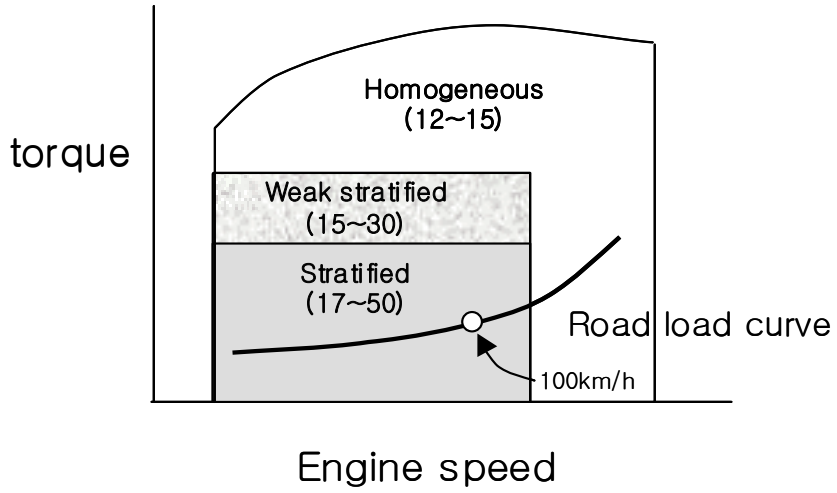

Figure 2.2 Combustion control scheme based on engine operating point (Numbers in parenthesis indicate air/fuel ratio range)

Table 2.3 shows the combustion control schemes. When the engine load is above a certain load threshold, the engine is working in the homogeneous charge mode. Other homogeneous charge control modes are during cold start, brake control and NOx control. During brake control, the engine goes stoichiometric throttled to supply a significant amount of negative pressure (vacuum) to the brake booster. For control of NOx in NOx the storage reduction catalyst, the engine control should be stoichiometric or rich to supply the reduction agent (HC and so on).

Table 2.3 Combustion control scheme

Control	Combustion	A/F ratio	Injection timing	Operating condition
Lean control	Stratified	50~17	Compression	Low load
	Weak Stratified (2 stage)	30~15	Compression & Intake	Middle load
Stoichiometric control	Homogeneous	15~12	Intake	High load
				Cold Start
				Brake control
				NOx control

The OPA has two catalysts as shown in Figure 2.3. In addition to the three way catalyst, a NOx storage reduction catalyst is installed downstream of the 3 way catalyst. It traps NOx as nitrate during lean operation. The stored NOx is reduced to N_2 in homogeneous control regeneration mode occurring once every 30~50 seconds. The reduction agents, such as HC in the stoichiometric/rich products of combustion are used to reduce the stored NOx.

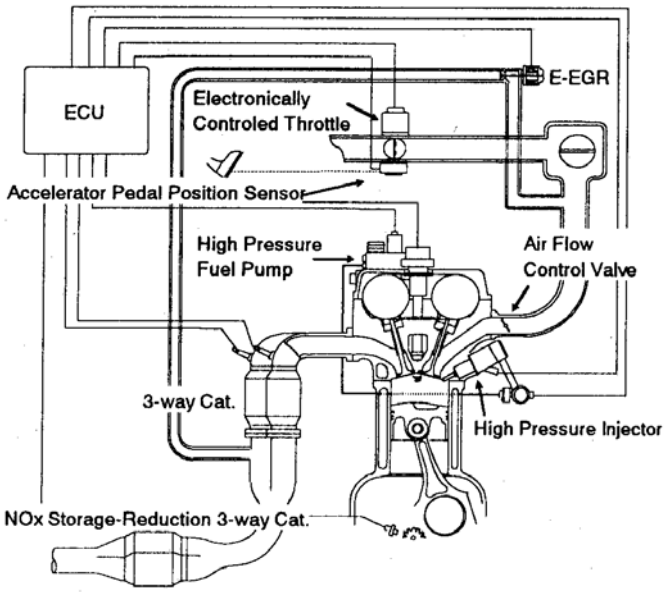

Figure 2.3 OPA emissions control system

CHAPTER 3: METHODOLOGY

This chapter describes the methodology used to estimate the benefit of DISI engine in two types of powertrains, conventional vehicle and HEV. For the conventional vehicle, an experimental method was used and a simulation was performed to support the experimental results. The procurement of the vehicle with state-of-the-art DISI engine made it possible to estimate experimentally this benefit but a different methodology was necessary for HEV. A virtual HEV was built and the resulting fuel economy, emission and performances were evaluated using a simulation method. The experimental approach, analysis method and simulation method are explained in this chapter.

3.1 CONVENTIONAL VEHICLE

Conventional methods to evaluate the factors on fuel economy are fuel economy test in driving cycle or collecting a 2 dimensional specific fuel consumption map from component testing. However, as the fuel economy of a vehicle is the combined result from all factors, it is not easy to distinguish the contribution of a specific factor from vehicle fuel economy testing. Also, the specific fuel consumption map can give only a clue to explain a difference in efficiency, not the overall efficiency itself. Therefore, in order to directly evaluate and compare the efficiency, it is necessary to directly measure the efficiency of the specific component during an actual driving cycle.

3.1.1 Direct measurement of powertrain component efficiency

In this research, the fuel consumption and power flow between the major powertrain components were collected during Phase 1 and Phase 3 of the FTP cycle. To assess the power flow through the major components, the fuel flow rate into the engine and the speeds and torques out of the engine and out of the CVT were measured as shown in Figure 3.1.

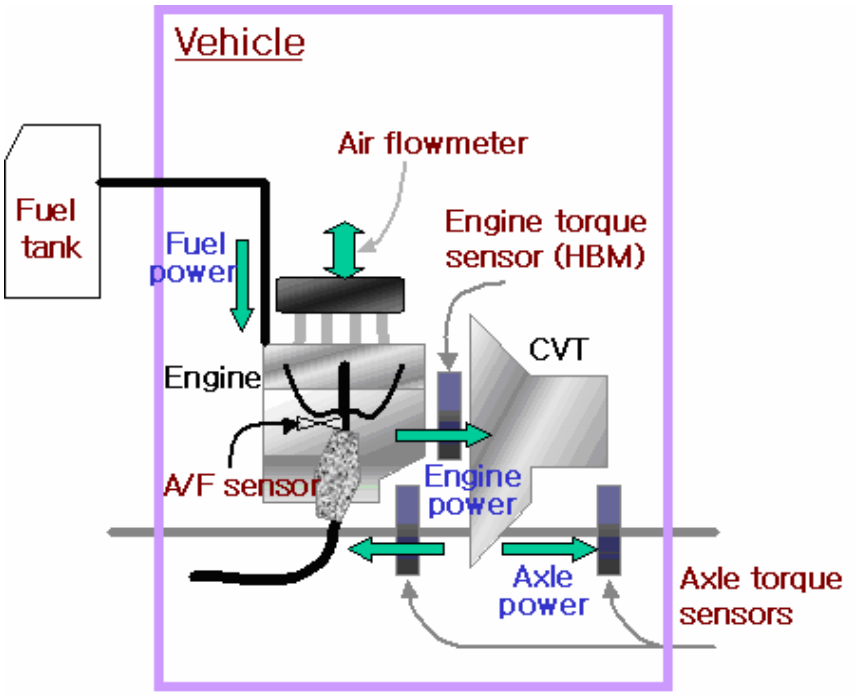

Figure 3.1 Schematic diagram of power flow measurements

The physical quantities measured for this experiment are summarized in Table 3.1. The fuel flowrate was deduced from the measured air flowrate and measured AF ratio. The accuracy of the fuel flow calculation was confirmed by comparing it with that of a direct fuel consumption meter during steady state tests.

Table 3.1 Measured Physical Quantities

Power	Formulae	Physical quantity	Instrument
Fuel power	$\frac{air\ flowrate}{A/F} \times Lower\ heating\ value$	Air flowrate	Laminar flow meter
		A/F ratio	λ sensor
	$fuel\ flowrate \times Lower\ heating\ value$	Fuel flowrate	AVL fuel consumption meter
Engine power	$\tau_{engine} \times \omega_{engine}$	Torque	HBM T10F
		Speed	
Axle power	$\tau_{axle} \times \omega_{axle}$	Torque	SDI sensor
		Speed	CVT speed signal

3.1.2 Power flow for each operation mode

The function of the powertrain in a vehicle can be defined as conversion of the chemical energy of the fuel into rotational mechanical energy and transmission of this energy to kinetic energy of the vehicle. Therefore, the loss of energy occurs during this conversion and during transmission. Therefore, to analyze those losses of energy, the vehicle operating mode should be defined first as shown in Figure 3.2.

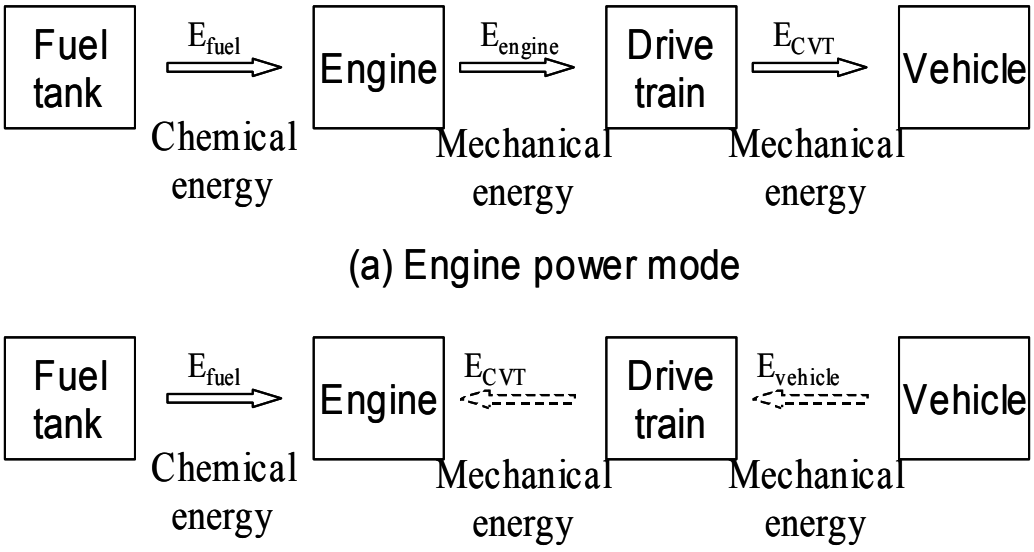

Figure 3.2 Power flow during vehicle operation

In Figure 3.2, the engine power mode means the engine power is transmitted to the vehicle for acceleration, cruising and powered deceleration. Therefore, the efficiency of the engine and drivetrain are important in this mode. During braking, the kinetic energy is lost if there is no regeneration device as in a hybrid electric vehicle. Moreover, fuel must be supplied to the engine to maintain stability. Accordingly, the overall efficiency of the engine is 0% and all the fuel energy supplied to the engine is lost during the standby mode.

Table 3.2 Energy Losses for Each Mode

Mode	Loss component	Energy loss
Engine power mode	Engine loss	Fuel energy – Engine output
	CVT loss	Engine output – CVT output
	Vehicle loss	Road load + Acceleration
Stand-by mode	Idle loss	Fuel energy
	Braking fuel loss	Fuel energy

In this analysis, the energy loss and efficiency of each component were investigated according to the vehicle modes and energy losses, as summarized in Table 3.2. The tests are performed with the engine in stratified charge unthrottled mode as well as in homogeneous throttled mode. As results of tests in two different combustion modes, the benefit of DISI engine is investigated.

3.1.3 Component efficiencies

Based on the measured fuel flowrate from the fuel tank and torque and speed of the engine and transmission, the overall efficiency can be calculated from the following formulae. For the various conditions of the engine and the vehicle, the overall efficiencies from the following formulae can be obtained. The efficiency of the DISI engine is obtained by running the vehicle at the normal operating mode and that of the PFI is obtained by manipulating the mode into the homogenous stoichiometric mode. Then, the overall efficiencies of both the lean burn mode and the homogenous mode can be compared.

$$\eta_{engine} = \frac{\int_{power\,mode} \tau_{engine} \cdot \omega_{engine}\, dt}{\int_{power\,mode} \dot{m}_{fuel}\,(LHV)\, dt}$$
$$\eta_{CVT} = \frac{\int_{power\,mode} \tau_{CVT} \cdot \omega_{CVT}\, dt}{\int_{power\,mode} \tau_{engine} \cdot \omega_{engine}\, dt} \qquad (1)$$

3.2 HYBRID ELECTRIC VEHICLE

The benefit of a DISI engine in a conventional vehicle can be estimated by actual vehicle testing. Similar tests could be performed on an HEV. However, it was not possible to build a vehicle for the purpose of this research. Therefore, a virtual HEV and a simulation tool which can predict the fuel economy and emissions are necessary. The required functions of the simulation tool are as shown in Figure 3.3. The simulation program should predict the fuel economy and emissions from the input data such as the vehicle resistance and powertrain efficiency and engine emissions maps and the cycle that the vehicle needs to run on. It also has various libraries of vehicle models from the conventional vehicle to the various types of HEVs such as series, parallel and power-split.

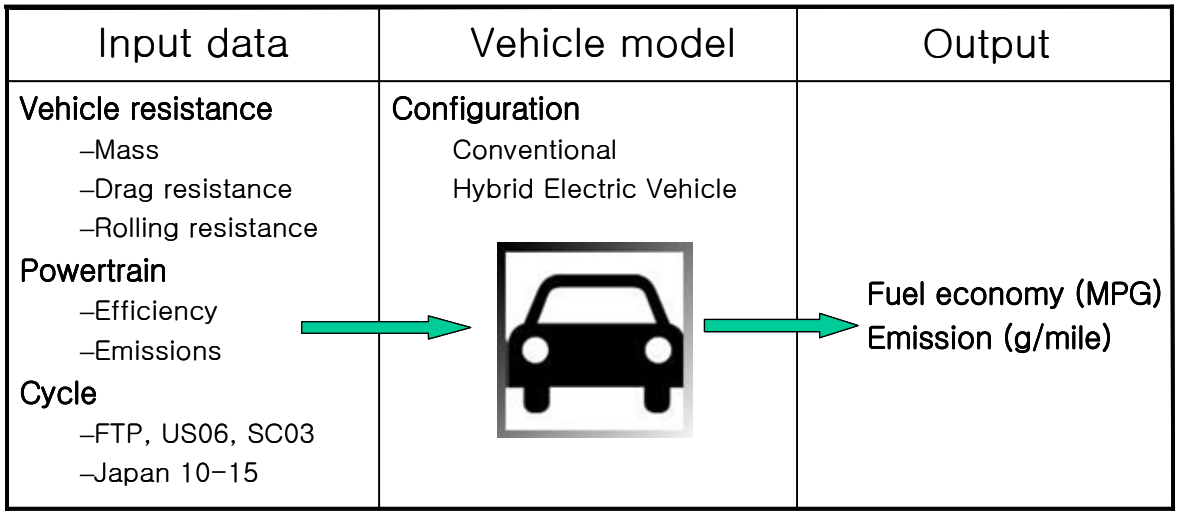

Figure 3.3 Vehicle simulation model

ADVISOR (ADvanced VehIcle SimulatOR) and PSAT (Powertrain Systems Analysis) were used as the simulation tools as shown below.

- ADVISOR version 2002
- PSAT version 5.1 Non-proprietary version

Brief descriptions for ADVISOR and PSAT are shown in Table 3.3. Both tools are based on a Bond graph model [19]. There are effort and flow for each component model. The efforts and flows change as they pass through the components.

Table 3.3 Comparisons of ADVISOR and PSAT [32]

<table>
<tr><th></th><th>PSAT</th><th>ADVISOR</th></tr>
<tr><td>Model</td><td colspan="2">Map based model
• For maximum/minimum characteristics
• Efficiency and emissions
Bond graph model
 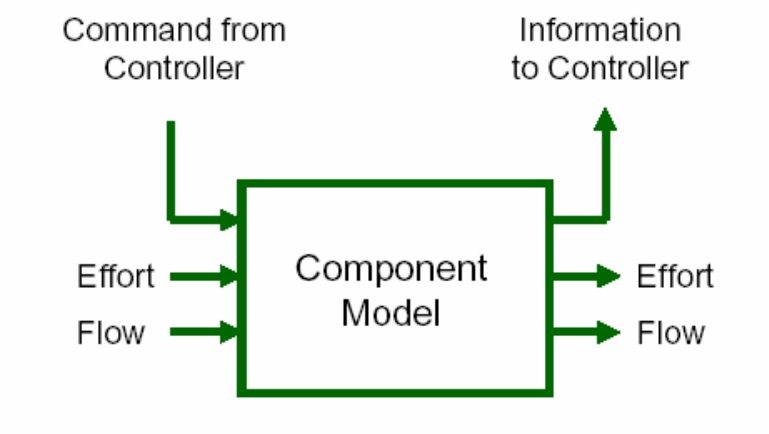

• Mechanical Component
○ Effort = Torque
○ Flow = Speed
• Electrical Component
○ Effort = Voltage
○ Flow = Current</td></tr>
<tr><td>History</td><td>• 1995 by USCAR (Contract to SwRI)
• 1999 transferred to ANL</td><td>• 1994 by USCAR (Contract to NREL)</td></tr>
<tr><td>Primary difference</td><td>• Forward facing</td><td>• Backward facing</td></tr>
</table>

The main difference between the two simulation tools is that PSAT is based on a forward facing model and ADVISOR is facing backward, as shown in Figure 3.4. The backward model means the desired vehicle goes from the vehicle model back to the engine to finally find out how each component should be used to follow the speed cycle.

Instead, the forward model used in PSAT goes from the driver. The driver determines the required power to drive the vehicle as close to the given cycle as possible. Then this power passes through the clutch, transmission, final drive, wheel and finally to the vehicle (i.e., the road). The efficiencies and dynamic effects of each component model affects the flows of speeds and torques between the component models.

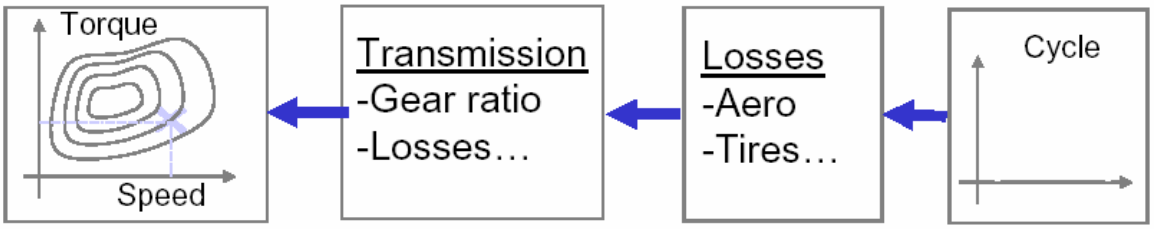

(a) Backward facing model

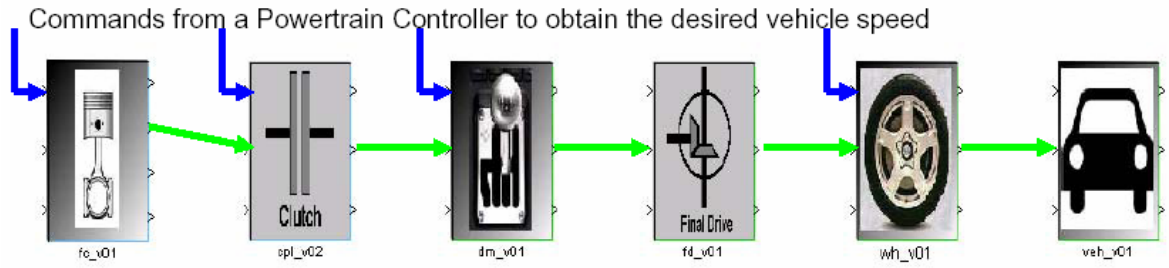

(b) Forward facing model

Figure 3.4 Comparison of forward and backward models [44]

The forward facing model is closer to the actual operation of the vehicle. Its advantages over the backward facing model can be summarized as follows [44];

- More realistic prediction for the transient component behavior and vehicle response
- Consistent with industry design practice
- Allows for the development of control strategies that can be utilized in hardware-in-the-loop or vehicle testing

In this research, PSAT and ADVISOR were used for the conventional vehicle simulation. The predictions of both programs were compared with the measured results. For the simulation of the HEV, PSAT was selected due to the advantages mentioned

above. Figure 3.5 shows an example of the block diagram of PSAT. The controller model determines the operation of each component based on the accelerator and brake pedal position from the driver model. The driver sees the vehicle speed of a given driving cycle and actual vehicle speed and controls accelerator and brake pedals. The controller determines the load of the engine, clutch engagement, gear shifting, brake on/off and the usage of the motor.

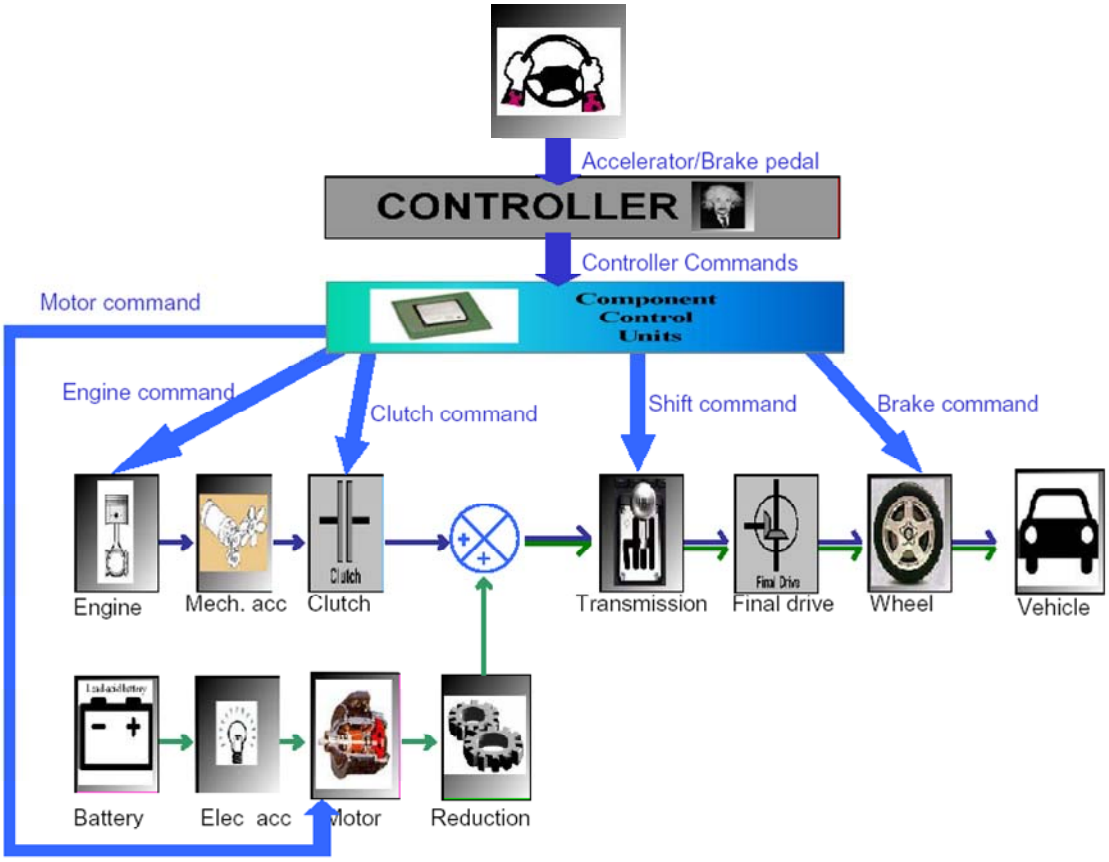

Figure 3.5 Block diagram of PSAT

CHAPTER 4: EXPERIMENTAL SETUP

For this project, the test vehicle, a 2001 OPA, was imported directly from Japan. The break-in time period was dictated by the catalyst's aging requirement needed for emissions certification. Due to time and cost, a dyno-controlled AMA cycle break-in period was not done on the vehicle. Instead a simulated AMA cycle was mapped out using the streets and highways of Chicago and the surrounding areas. Several workers at ANL, including this author, drove the vehicle until the 4000 miles were accumulated.

Special concern regarding the contamination of the lean NOx trap catalyst required the use of special fuel during not only the actual testing but also the break-in period. A gasoline with high sulfur concentration, which is usually available in any gas station, may affect dramatically the lean NOx trap catalyst's efficiency. Inappropriate use of fuel would result in an inaccurate representation of the tailpipe emissions of the production vehicle. The fuel used throughout this research is commercially known as EEE. The EEE fuel is an unleaded low sulfur fuel used as a certification gasoline. Its specifications are presented in Table 4.1.

Table 4.1 Specifications of test fuel, EEE

Specification	Units	Value
Gravity	°API	59.3
Density	kg/liter	.741
Reid vapor pressure	psi	9.2
Hydrogen/Carbon ratio	mole/mole	1.806
Oxygen	wt %	<0.05
Sulfur	wt %	0.0035
Lead	g/gal	<0.01
Phosphorus	g/gal	<0.0008
Aromatics	vol %	29.2
Olefins	vol %	0.7
Saturates	vol %	70.1
Net heating value	BTU/lb	18430
Research octane number		97.6
Motor octane number		88.5

4.1 SENSOR INSTALLATION

A special technique of sensor installation used in the present research is torque sensor installation in the vehicle so that it can be tested on the chassis dynamometer. The engine and axle shaft torque measuring methods are explained. The installation of thermocouples on the catalyst is explained as well.

4.1.1 Torque sensor installation

Two kinds of torque sensors were installed to measure the power output of the engine and CVT. In the present experiments, an engine torque sensor was installed between the engine and CVT, as shown in Figure 4.1, so that the engine-out torque and speed could be measured during chassis dynamometer testing.

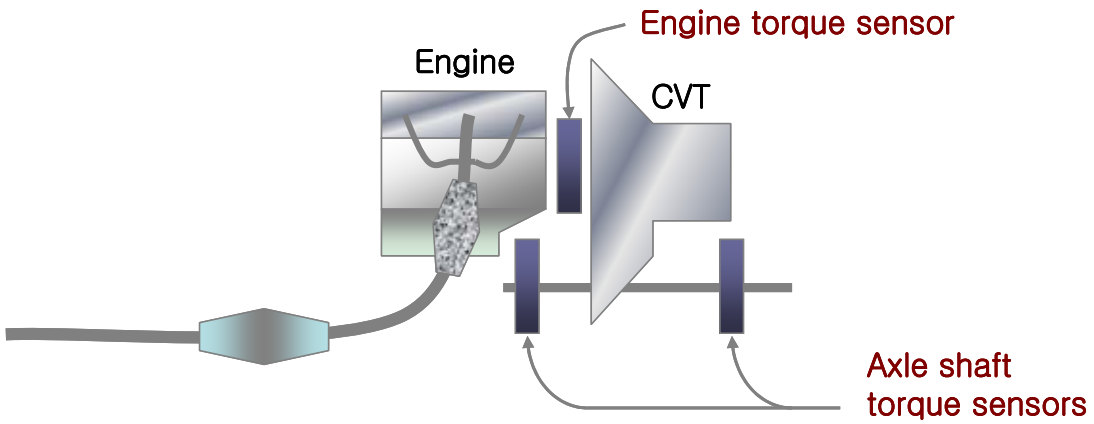

Figure 4.1 Positions for torque sensor installation

Though the apparent functions of both torque sensors are the same, the torque sensors and installations of them are different from each other. An engine torque sensor was purchased from HBM GmbH and installed between the engine and CVT. The necessary parts and modifications were accomplished at ANL. For the measurement of axle shaft torque, the axle shafts were take out from the vehicle and sent to the Sensor

Development Inc.. This sensor company attached strain gauges on the axle shafts and sent them back to ANL with a telemetry system.

The engine torque sensor is composed of a rotor and stator as shown in Figure 4.2. The rotor is installed between the crankshaft and torque converter and rotates together with them. The stator is a kind of signal receiver and was installed on the housing located between the engine and transmission case. The specifications of the torque sensor are shown in Table 4.2.

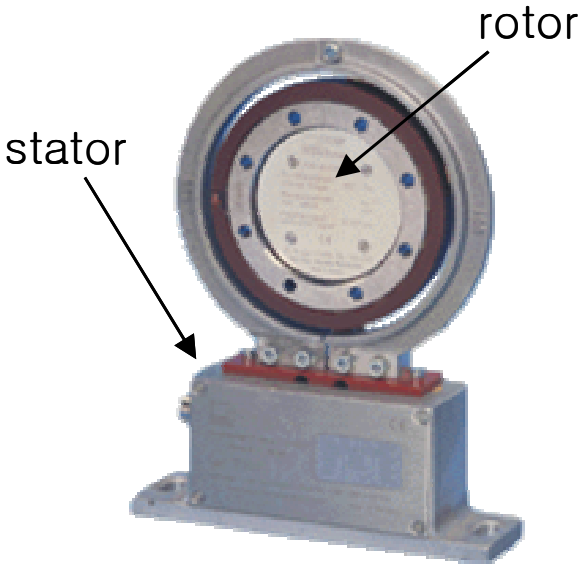

Figure 4.2 Torque sensor used

Table 4.2 Specifications of the engine torque sensor

Manufacturer	HBM
Model	T10F-200
Measuring system	Strain gauge
Load limits	200 N-m
Limit torque	400 N-m
Breaking torque	800 N-m
Maximum speed	8000~15000 rpm
Temperature range	10~60 °C
Signal transfer	Non-contact
Output signal	Voltage, frequency

This torque sensor has a finite thickness so the total length of the powertrain must be increased. In the case of this OPA, the total length increased by 3 inches. There are two kinds of work necessary for the torque sensor installation as shown below.

- Sensor work: Machining the adapter and sensor housing
- Engine room work: Modification for increased powertrain length

Photos of the torque sensor installation are shown in Figure 4.3. At first, the powertrain was taken out from the vehicle. Then, the sensor work and engine room work proceeded separately.

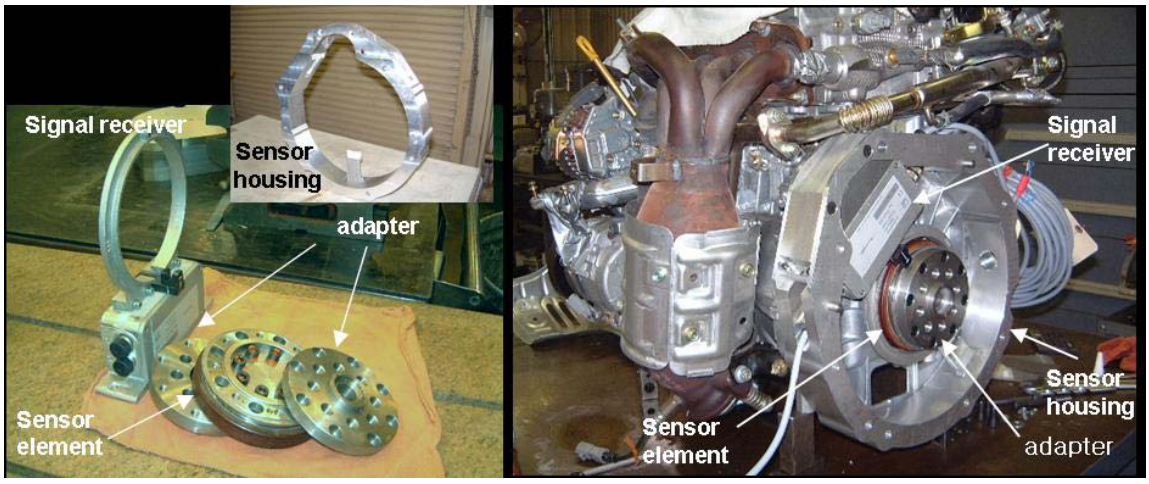

(a) Sensor work

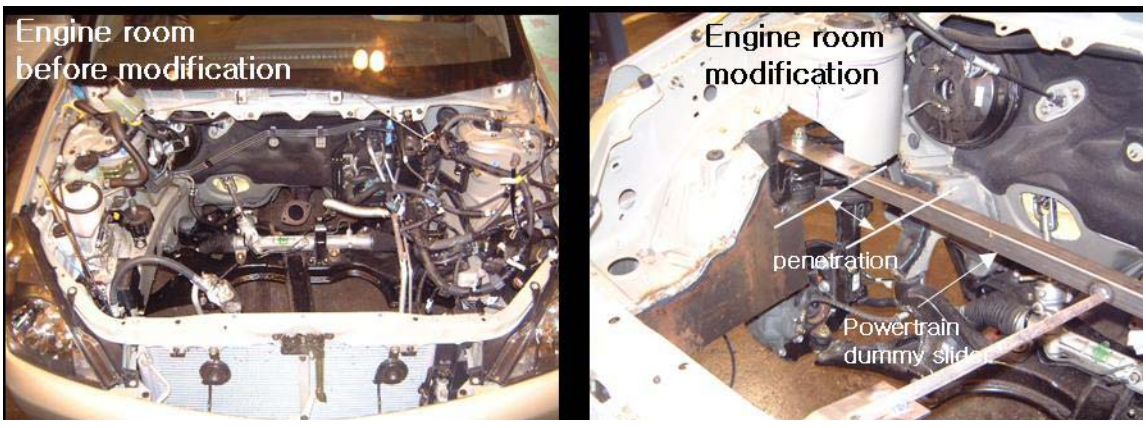

(b) Engine room work

Figure 4.3 Engine torque sensor installation

After the sensor work and engine room work, the powertrain was installed into the vehicle to be ready to go. The completed powertrain and vehicle are shown in Figure 4.4. There were additional modifications done due to the sensor installation. The engine room cover and the brake booster were removed. Thus, the tests were done without the brake booster.

(a) Assembled powertrain (b) Vehicle after the powertrain installed

Figure 4.4 Powertrain and vehicle after the torque sensor installation

For the measurement of axle shaft torques, a strain gauge was attached on the surface of each axle shaft. The axle shaft torque measurement system is shown in Figure 4.5.

Figure 4.5 Axle shaft torque measurement system

As the sensor is installed on a rotating shaft, a wireless signal transmission is necessary. A signal transmission collar is installed on the shaft and the data was obtained using a signal receiver. The left photo of Figure 4.5 shows the signal transmission collar and signal receiver and the right photo shows the axle shaft with the sensor and transmission collar installed.

4.1.2 Temperature measurement

The measurement of temperatures of the exhaust gas and catalyst is essential to examine the characteristics of the catalyst. Four thermocouples were installed as shown in Figure 4.6. Two of them were for exhaust gas temperature and the others were for catalyst temperature.

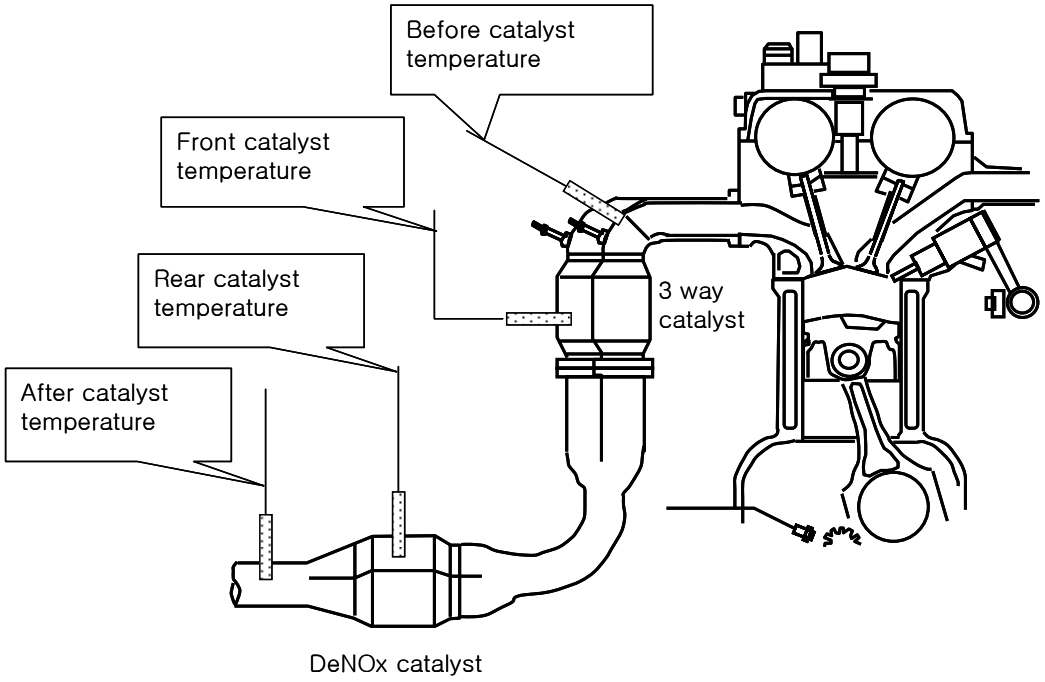

Figure 4.6 Temperature measuring positions

In order to minimize the machine work on the catalyst, two thermocouples of similar diameter with the hole in the substrate were inserted into one of the holes of the

substrate. The thermocouples are located in the middle of the catalyst so that the measured temperature represents the average temperature of the catalyst.

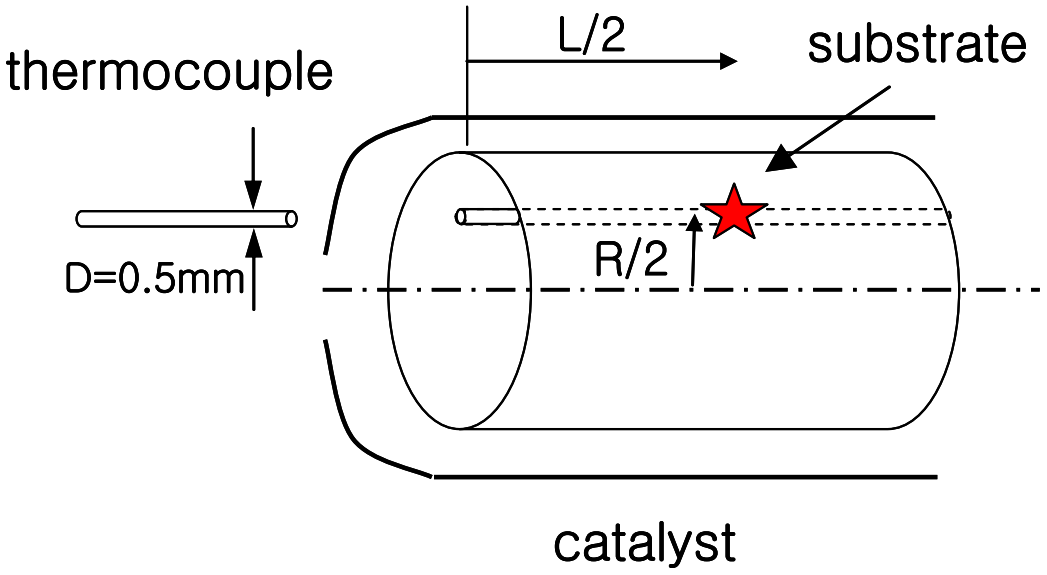

Figure 4.7 Location of catalyst temperature measurement

4.2 FACILITIES

The experiments were done in three different test cells as summarized in Table 4.3. This research started at ANL and finished at UT. The chassis dynamometer emission benches in UT are not capable of FTP testing. Thus, with the help of SwRI staff engineers, the FTPs were performed at SwRI. SwRI has both a CVS and modal emission measurement system. Only the steady state tests were performed at UT.

Table 4.3 Test cells

Test cell	ANL	SwRI	UT
Test duration	Jan. 2001~Aug. 2001	Mar. 2004	Apr. 2004~June 2004
Cell type	Twin roll	48" single roll	Twin roll
Performed test	Overall efficiency measurement	FTPs	Steady state test

The photos, taken at ANL where the initial experiments were carried out, are shown in Figure 4.8 and the facilities are summarized in Table 4.4. The fuel consumption was obtained using both the fuel consumption meter and air flow meter together with an air/fuel ratio meter.

Figure 4.8 OPA testing at ANL

Table 4.4 Test facilities at ANL

Facility	Maker	Model
Dynamometer	Clayton	
Emission bench	Pierburg	AMA 2000 AMA 4000
AF ratio	E-TAS	λ sensor
Intake air flowrate	Sierra	600-L04
Fuel consumption meter	Pierburg	
Data acquisition	National Instrument	SCXI-1100 SCXI-1126

The chassis dynamometer at the University of Texas is a water brake type dynamometer. The inertia masses were not hooked up to the dynamometer. Therefore, only steady state tests were possible with this dynamometer. The fuel consumption rate was measured using an AVL fuel consumption meter. The available facilities at UT are

summarized in the following Table 4.5. The OPA on the chassis dynamometer at UT is shown in Figure 4.9.

The dynamometer settings used for the FTP test are as follows.

Test inertia: 3125 lbs

Road load:

$$F = f_0 + f_2 \cdot v^2$$

$$where\ f_0 = 38.93\ (lbf)$$

$$f_2 = 0.02055\,(lbf / mph^2)$$

Figure 4.9 OPA testing in UT

Table 4.5 Test facilities at UT

Facility	Maker	Model	Specification/Remarks	
Dynamometer	Clayton	CT-200	Water brake type Capacity: 200 hp	
Fuel consumption meter	AVL	730 Dynamic	Accuracy: 0.12% of consumed mass Measuring frequency: 1 Hz	
Emissions bench	Horiba	CLA 53	<u>NO/NOx analyzer</u> Measuring range : 0–10~5,000 ppm Repeatability: ±1% of full scale Linearity: ±1% of full scale	
		FIA-34A-2	<u>HC analyzer</u> Measuring range : 0–10~30,000 ppm	
	Horiba	MEXA-554J	HC	Range: 0-10000 ppm vol. Repeatability: within 1/3 of (±12ppm or ±5 % of readout)
			CO	Range: 0-10 % Repeatability: within 1/3 of (±0.06 % or ±5 % of readout)
			CO_2	0-20 % Repeatability: within 1/3 of (±0.5 % or ±5 % of readout)
Data acquisition system	Fluke	2640 NetDAQ	Measurement: DC, AC, Resistance, Frequency, Thermocouple Channel: 20 ea Scan speed: Slow: 6 channels/sec Medium: 48 channels/sec Fast: 100 channels/sec	
A/F ratio sensor	Horiba	MEXA-110λ	Range: 0.0-99.9 (with gasoline) Within ± 0.1 A/F (at stoichiometry)	

CHAPTER 5: FTP TEST RESULTS

The main reason for investigating a DISI engine is the benefit in fuel economy and the barrier is strict emissions regulations in the U.S. The OPA with Toyota's 2nd generation D-4 engine and super CVT was tested for fuel economy and emissions on the Federal Test Procedure. The measured fuel economy and emissions are compared with those of the vehicle with the 1st generation D-4 engine. UT has already completed a project of testing the Corona Premio which employs the previous version of Toyota's DISI engine in 1999. The Corona test data used for comparison are based on several references [35] [37].

Selected topics and comparison issues are addressed in this section. Air/fuel ratio control for the OPA is compared to that for the Corona in the following section. Fuel economy and emissions are discussed in Sections 5.2 and 5.3 respectively. Additional FTP results are provided in Appendix A.

5.1 AIR/FUEL RATIO CONTROL

Figure 5.1 shows the air/fuel ratio histories for the OPA and Corona during the FTP cycle. Both the OPA and Corona begin the cycle with stoichiometric combustion and, after a while, lean combustion starts. The onset of lean combustion for the Corona was 256 seconds whereas that for the OPA is 416~529 seconds after vehicle start-up.

The main factor on this timing is the catalyst light-off. The temperatures of the exhaust gas and catalysts are shown in Figure 5.2. For the Corona, only the exhaust temperature is available so the catalyst temperature is plotted only for the OPA. The exhaust temperatures of both vehicles are similar to each other as long as the combustion control scheme is the same as each other, about 250 seconds after start-up. After that, the exhaust temperature of the OPA is about 20~30 °C higher than that of the Corona because its combustion remains stoichiometric.

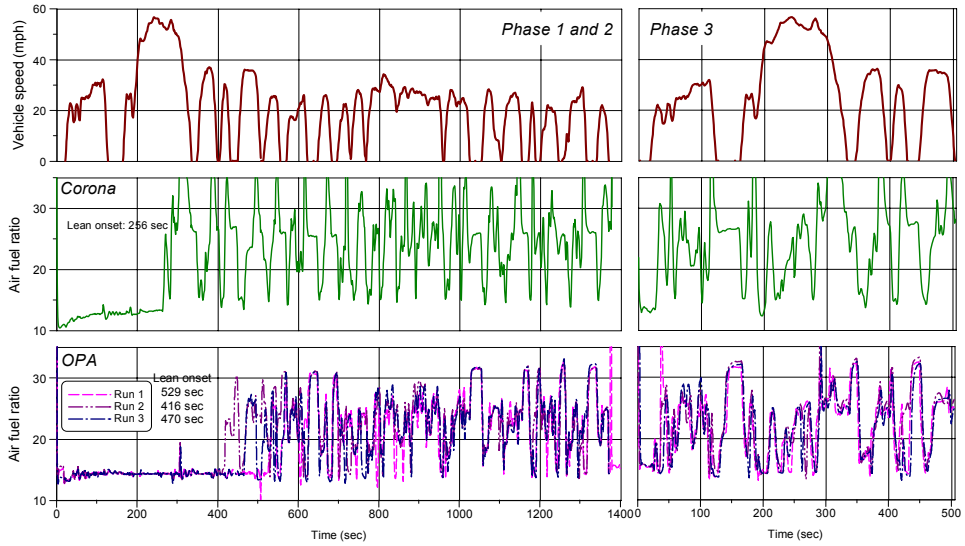

Figure 5.1 Comparison of air/fuel ratio control

The catalyst is heated by hot exhaust gas and reaction heat within the catalyst. The onset of lean combustion might be dependent on the temperature of the rear catalyst because it is used to convert NOx emissions. The front catalyst temperature passes 500°C at 32 seconds and the rear catalyst passes at 259 seconds. Therefore, it is reasonable to program the engine to begin the lean combustion at around 250 seconds. It is not clear why the onset of the lean combustion is after 400 seconds for the OPA.

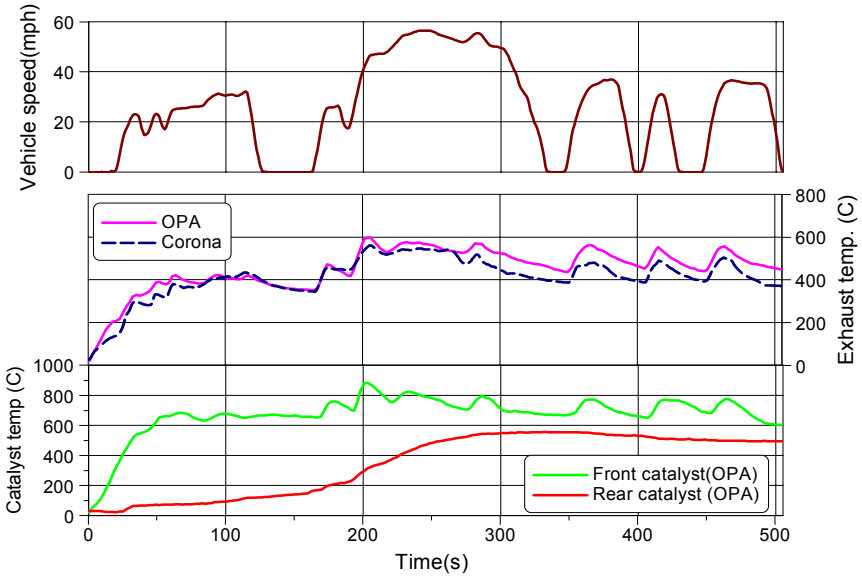

Figure 5.2 Temperatures of the exhaust gas and catalysts

The D-4 engine is supposed to work in the lean combustion mode after catalyst light-off. During lean combustion, the tailpipe NOx emissions are reduced by a NOx storage reduction catalyst [17]. The mechanism is that NOx is stored and held in the catalyst as nitrate at lean air/fuel ratios, then desorbed from the catalyst and reduced to nitrogen using the reduction agent exhausted during stoichiometric combustion. Therefore, the regular repetition of stoichiometric combustion is necessary. Figure 5.3 shows this operation during steady state and transient running of the vehicle. At constant speed running as shown in Figure 5.3(a), the air/fuel ratio is kept constant and the rich spikes occur periodically. At this rich spike, the throttle valve closes to reduce the amount of air with the constant accelerator position. During the transient operation shown in Figure 5.3(b), the stoichiometric combustions are seen for both the high load and rich spikes for NOx regeneration.

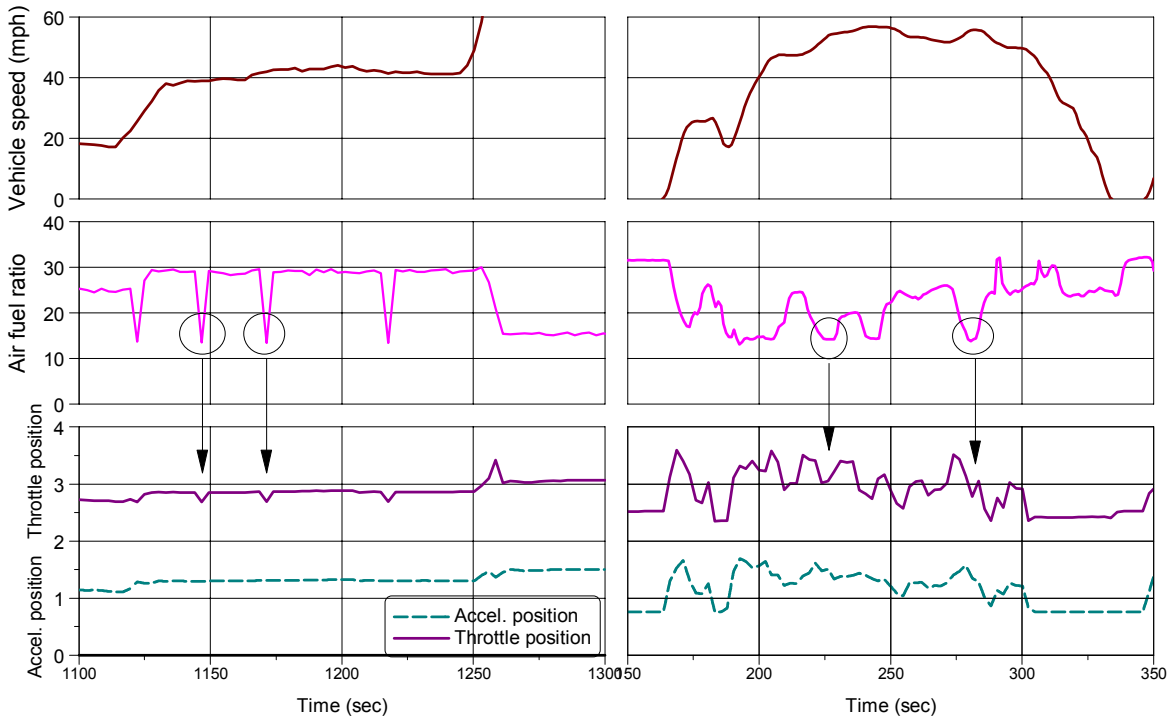

(a) Steady state operation (b) Transient operation

Figure 5.3 Engine operation for NOx regeneration

Figure 5.4 shows the comparison between the OPA and Corona for the engine operation, air/fuel ratio and engine speed. Even though the air/fuel ratio is transient and complex, the range of air/fuel ratio for the OPA and Corona is similar to each other. The air/fuel ratio during the idle for the OPA is 32 whereas that for the Corona is 27. The engine speed of the OPA is controlled lower than that of the Corona due to the use of a CVT.

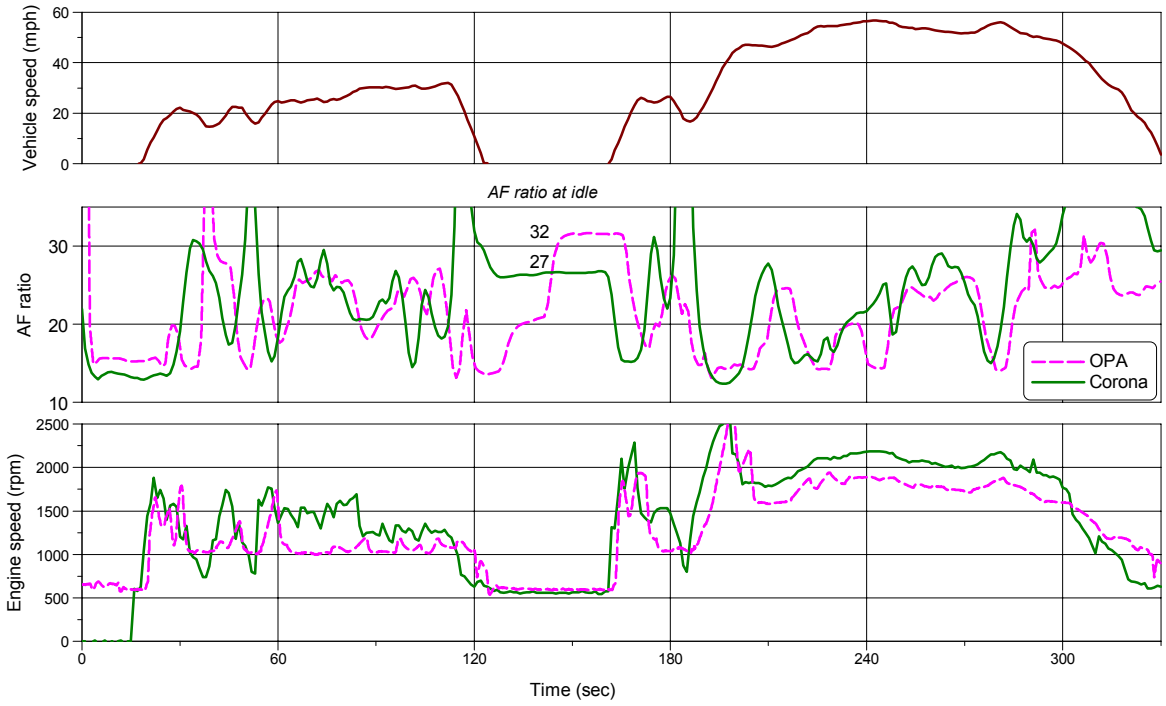

Figure 5.4 Comparison of engine operation for the OPA and Corona.

5.2 FUEL ECONOMY

The OPA was tested 3 times on the FTP cycle. The fuel economy results are shown in Table 5.1 along with the fuel economy of the Corona. The Corona was the first Toyota vehicle with the 1st generation D-4 engine. UT has conducted experiments on this vehicle and presented the fuel economy and emissions results and examined the potential of the DISI engine [36]. The FTP fuel economy of the OPA is 30.5 mpg, 10% less than that of the Corona. There are two possibilities for this unexpected finding. One

possibility is that there is an actual difference in fuel economy and the other one is the test variation. The weight of the OPA is 50 kg heavier than the Corona and the OPA is a station wagon while the Corona is a sedan and thus should have a higher drag coefficient. The specifications can affect the fuel economy difference. The test-to-test variation in fuel economy for tests performed at the same lab is usually said to be 3%. However, the OPA was tested on a chassis dynamometer at SwRI and the Corona was tested at GM. The test-to-test variation together with the lab-to-lab variation can result in a 10% difference in fuel economy. Therefore, it can not be stated with certainty that the fuel economy of the OPA is 10% less than that of the Corona.

Table 5.1 Fuel economy of the OPA and Corona (mpg) [37]

	Phase 1	Phase 2	Phase 3	Weighted results
Run 1	25.812	31.876	34.877	31.079
Run 2	25.597	31.213	34.341	30.575
Run 3	24.968	30.535	33.444	29.804
Average	**25.453**	**31.208**	**34.221**	**30.486**
Corona				**33.495**

The fuel flowrate during the FTP cycle is shown in Figure 5.5. There is a small difference in fuel consumption rate. In fact, the fuel economy data in the above table is obtained from the CO_2 concentration bag measurements and the fuel consumption rate in Figure 5.5 is obtained from the instantaneous modal CO_2 concentration and exhaust gas flowrate. There is usually a discrepancy between the modal data and bag data. That is the reason that the fuel consumption rates in Figure 5.5 do not show a big difference. Anyway, what we can see from the fuel flowrate is that the fuel consumption patterns of the OPA and Corona are similar to each other.

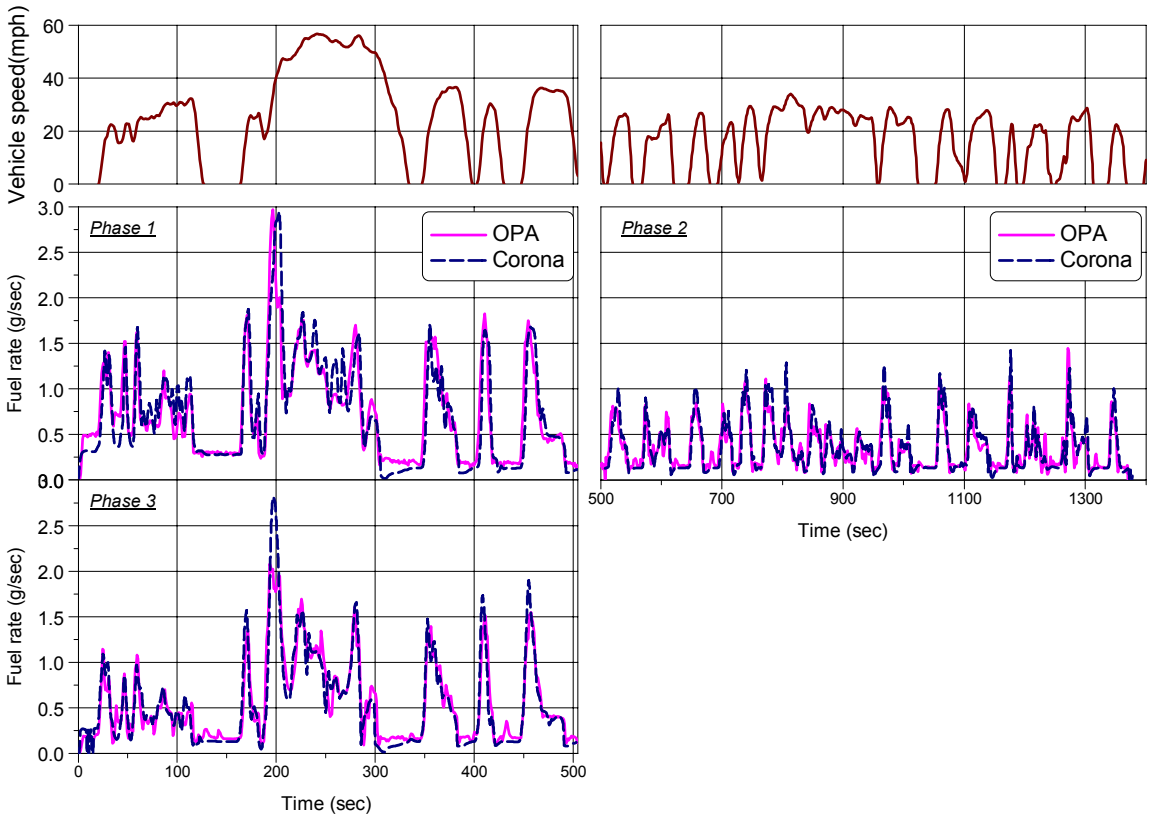

Figure 5.5 Fuel flowrate during FTP cycle

5.3 EMISSIONS

The tailpipe emissions from the OPA on the FTP cycle are summarized in Table 5.2. The comparison of these emissions with the previous version D4 engine is shown in Figure 5.6, which also shows the regulated levels. For this comparison, two sets of standards were used. The first set is the intermediate useful life (50 kmile) Low Emission Vehicle (LEV) standards fro the National Low Emission Vehicle (NLEV) program. The FTP emissions are also compared to the intermediate life Tier 2 bins, which is effective for 2004~2009 MY. Specifically, the emissions of the OPA are compared with Bin 10. Regulators recognize the fact that some HC species are more ozone-forming than others. Methane is essentially non-reactive and excluded from most regulations. Thus, California hydrocarbon emissions are regulated in terms of Non-Methane Organic Gas (NMOG) and Federal HC emissions as Non-Methane Hydrocarbons (NMHC). To

compare the measured emissions results with the emissions regulations, it is necessary to convert the amount of THC into the terms actually used in the regulations. In this research, the measured THC is converted into the NMOG using the factors suggested by Lindhjem [27].

Table 5.2 FTP emissions test results for the OPA (unit: g/mile)

Phase 1			
THC	NOx	CO	CO2
0.480	0.167	3.141	338.15

Phase 2			
THC	NOx	CO	CO2
0.049	0.224	0.613	277.52

Phase 3			
THC	NOx	CO	CO2
0.056	0.342	0.531	258.90

Weighted average			
THC	NOx	CO	CO2
0.141	0.245	1.114	283.52

As seen in Figure 5.6, the OPA meets only the CO standard for both regulations. The NOx of the OPA meets Bin 10 of the Tier 2 EPA Bins but still needs improvement to meet Bin 9, or LEV in the NLEV program. For the NMOG, the barrier is larger than for the NOx. Although the D-4 engine is not calibrated for U.S. standards, this result implies that the barriers for the DISI engine in the U.S. market are NOx and HC emissions, even though Toyota has made considerable improvements to both with their second generation D-4.

For all species except for carbon monoxide (CO), the tailpipe emissions of the OPA are smaller than those of the Corona. The weighted average NMOG emissions from the OPA are 30% less than that from the Corona. The NOx emissions of the OPA are almost half of that from the previous D-4 vehicle. Even though the CO emissions increase, its level is still below the regulated amount. Therefore, we can see that there is a significant improvement in the development of the 2nd generation D-4 engine. The following is a detailed analysis about the sources of these improvements.

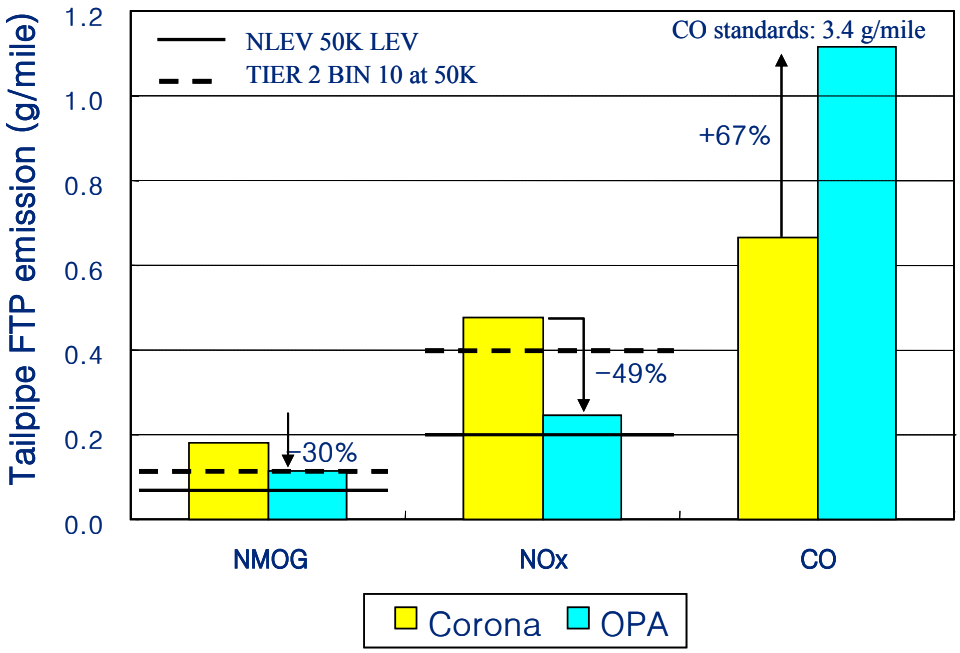

Figure 5.6 Comparison of tailpipe emissions

5.3.1 THC emissions

The reason for the difference in emissions can be considered in two ways, engine-out and after-treatment. To make this reason clear, the engine-out and tailpipe THC and catalyst efficiencies are shown in Figure 5.7. The difference in the amount of engine-out THC appears in the same quantitative way. The catalyst efficiencies are almost the same as each other. The change in combustion system using slit nozzle injector seems to be effective for the reduction of engine-out HC. According to Toyota [18], [23], the fuel spray from the slit nozzle injector can be mixed well with air more evenly than the previous cone spray and the reduced under-mixing and over-mixing can effectively reduce HC emissions.

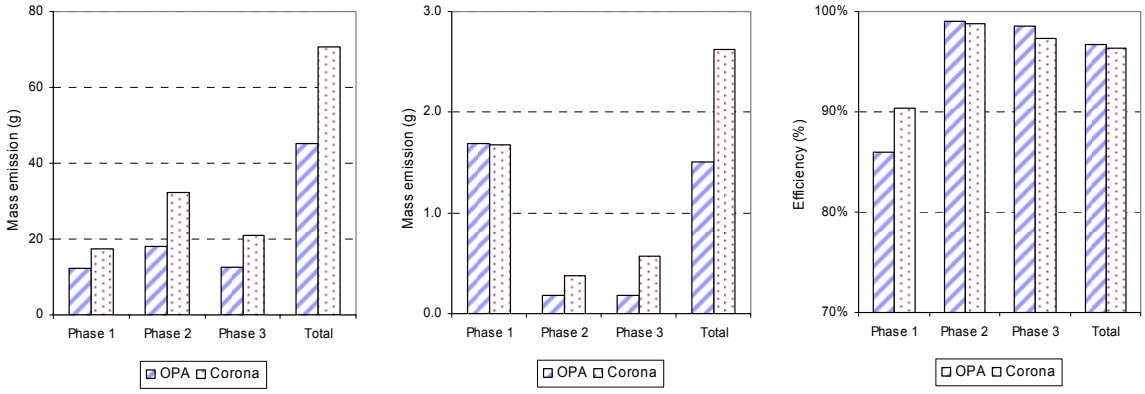

(a) Engine-out emissions (b) Tailpipe emissions (c) Catalyst efficiency

Figure 5.7 Source of THC difference between the OPA and Corona

Figure 5.8 shows the second by second HC emissions for Phases 1~3 of the FTP cycle. It is seen in this figure that the OPA emits less HC than the Corona except for the initial period until 250 seconds while both engines are working in a stoichiometric combustion mode.

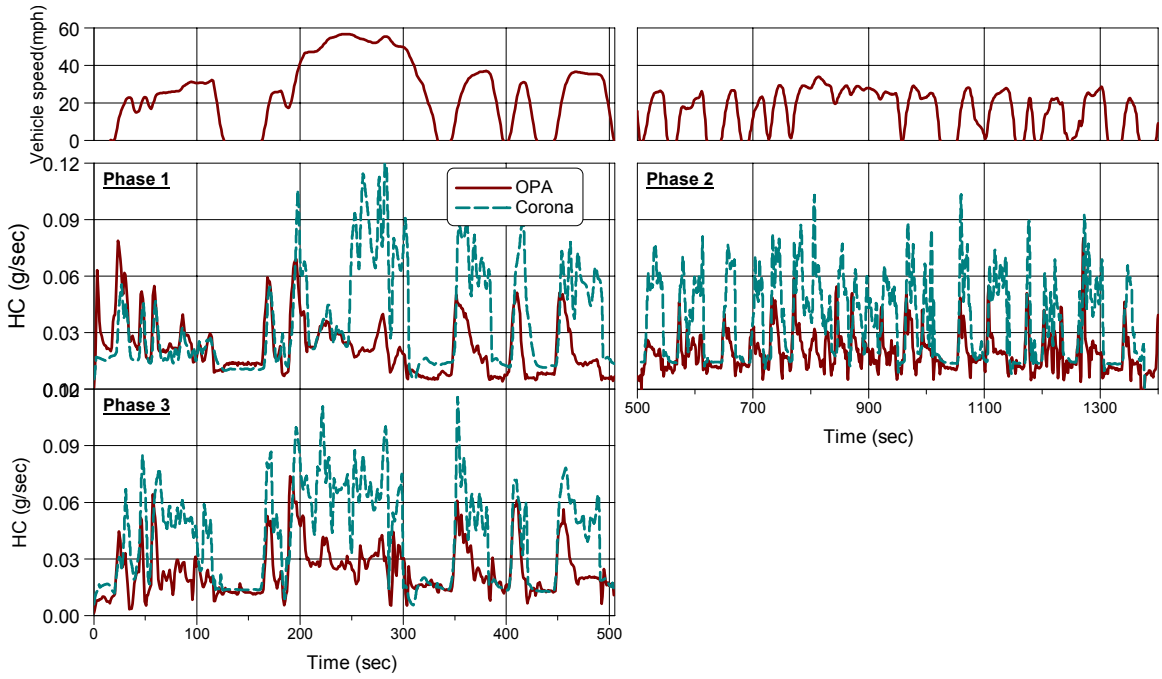

Figure 5.8 Comparison of engine-out THC between the OPA and Corona during the FTP cycle

5.3.2 NOx emission

The reasons for decreased NOx emissions are investigated in the same way as for THC. The engine-out and tailpipe NOx and catalyst efficiencies are shown in Figure 5.9 to see which factor dominates the reduced tailpipe NOx emissions. The dominant factor seems to be different from that for THC. In the case of THC, the catalyst efficiency is similar to each other and the decrease in engine-out emissions is the reason for the decreased tailpipe emission. In contrast, the engine-out NOx emissions for the OPA are more than that of the Corona but the tailpipe emissions are less than the Corona. This means that the catalyst plays a significant role in the reduction of tailpipe emissions in the case of NOx. As shown in Figure 5.9(c), the NOx purification efficiency of the catalyst of the OPA is far better than that of the Corona in every phase of the FTP cycle. Toyota increased the capacity of the NOx absorption reduction catalyst by 1.5 times compared to the previous version and used a lot more EGR to decrease the engine-out NOx emissions. From this result, it can be concluded that the improvement in after-treatment is more effective than the changes to the combustion process (EGR).

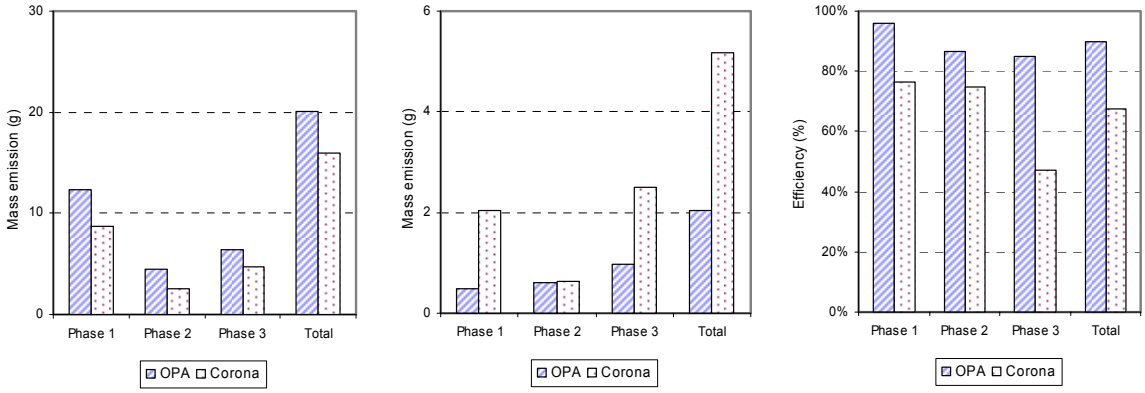

(a) Engine-out emissions (b) Tailpipe emissions (c) Catalyst efficiency

Figure 5.9 Source of NOx difference between the OPA and Corona

Figure 5.10 shows the NOx conversion efficiency of the catalyst during the FTP cycle. As the catalyst repeats absorption and regeneration during the transient operation, the second by second conversion efficiency does not give the insight for the actual

conversion efficiency. Therefore, the efficiency is calculated within the interval between the stoichiometric combustions as shown in the lower right graph of Figure 5.10.

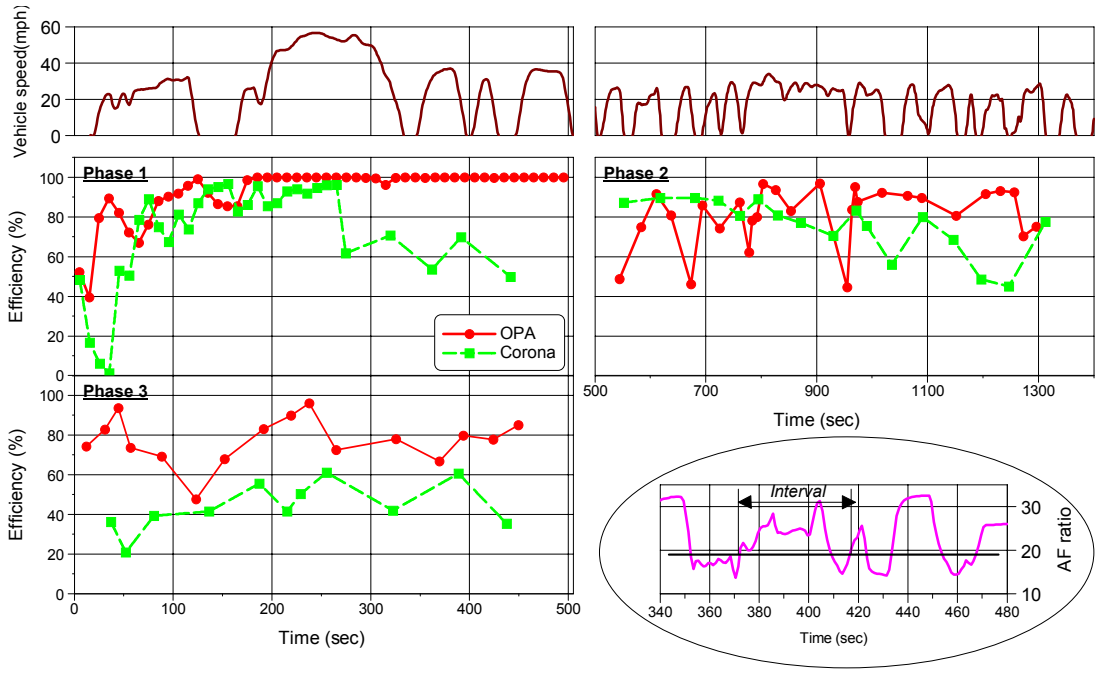

Figure 5.10 Comparison of NOx conversion efficiencies between the OPA and Corona during the FTP cycle. The interval during which the efficiency is calculated is also illustrated.

Except for the initial 250 seconds before the catalyst light-off, the catalyst of the OPA is more efficient than that of the Corona. For the latter part of Phase 1, the difference is caused by the combustion scheme. The efficiency of the OPA is almost 100% because it is working in stoichiometric mode whereas the Corona is in lean combustion mode. For Phases 2 and 3, where both vehicles are in the lean combustion mode, the efficiency of the OPA catalyst is better than that of the Corona. Especially for Phase 3, the difference in efficiency is larger than that for Phase 2. The engine load in Phase 3 is larger than that of Phase 2 because the average vehicle speed is higher. Therefore, the capacity of the Corona seems to be insufficient to purify the engine-out NOx. That is why the efficiencies of the OPA for Phases 1~3 are similar to each other but the efficiencies of the Corona for the 3 Phases are different from each other. For the

Corona, the efficiency during Phase 3 is worst and only 47.3% whereas that of the OPA is 84.8%. The overall efficiency of the OPA is 89.9% and that of the Corona is 67.5%.

5.3.2 CO emissions

For the analysis of the increased tailpipe CO emissions, the engine-out and tailpipe CO and catalyst efficiencies are shown in Figure 5.11. Both the engine-out and tailpipe CO of the OPA are more than that of Corona. The catalyst efficiency of the OPA is worse than those of the Corona. Every factor contributes to the increase in CO emissions. However, the CO emissions are still within the regulated level even in the strict U.S. standards.

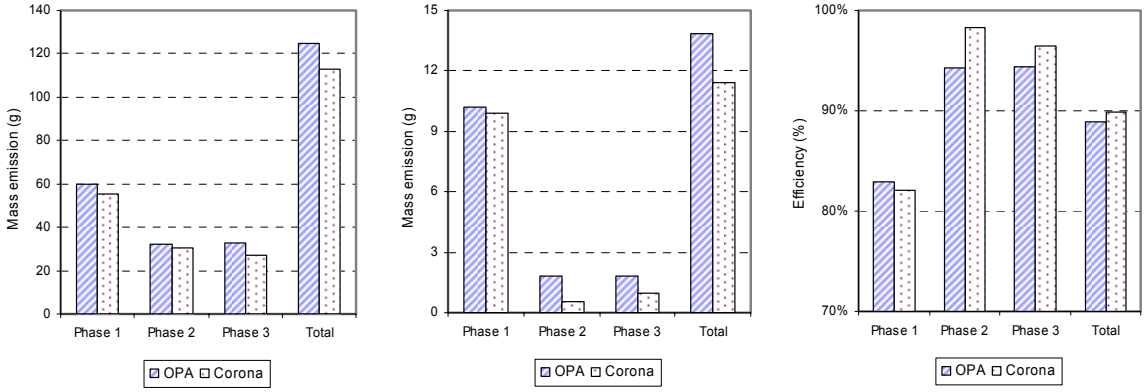

(a) Engine-out emissions (b) Tailpipe emissions (c) Catalyst efficiency

Figure 5.11 Source of CO difference between the OPA and Corona

5.3 CHAPTER SUMMARY

The OPA was driven on the chassis dynamometer following the FTP cycle. The operations of the OPA are compared with those of the Corona. The fuel economy and emissions were measured and compared with those of the Corona. The factors affecting the fuel economy and emissions were analyzed.

Both the OPA and Corona begin the FTP cycle with stoichiometric combustion and, after a while, lean combustion starts and lasts until the end of the FTP. For the OPA, the onset of lean combustion was 416~529 seconds after vehicle start-up. This onset timing is delayed compared with that of the Corona. The fuel economy of the OPA is 30.5 mpg, 10% less than that of the Corona. This is because the vehicle resistance of the OPA is larger than that of the Corona.

Toyota has made considerable improvements in tailpipe HC and NOx emissions with their second generation D-4. For the HC emissions, the change in combustion system using their slit nozzle injector seems to be effective. It was reported by Toyota that the fuel spray from the slit nozzle injector can be mixed well with air more evenly than the previous cone spray. In contrast, the dominant factor for the NOx reduction turns out to be the catalyst efficiency. Due to the increase in the capacity of the catalyst, the average catalyst efficiency for NOx is improved from 67.5% for the Corona to 89.9% for the OPA.

Even with these improvements, the barrier of the U.S. market seems to remain high for the DISI engine. The tailpipe NMOG and NOx do not meet the LEV standards in the NLEV program.

CHAPTER 6: STEADY STATE RESULTS

Chapter 6 describes the steady state test results. The purpose of these steady state tests was to examine the feasibility of an in-situ mapping technique and obtain the map data for the OPA's DISI engine and CVT. The in-situ mapping technique is a method of getting map data in the actual vehicle on the chassis dynamometer instead of via engine dynamometer testing. The key problem in this method is how to get the engine torque with the engine in the vehicle. The installation of torque sensors at the output shafts of the engine and CVT was developed and used. Part of this experiment was done with both torque sensors and the remaining part was done with only the axle torque sensor. In the latter case, the efficiency map of the CVT, which was obtained from the previous tests with both torque sensors, was used to estimate the engine torque.

The measured map plots of steady state results are presented in Appendix B. Some of the important issues are selected and addressed in the following sections.

6.1 STEADY STATE VEHICLE OPERATION

The emissions were measured at constant vehicle speed under road load conditions and the measured results are shown in Figure 6.1. The air/fuel ratio is controlled at around 30 at 20 mph and decreases as the vehicle speed increases. In this figure, two kinds of rich spikes are observed. The air/fuel ratio goes down to near stoichiometry when the vehicle is accelerated because the engine load goes beyond the lean combustion region. The other kind of spikes occurs regularly to regenerate the NOx catalyst.

Every species, both engine-out and tailpipe, change according to the change in load and air/fuel ratio. The behaviors of both HC and CO concentrations are directly linked to the air/fuel ratio. Their peaks coincide with the rich spikes. Similar trends can be seen in the NOx concentration. During lean combustion, the engine-out NOx remains constant but the tailpipe NOx concentration increases gradually. This indicates that the

catalyst efficiency decreases with time as the NOx is absorbed in the catalyst until the next regeneration occurs to purge the absorbed NOx and increases the efficiency again.

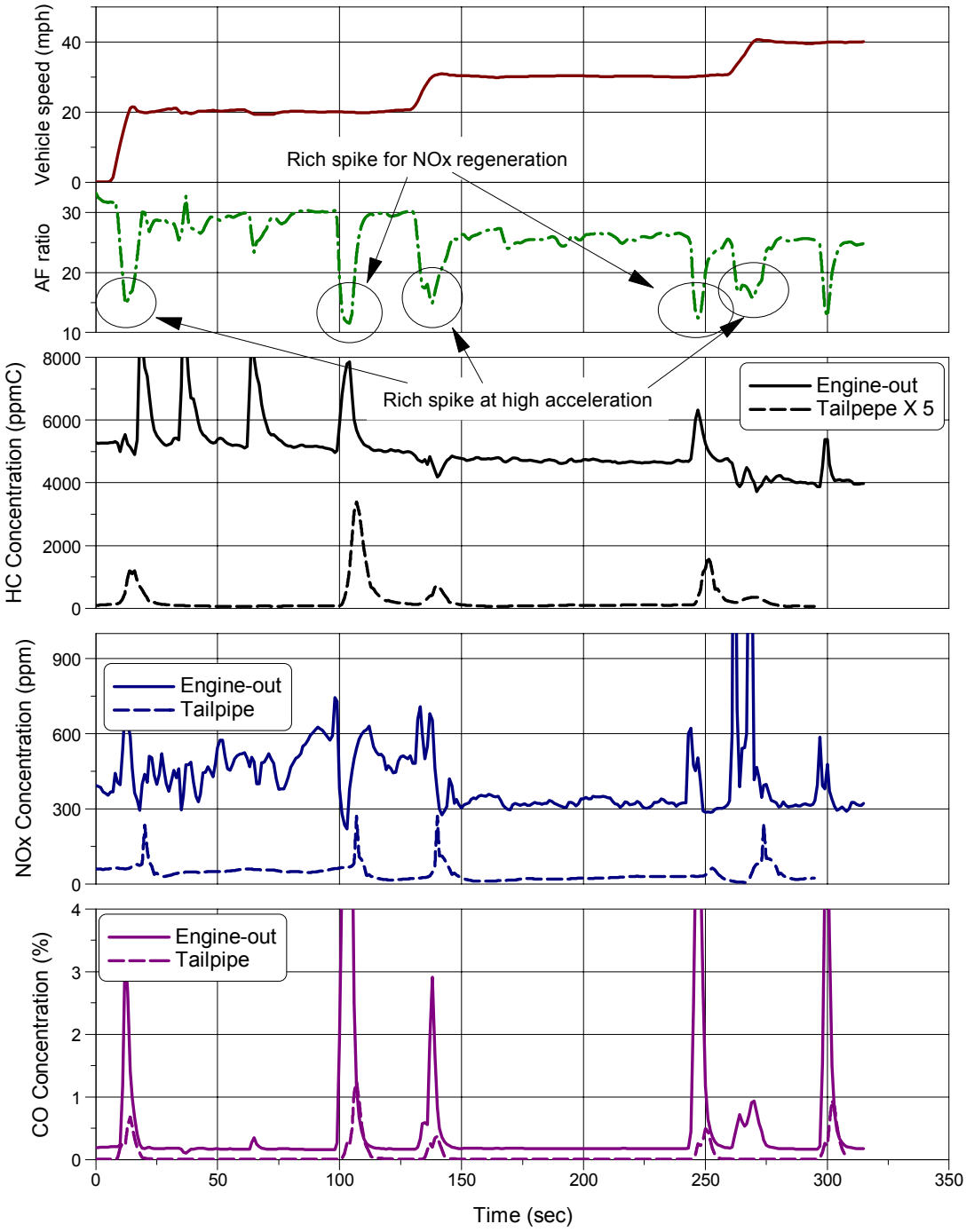

Figure 6.1 Emissions during steady state engine operation

6.2 CVT EFFICIENCY

The fuel consumption and emissions of the engine and the efficiency of the CVT were obtained using the in-situ mapping technique. The torque sensors between the engine and the CVT and those between the CVT and wheels enable the measurement of the CVT efficiency. The efficiency of the CVT is defined as the ratio of the output power to the input power as shown in the following equation. Table 6.1 shows the physical quantities in this equation.

$$\eta_{CVT} = \frac{Axle\ power}{Engine\ power} = \frac{\tau_{axle} \times \omega_{axle}}{\tau_{engine} \times \omega_{engine}} \tag{6.1}$$

Table 6.1 Measured physical quantities used to calculate the CVT efficiency

Power	Formulae	Physical quantity	Measurement
Engine power	$\tau_{engine} \times \omega_{engine}$	Torque	Engine torque sensor (HBM T10F)
		Speed	CPS(Crank Position Sensor) signal
Axle power	$\tau_{axle} \times \varpi_{axle}$	Torque	Two torque sensors, one on each axle shaft
		Speed	CVT output speed signal

For the measurement of fuel consumption and emissions, the engine torque sensor was used while the chassis dynamometer absorbs the power of the engine as if the engine is mounted on the engine dynamometer. A part of this experiment was done with both torque sensors and the other part was done without the engine torque sensor because the engine torque sensor got out of order. For the latter part of this experiment, the efficiency of the CVT was used to estimate the engine torque from the axle torques.

Figure 6.2 shows the measured efficiency of the CVT. The losses in the CVT are composed of oil pump power, belt drag and frictional losses in the gears and bearings [22]. In Figure 6.1, it is seen that the input engine torque, expressed as BMEP, is the dominant factor and engine speed and gear ratio also affect the efficiency of the CVT. As the input torque increases, the efficiency increases and as the engine speed increases,

the efficiency decreases. At the same engine speed and torque, the efficiency at middle ratio with the similar radius of belt pulley is better than that of high or low ratio.

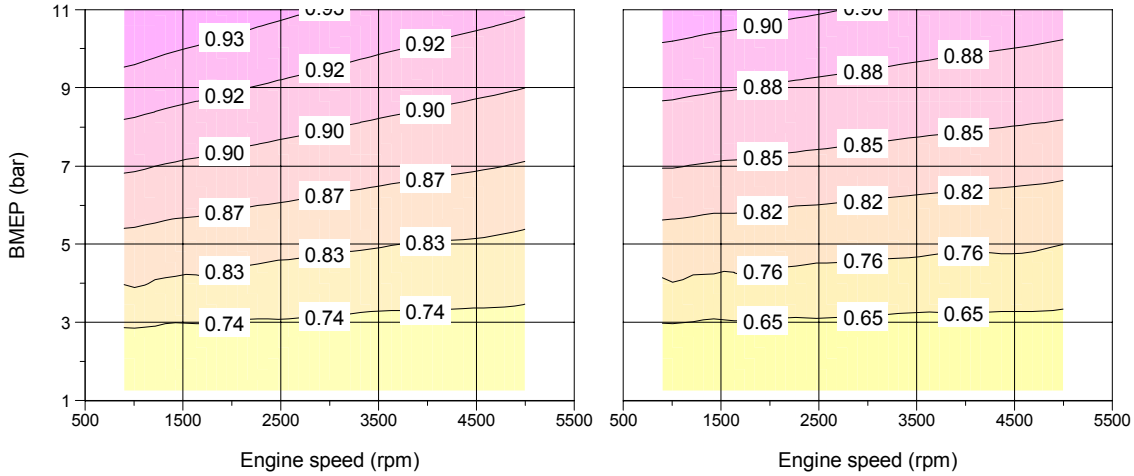

(a) At middle ratio ($\frac{\omega_{in}}{\omega_{out}} \approx 1$) (b) At high or low ratio

Figure 6.2 Efficiencies of the CVT

Direct measurement of the engine torque is the best way for the engine map test but an indirect method was used due to the problems with the engine torque sensor. To check the validity of this approach, the errors of engine torque were estimated from the measured torque, as shown in Figure 6.3. The actual torques directly measured from the engine torque sensor are compared with those estimated from the axle shaft torque and rotational speed on both sides of the CVT using the efficiency map in Figure 6.3. The frequency of the error at each range is counted and shown in this figure for the 43 measurement points. The maximum error is 1.6 N-m and more than 90% of the measurements are within 1 N-m.

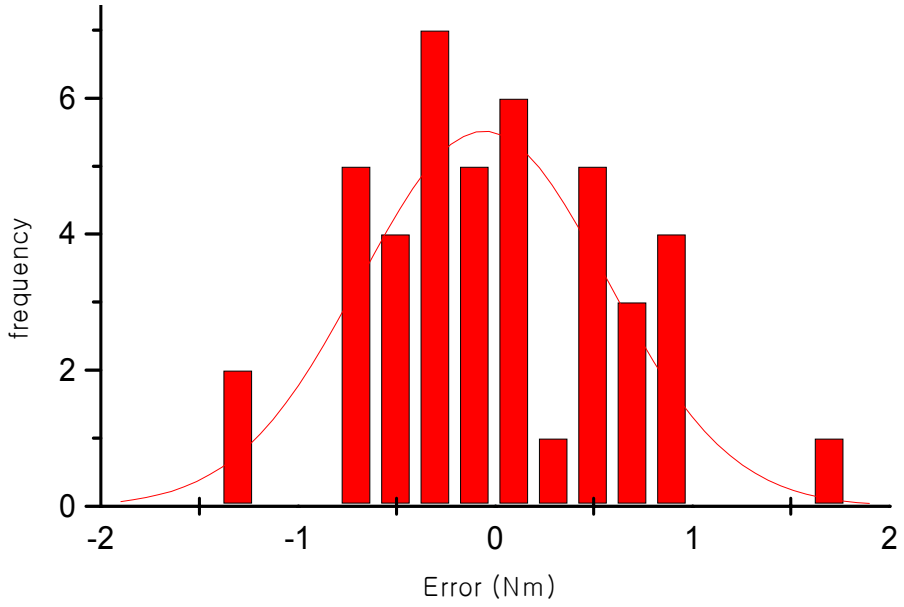

Figure 6.3 Estimated error in engine torque calculation

The CVT efficiency map was used to estimate the engine torque for both engine map testing and simulation. From the results in Figure 6.3, it appears that this method for engine torque estimation is reliable even though it is not measured directly.

6.3 AIR/FUEL RATIO DISTRIBUTION

As the in-situ mapping test was done in an actual vehicle, the operation is different from testing on an engine dynamometer. It was not possible to locate the operating point on the exact point of pre-selected engine speed and torque. The operating point was controlled as close to the target as possible by manipulating the throttle pedal and the load of the chassis dynamometer.

Experiments were done in both the lean and stoichiometric combustion mode. The operating points are shown in Figure 6.4 for normal operating conditions. The markers indicated as stoichiometric mean that the operating points go beyond the lean combustion range.

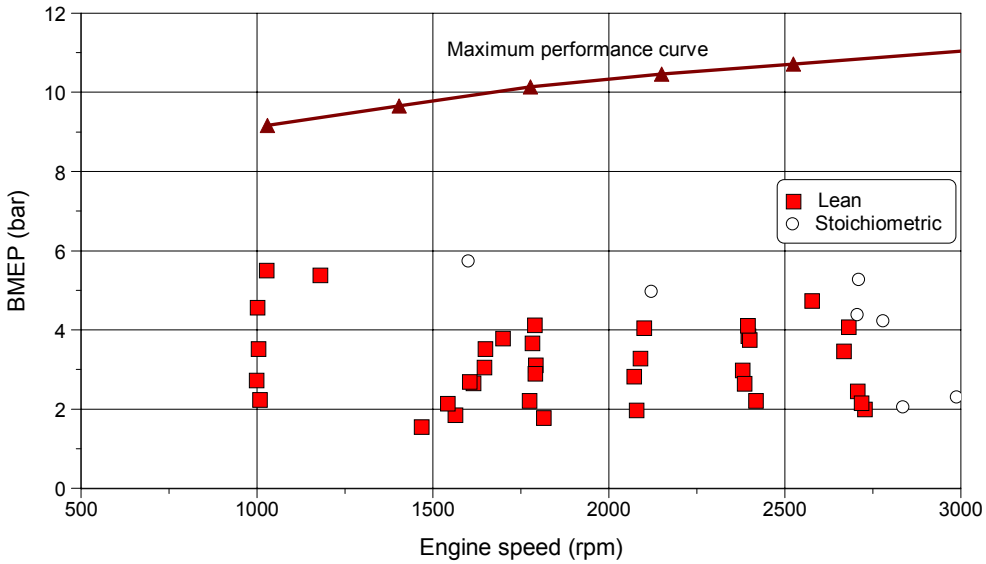

Figure 6.4 Operating points used in steady state tests

Based on the measured air/fuel ratio and operating engine speed and torque, the revealed lean operating region is as shown in Table 6.2.

Table 6.2 Lean combustion region of the 2nd generation Toyota D-4 engine

Engine speed	Load in BMEP
1000 ~ 1500 rpm	≤ 6 bar
1500 ~ 2550 rpm	≤ 5 bar
2550 ~ 2750 rpm	≤ 4 bar

The maximum load for lean combustion with the engine speed less than 1500 rpm is regarded as 6 bar BMEP. As the engine speed increases, the maximum load decreases a little to 5 and 4 bar BMEP.

The lean combustion region is plotted in Figure 6.5 with the engine operating points during the Hot 505 cycle. In this figure, most of the engine operating points are within the lean combustion region. With the help of the CVT, the engine operation is controlled at low engine speed and high load. It seems that Toyota tried to increase the lean combustion region toward the load direction instead of toward increased engine speed.

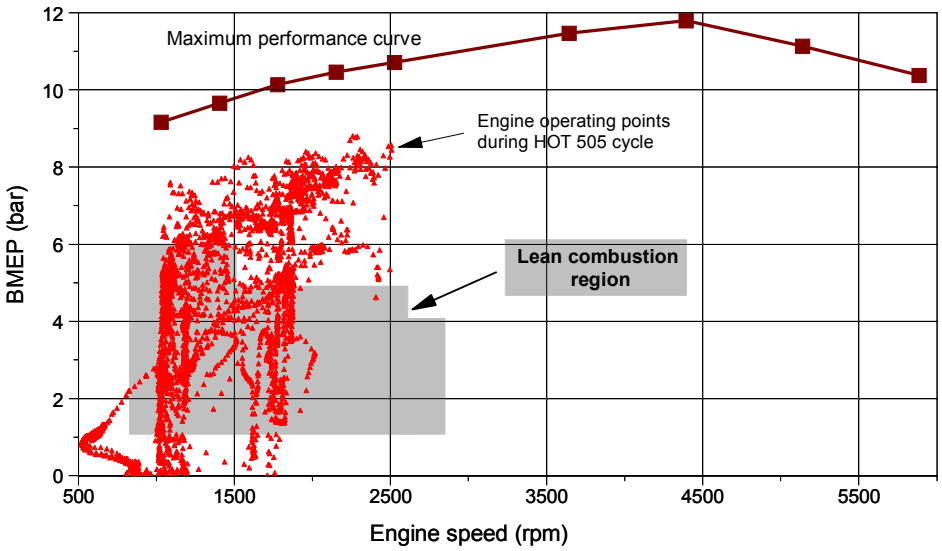

Figure 6.5 Measured lean combustion region

The air/fuel ratio distribution is shown in Figure 6.6. At low engine speed and low load, the air/fuel ratio is controlled high and decreases as the engine speed and load increase. In the manual for the OPA published by Toyota, it is stated that the maximum air/fuel ratio is 50. However, in these experiments, the measured maximum air/fuel ratio was 30 as shown as a marker in Figure 6.6.

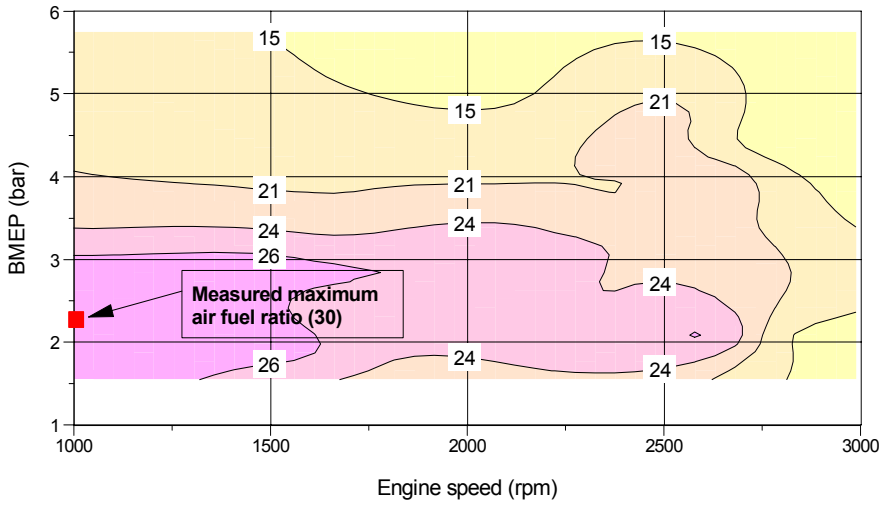

Figure 6.6 Air/fuel ratio distribution

6.4 FUEL CONSUMPTION

The measured brake specific fuel consumption maps, in g/kW-hr, for both the lean and stoichiometric combustion modes are shown in Figure 6.7. The fuel consumption rate used to calculate the BSFC in this figure is the average fuel consumption rate for at least 2 minutes. Therefore, the fuel consumption includes the effect of fuel enrichment for NOx regeneration. As the load increases, the specific fuel consumption decreases monotonically in the stoichiometric combustion mode. In contrast, the specific fuel consumption for the lean combustion mode decreases rapidly at low load and then the rate of decrease becomes small.

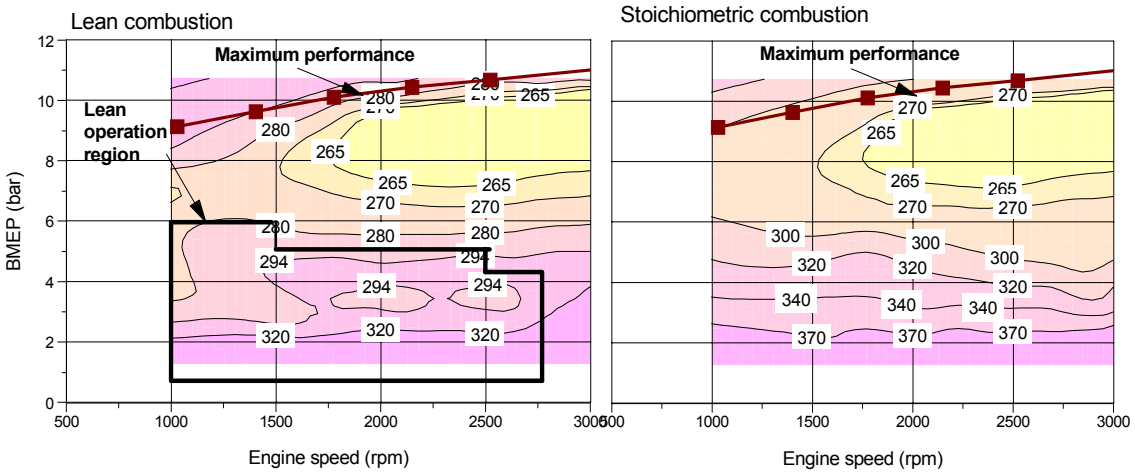

(a) Map

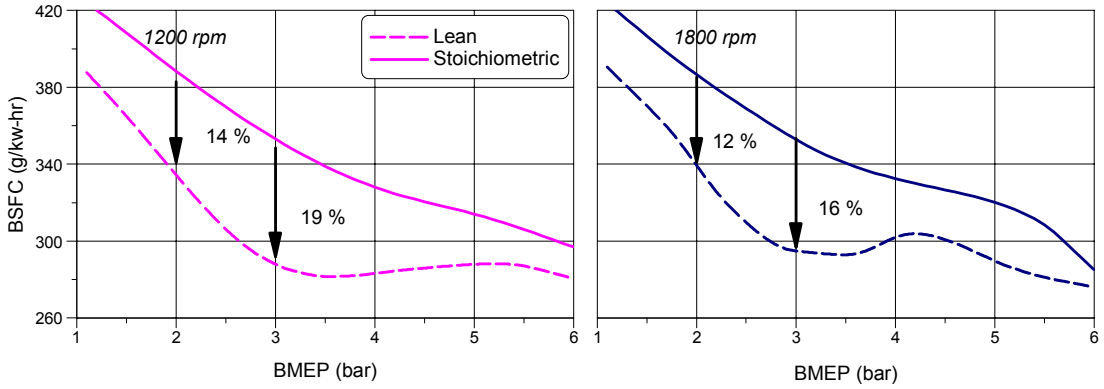

(b) Plots at 1200 rpm and 1800 rpm

Figure 6.7 Brake specific fuel consumption of the 2nd generation D4 engine

Figure 6.8 shows the relative SFC decrease in lean combustion mode compared to the SFC in stoichiometric combustion mode. Within the lean operation region, the improvement in fuel consumption is best at low engine speed and 3 bar BMEP. From this figure, the fuel consumption improvement at low speed and 2~4 bar is about 20%.

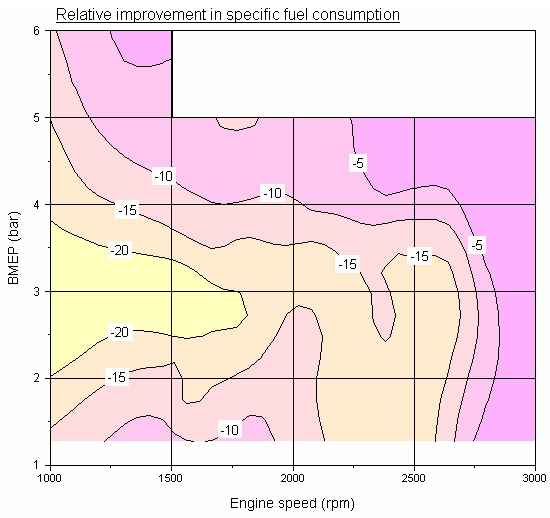

Figure 6.8 Relative improvement in SFC ($=100\times\frac{sfc_{lean}-sfc_{stoichiometric}}{sfc_{stoichiometric}}$)

6.5 EMISSIONS

The emission rates are expressed in terms of BSHC(Brake Specific HC) and BSNOx(Brake specific NOx). The definitions are as followings.

$$BSHC\left(\frac{g}{kW\cdot hr}\right)=\frac{\dot{m}_{HC}}{bp}$$

$$BSNOx\left(\frac{g}{kW\cdot hr}\right)=\frac{\dot{m}_{NOx}}{bp}$$

$$\begin{aligned}&Where\ \dot{m}_{HC}: mass\ flowrate\ of\ HC\ (g/hr)\\ &\qquad \dot{m}_{NOx}: mass\ flowrate\ of\ NOx\ (g/hr)\\ &\qquad bp: brake\ power\ (kW)\end{aligned} \tag{6.2}$$

The change in BSHC and BSNOx according to the load at 1200 and 1800 rpm are shown in Figure 6.9. BSHC in lean combustion is 2~3 times of that in the stoichiometric combustion mode. On the other hand, the lean BSNOx is about one-half to one sixth compared to that in the stoichiometric combustion mode.

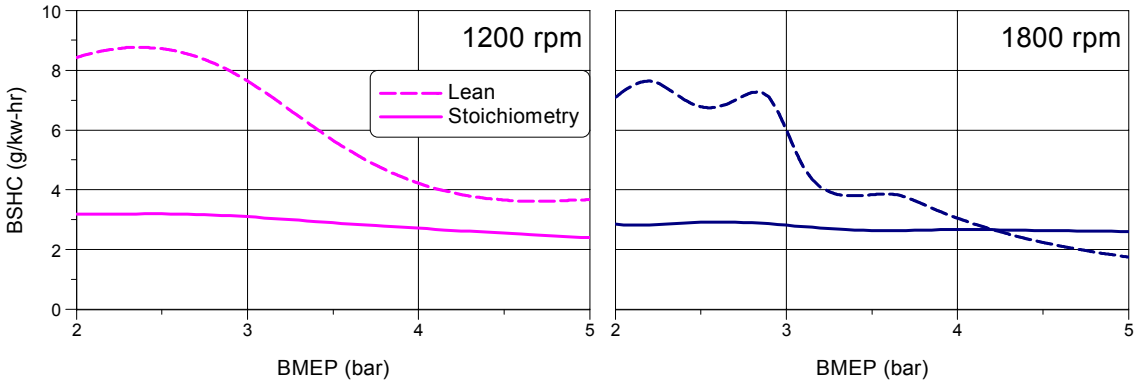

(a) BSHC (g/kW-hr)

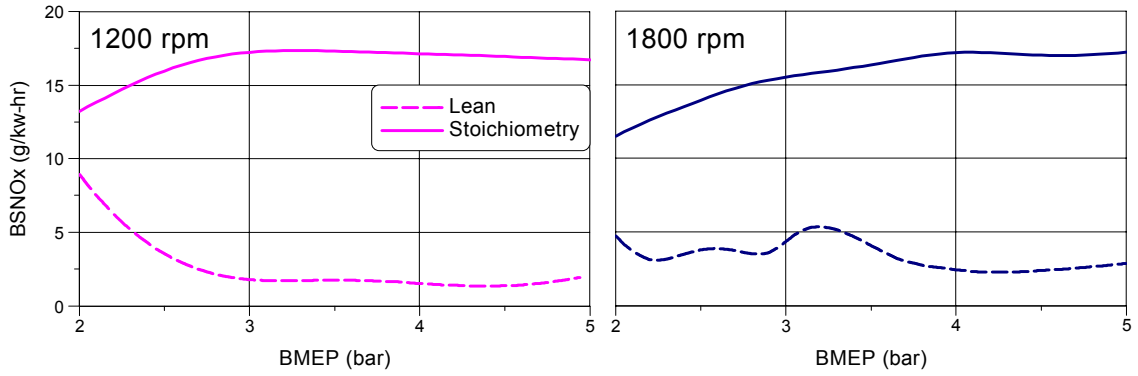

(a) BSNOx (g/kW-hr)
Figure 6.9 Steady state emissions

The FTP test results for the 1st generation D-4 of Toyota were reported by Chad and coworkers [36] and those for the Mitsubish Legnum with a 1.8L GDI engine were reported by Cole and coworkers [8]. They compared the engine-out and tailpipe emissions with those of comparable PFI(Port Fuel Injection) engine. According to the results of Chad and coworkers [36], the difficulties for the HC emissions are the engine-out HC emissions for all modes of operation during the FTP cycle. Those for the NOx emissions stem from the low efficiency of the lean NOx catalyst in the DISI vehicle. The

rich and lean ends of the gradient in the DISI engine working under stratified charge mode give rise to unburned HC. Another source is wall wetting on the piston and cylinder liner. These are the cause of increased HC in DISI engine.

The NOx emissions decrease as the load increases in the lean mode whereas that in the stoichiometry mode increases. This is because the usage of EGR is different for lean stoichiometric operation. The stock ECU does not control the EGR valve during stoichiometric operation. In contrast, during the lean combustion mode, the EGR rate increases as the load increases as shown in Figure 6.10. Due to the restriction in facilities at UT, the actual EGR ratio could not be measured and the EGR step number shown on the scan tool was recorded and shown in Figure 6.10.

To compare the difference in emissions for the lean and stoichiometric combustion modes, the emissions during the last 160 seconds in Phase 1 and 3 are shown Figure 6.10. As the engine is warmed-up during this period, the only difference is the air/fuel control scheme as shown in Figure 6.10(b). As expected from the measured steady state emissions results, the engine-out HC in the lean mode is more than that in the stoichiometric mode and the engine-out NOx in the lean mode is far less than that in the stoichiometric mode.

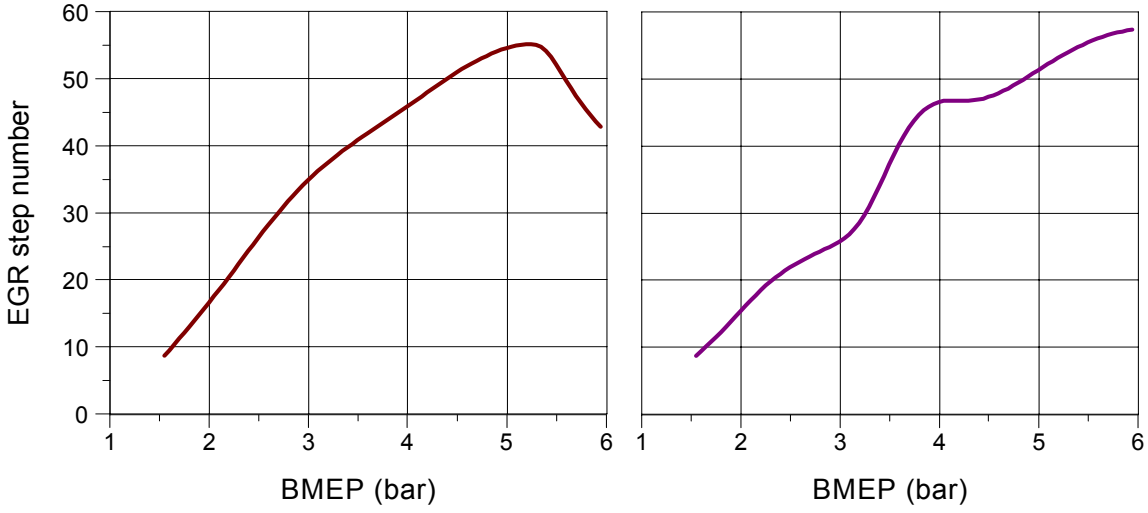

(a) 1200 rpm (b) 1800 rpm

Figure 6.10 Change in EGR step according to load

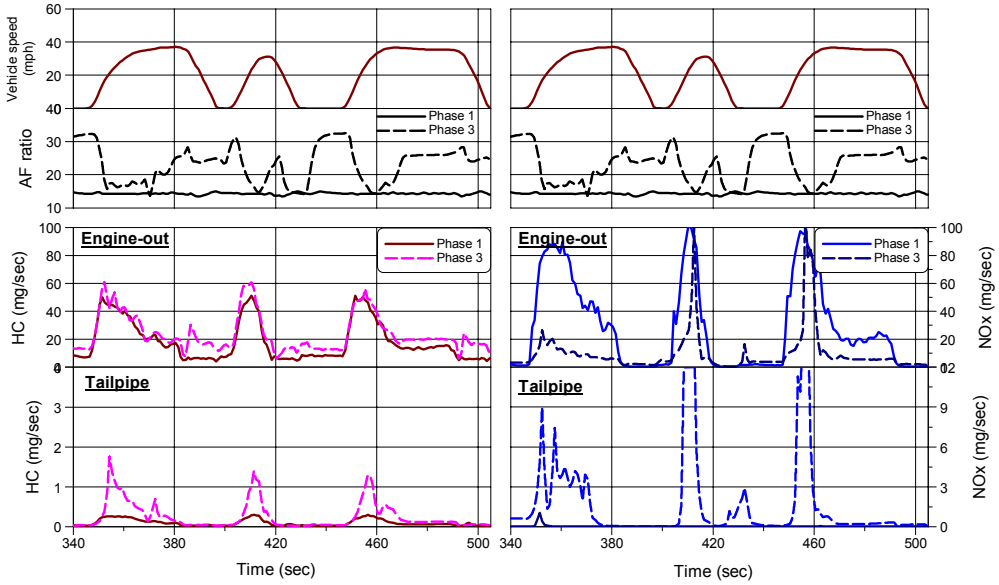

Figure 6.11 Effect of combustion mode on the emissions during the last 140 seconds of FTP Phase 1 and 3

6.6 IGNITION AND INJECTION TIMING

The strategies for ignition timing calibration are either MBT or retardation for emissions reduction. Figure 6.12 shows the mapped ignition timing for the lean and stoichiometric modes. Both ignition timings at 1200 rpm are similar to each other but those in the lean burn mode are retarded by 5 ° compared to those in stoichiometric combustion mode. This indicates that the burning speed in the lean stratified charge mode is faster than that in homogeneous stoichiometric mode. Makato and coworkers [18] who presented a paper regarding this D-4 engine claimed that the stratified combustion has a short ignition delay and a large heat release at the beginning. It seems that the mapped ignition timing in the lean combustion mode is close to the TDC as a result of faster burning speed.

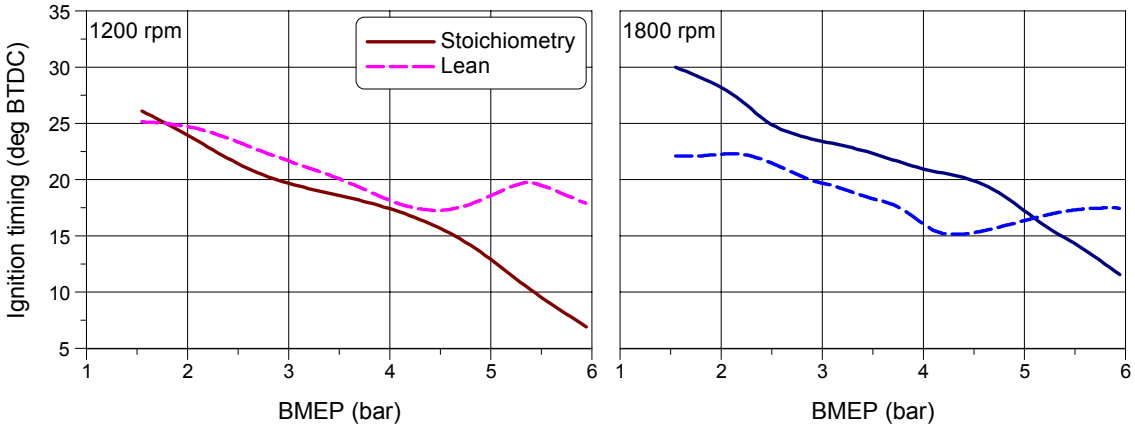

Figure 6.12 Comparison of ignition timing

The injection timing shown in Figure 6.13 is mostly dependent on the engine speed. As the engine speed increases, the duration for mixture preparation in terms of crank angle increases. The advance in injection timing with load is also observed.

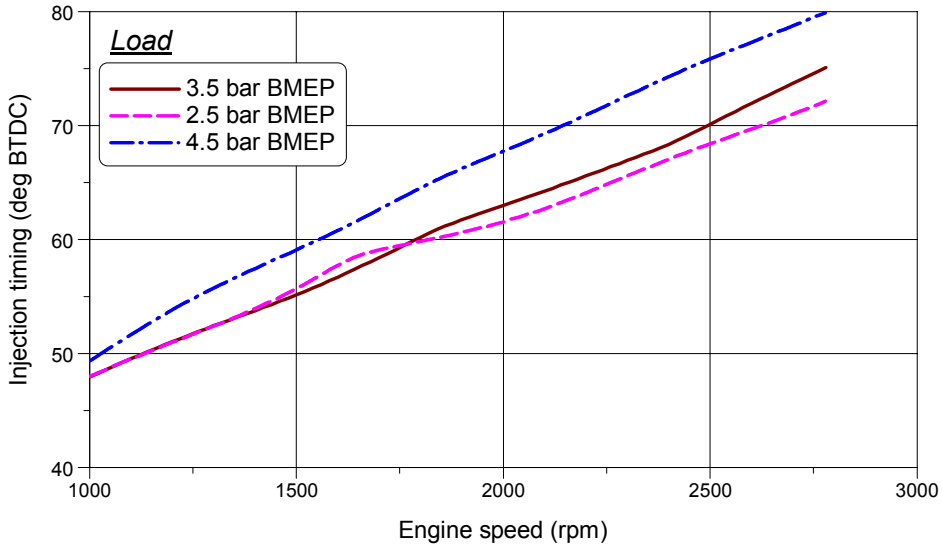

Figure 6.13 Injection timing

6.7 CATALYST EFFICIENCY

As the facility at UT does not allow measurement of catalyst efficiency, the efficiency of the catalysts, 3 way and DeNOx, in the OPA were obtained from the FTP test results. The typical behaviors of catalysts are shown in Figure 6.14 for both stoichiometric and lean combustion modes. As shown in this figure, the efficiency fluctuation is severe due to the variation in engine operation and response in the emissions measuring system, especially in the lean combustion mode with the rich spikes for NOx regeneration.

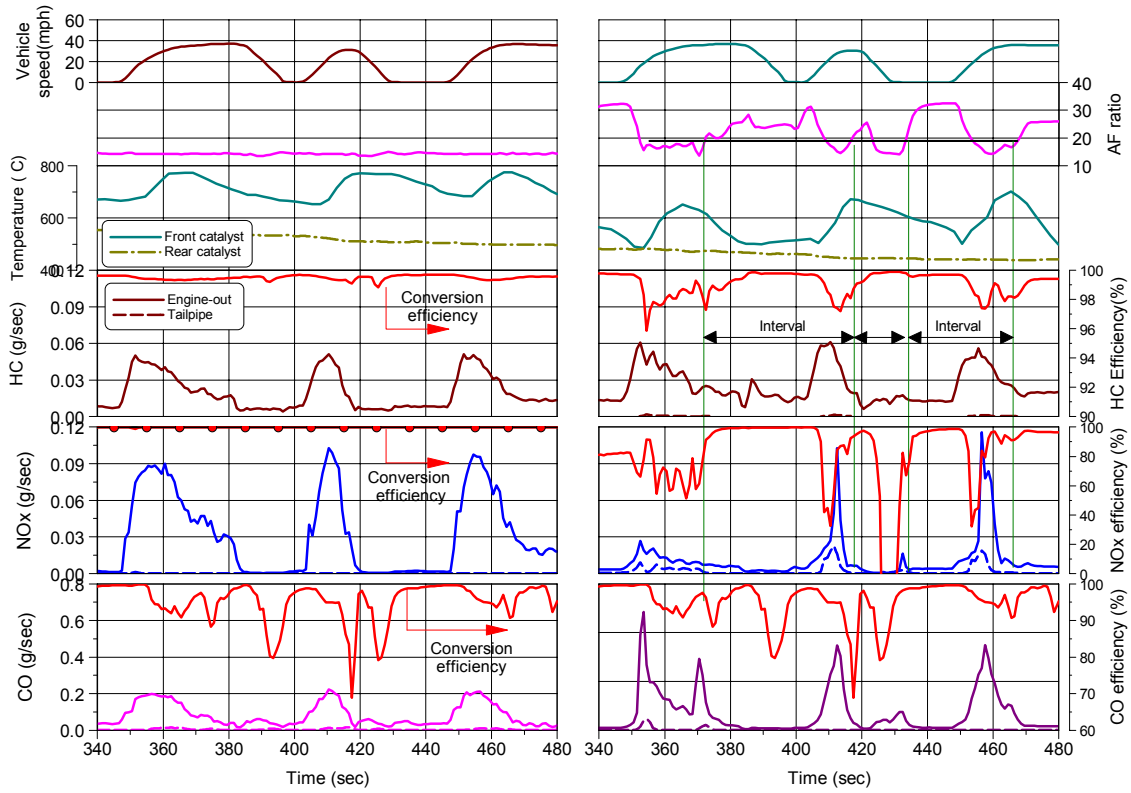

(a) Stoichiometric combustion (b) Lean combustion

Figure 6.14 Behavior of the catalysts

The catalyst efficiency is usually assumed to be a function of temperature. In this research, the catalyst efficiency was calculated during the finite time intervals as shown in Figure 6.14. The catalyst efficiencies are shown in Figure 6.15. In stoichiometric combustion, the efficiency was calculated based on the average engine-out and tailpipe emissions for 10 seconds. In the emission behavior during lean operation, all species of the emissions increase during the intermittent stoichiometric operation and the efficiencies decrease correspondingly. In lean operation where the rich spikes exist, the emissions were averaged over the interval between the rich spikes.

Except for the NOx conversion efficiency, HC and CO conversion efficiencies do not change according to the combustion mode. In contrast, NOx conversion efficiency during lean combustion is far less than that during the stoichiometric combustion mode. Above 350 °C, the efficiency for HC is mostly more than 95% and that for CO is distributed from 80~100% regardless of combustion modes.

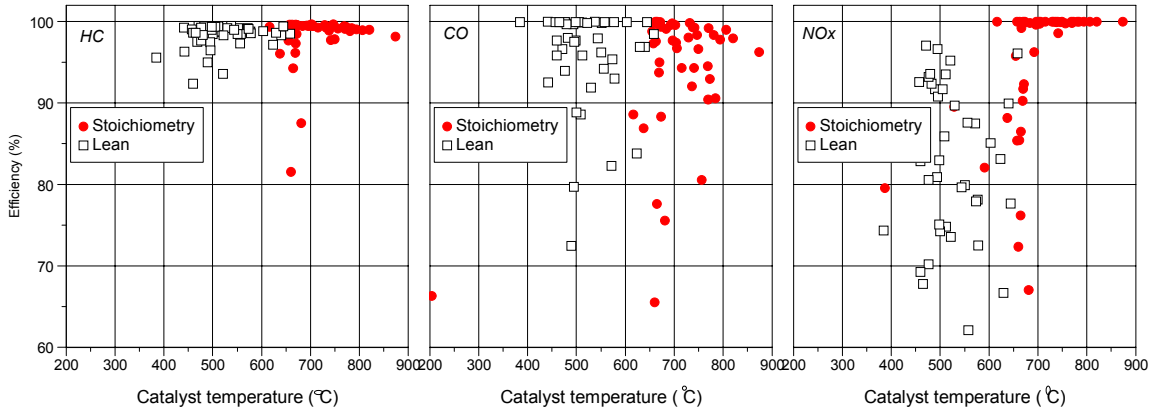

(a) HC (b) CO (c) NOx

Figure 6.15 Catalyst conversion efficiencies for stoichiometry and lean combustion modes

6.8 CHAPTER SUMMARY

The in-situ mapping technique turns out to be feasible to measure the map data for the engine and transmission in case that the dynamometer test for the engine and transmission itself is hard to perform. In this research, the steady state characteristics of DISI engine and CVT in Toyota's OPA was collected using the in-situ mapping technique.

The operating range of the lean combustion control was revealed. The maximum load for the lean combustion decreases as the engine speed increases and that for less than 1500 rpm was 6 bar BMEP. The maximum engine speed for lean combustion was found to be 2750 rpm. The mapped air/fuel ratio decreases as the engine speed and load increases. The measured maximum air/fuel ratio was 30 at 1000 rpm and 2.3 bar BMEP.

The improvement in steady state fuel consumption is about 20% at low speed and around 3 bar BMEP. This improvement decreases at lower and higher load and higher engine speed. The engine-out HC emissions in terms of BSHC for the lean combustion are 2~3 times of that in the stoichiometric combustion mode. The engine-out NOx emissions are about one-half to one-sixth compared to that in the stoichiometric combustion mode. It was confirmed again that the higher level of HC emissions in lean combustion mode come from the engine-out emission and that of NOx emission stem from the less efficiency of catalyst.

CHAPTER 7: OVERALL EFFICIENCY MEASUREMENTS

In order to determine the factors that affect fuel economy quantitatively, the power flows through the major powertrain components were measured during operation over transient cycles. The fuel consumption rate and torque and speed of the engine output and axle shafts were measured to assess the power flows in a vehicle with a CVT. The measured power flows were converted to the energy loss for each component to obtain the efficiency. Tests were done for Phase 1 and Phase 3 of the FTP and for two different CVT shift modes. The measured energy distributions were compared with those from the ADVISOR simulation and to results from the PNGV study.

The baseline combustion mode was the stoichiometric mode. As most of this experiment was done when the lean mode engine control was unstable, there was not enough data for the normal operation of the D-4 engine. Therefore, the data were obtained by manipulating the engine combustion mode to stoichiometric mode. The normal combustion mode data was added later and compared with the stoichiometric mode data.

The measured torque and speed are used to locate the operating point on the efficiency map as well as to calculate the energy flows and losses. The measured powers and calculated energy flows are plotted and related issues are discussed in the following sections.

7.1 MEASURED TORQUE AND POWER

The engine torque and axle torque measured using the installed torque sensors are shown in Figure 7.1 and Figure 7.2. Figure 7.1 shows the operating points during the Hot 505 cycle, based on the measured speeds and torques, superimposed on the engine's efficiency map.

In Figure 7.1, the engine efficiency map was obtained from the steady state experiments with the same measurement system as explained in the previous chapter. Fuel consumption rates at steady state were measured by changing gear ratio and vehicle

speed so that fuel consumption data would be obtained at several engine operating points. From Figure 7.1, it can be seen that the CVT allows the engine to operate close to the best efficiency line during much of the cycle. As noted previously, the test vehicle is equipped with a CVT, for which a continuously variable gear ratio is available.

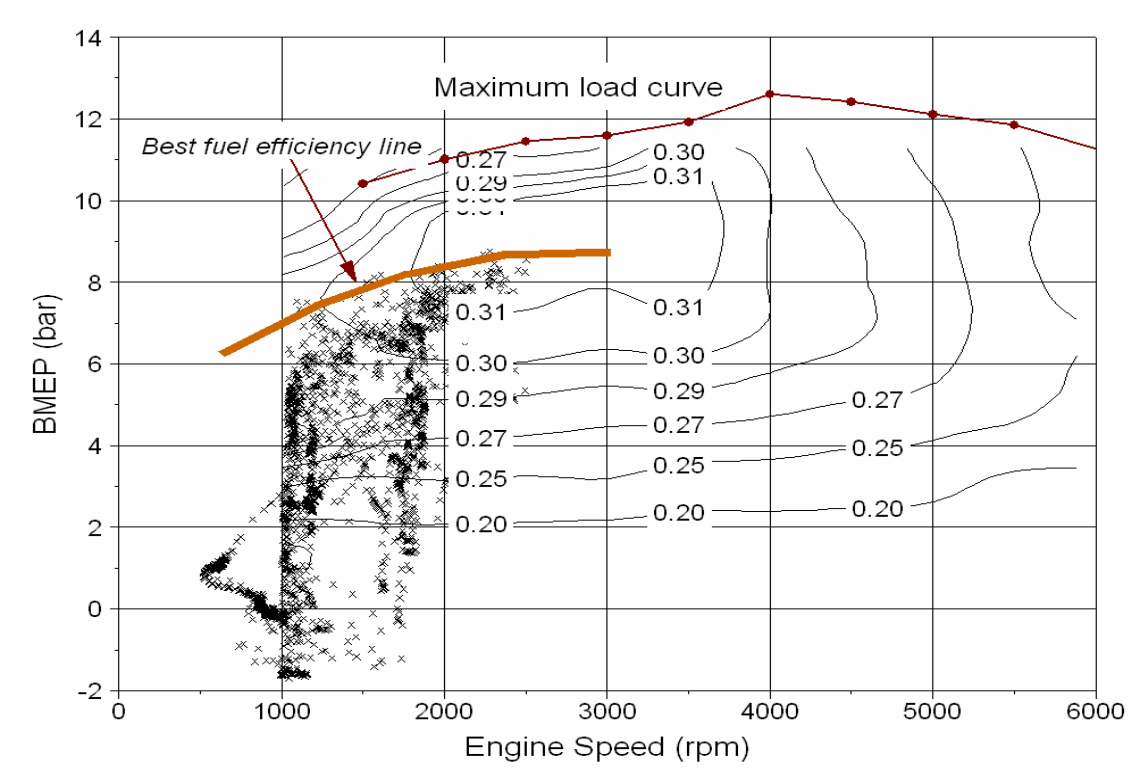

Figure 7.1 Engine operating points during the Hot 505 cycle.

Figure 7.2 shows the engine and axle torque changes as the vehicle accelerates and decelerates. The two measured axle torques are not exactly in accord with each other. It is seen that the engine torque is around 18 N·m and axle torques are around 100 N·m during idling. While decelerating, the engine torque becomes negative due to the transmitted power from the vehicle's inertia.

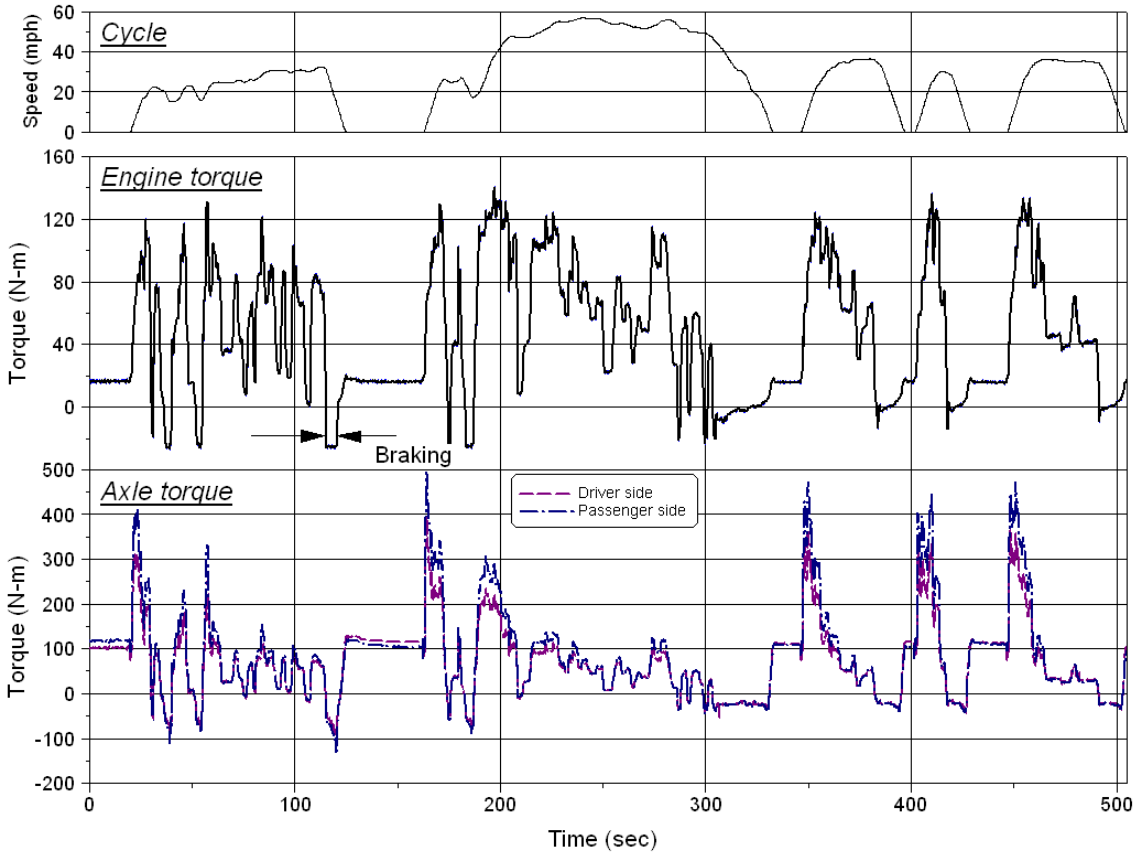

Figure 7.2 Measured engine and axle torques during the Hot 505 cycle

The power flows from the fuel through the powertrain to the vehicle can be calculated from the measured fuel rate, torques and speeds. Figure 7.3(a) shows the measured fuel energy addition rate ("fuel power"), engine power and axle power. The cumulative energies are shown in Figure 7.3(b).

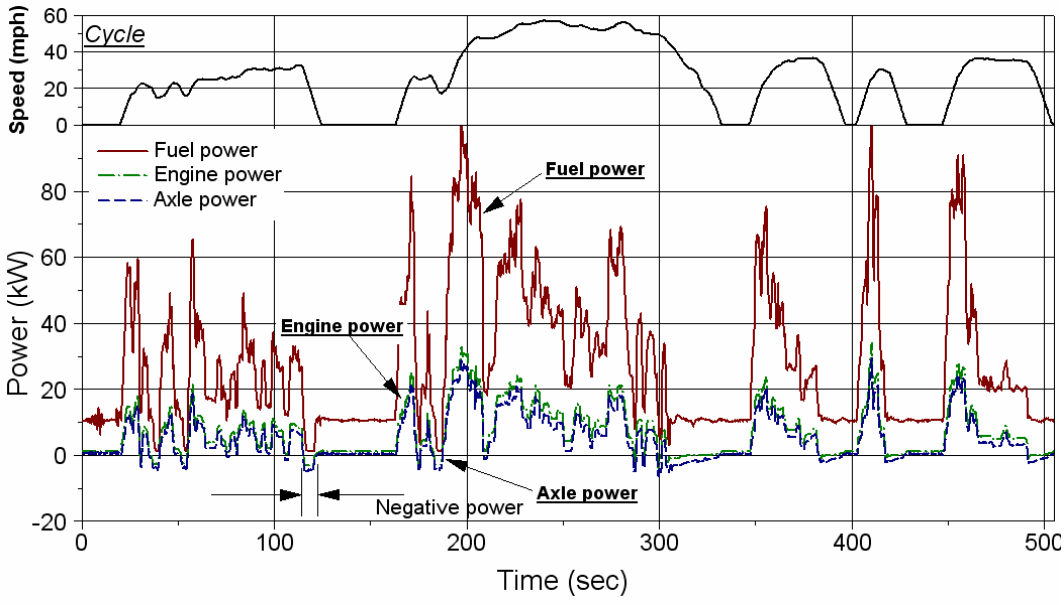

(a) Power flows

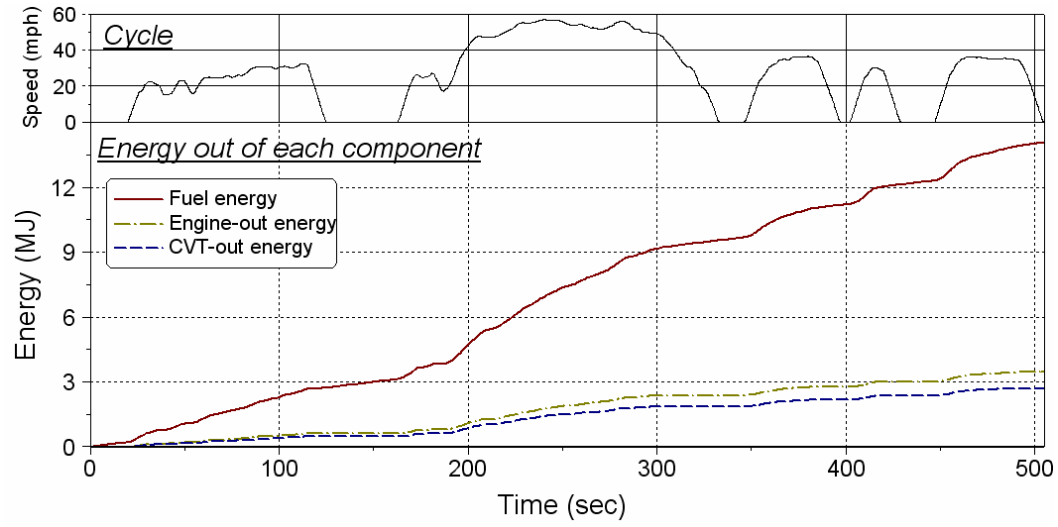

(b) Cumulative energy of each component

Figure 7.3 Measured power and energy during the Hot 505 cycle.

Figure 7.4 shows the instantaneous efficiency of the engine and drivetrain during the engine power mode. As shown via the engine operating points on the efficiency map in Figure 7.2, the efficiency of the engine varies between 0 (during deceleration) to 34% over the Hot 505 cycle. However, as shown in Figure 7.4, during engine power mode

operation, the engine efficiency varies from 20~34% and the average engine efficiency is 29.3%.

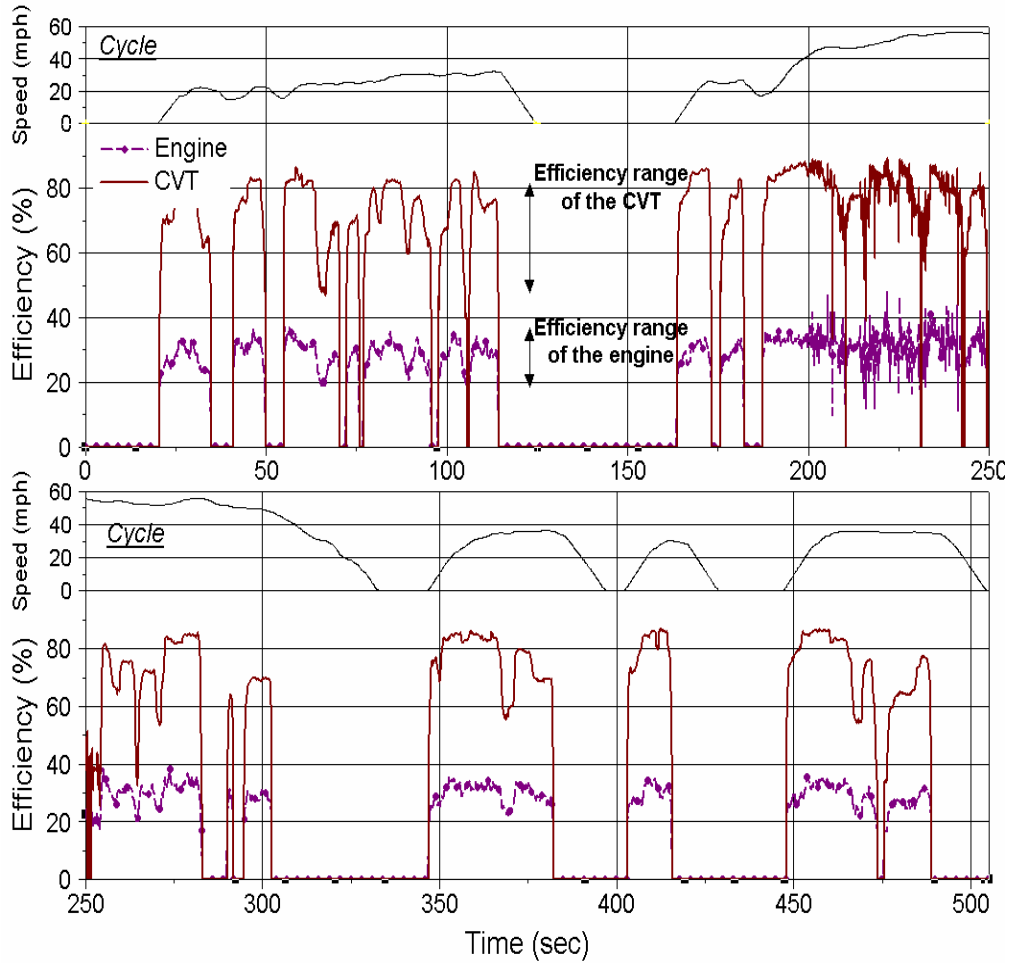

Figure 7.4 Measured efficiencies of the engine and CVT during the Hot 505 cycle.

The efficiency of the CVT is low during the early stages of acceleration, when the clutch is not yet locked up. It is seen in Figure 7.5 that the efficiency of the CVT does not exceed 80% with the unlocked clutch, but once the clutch is locked-up the efficiency goes beyond 80%. The measured CVT efficiency is in the range of 50~90% with an average of 78.4% during power mode operation.

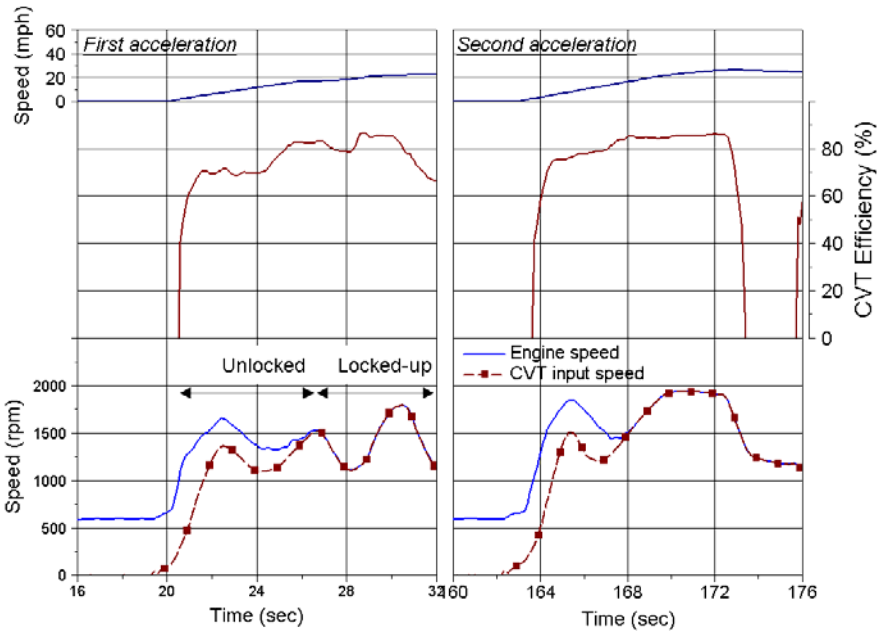

Figure 7.5 Change of the CVT efficiency according to the clutch state.

7.2 ENERGY LOSS DISTRIBUTION

The energy losses for each major component were calculated for the two operating modes, engine power and standby, and are shown in Figure 7.6. In the Hot 505 cycle experiments, 12% of the fuel energy was consumed for idling and braking for this test vehicle.

In Figure 7.6 it can be seen that the most energy was consumed by the engine. The CVT loss was only 5.6% of total fuel consumption. The energy conversion efficiency from fuel to engine-out mechanical energy is quite low compared to that of mechanical power transmission via the CVT. Nevertheless, the efficiency of the transmission is significant because a relatively small loss in the transmission can cause a relatively larger energy loss in the engine due to the limited efficiency of the engine.

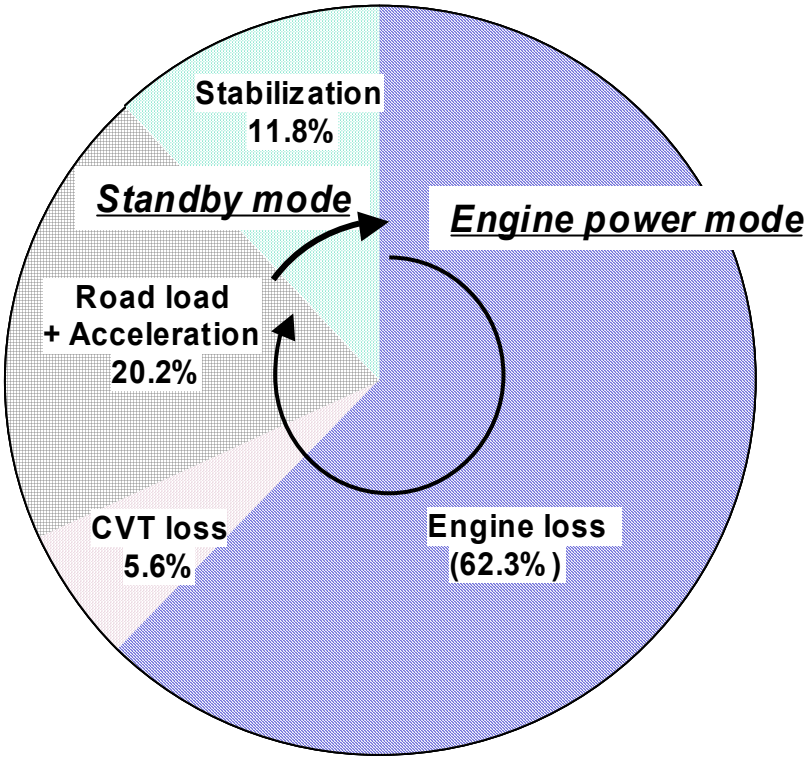

Figure 7.6 Energy loss distributions.

7.3 EFFECT OF ADDITIONAL PARAMETERS

In addition to the results shown above, more experiments were performed to examine the effect of cold vs. warm start and of the shift mode and of the combustion mode, as discussed below.

7.3.1 Effect of warm-up

In addition to the Hot 505 cycle, the Cold start 505 cycle (Phase 1 of the FTP) was performed to quantify the effect of the powertrain warm-up on the energy distribution. Based on the measured energy flow through each powertrain component, the energy losses and efficiencies were calculated, as shown in Figure 7.7.

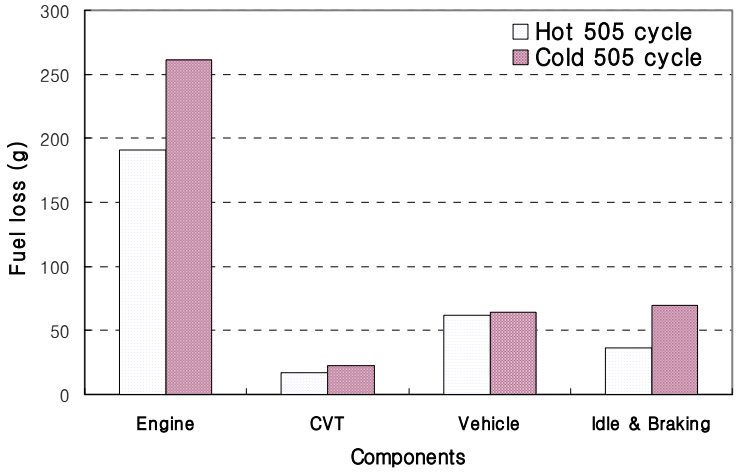

(a) Energy losses in terms of fuel consumption

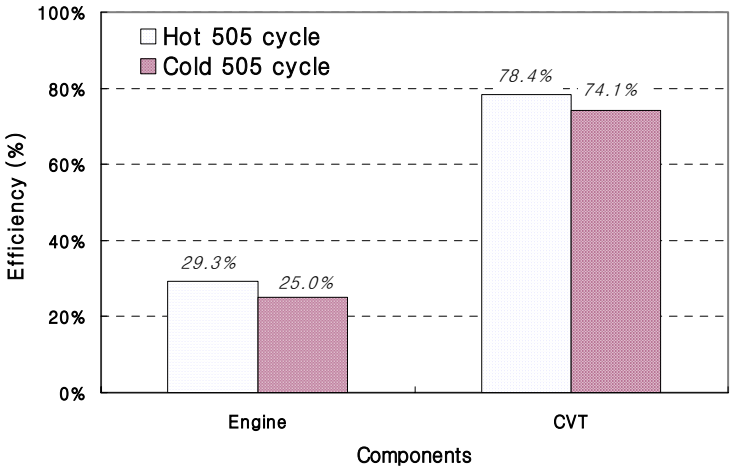

(b) Efficiencies of engine and CVT

Figure 7.7 Comparison of the energy loss and efficiency according to the warm-up

For cold starts, more fuel must be supplied to overcome the increased friction of the engine and CVT and to compensate for incomplete vaporization of the fuel. Moreover, the increased idle speed consumes more fuel. Thus, it is shown in Figure 7.7 that the energy losses for the cold start test are larger than those for the hot start test, especially in the engine. The change in the average efficiency of the engine and CVT

was 4.3 percentage points for both, even though the effect on the engine was expected to be larger than for the CVT.

Even though the average (over the cycle) efficiency changed by 4.3 percentage points for both the engine and CVT for the hot vs. cold starts, the effect on the engine is much more important because its baseline efficiency (29.3%) is much lower than for the CVT (78.4%). That is, the 4.3% percentage point decrease in engine efficiency translates to a 14.7% loss in efficiency, whereas the CVT experienced only a 5.5% loss in efficiency. Of course, the product of the two efficiencies affects fuel economy.

Table 7.1 Fuel economies according to warm-up state

Operation	Cold start	Hot start	Difference
Fuel economy (mpg)	24.27	32.99	8.72 mpg (26.4%)

As a result of this increased energy loss, the fuel economy deteriorated, as shown in Table 7.1. About 36% more fuel was used to run the same distance with the same driving schedule. This additional fuel input contributes to the worse fuel economy. From the measured energy losses for each component, the factors which affect the change in fuel economy were quantified, as shown in Figure 7.8. More than 93% of the decrease in fuel economy for the cold start test can be attributed to the engine.

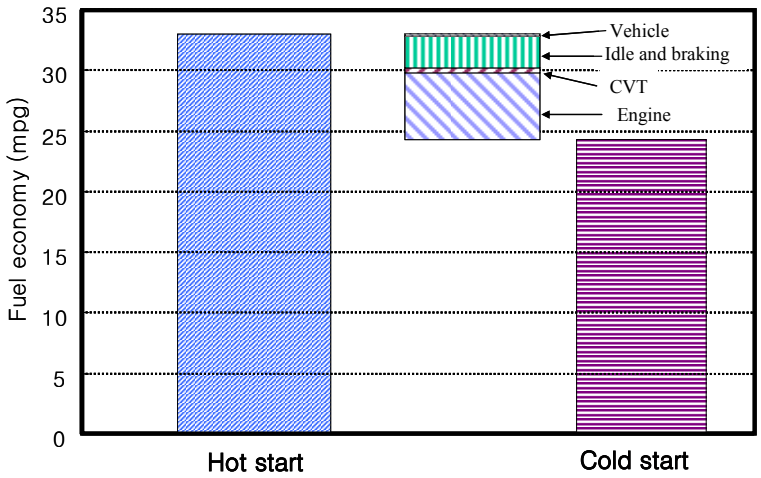

Figure 7.8 Change in fuel economy and contribution of each component

7.3.2 Effect of shift mode

The test vehicle in this research has two modes of gear shifting. One is the normal mode, seeking fuel economy, and the other is a sports mode, seeking torque and acceleration. In the sports mode, the engine operates mainly at high speed to realize a high level of acceleration. However, as there is a trade-off between the power and fuel economy, the sports mode is expected to increase fuel consumption. In this research, with the measurement of the fuel consumption and efficiencies of the engine and CVT, the effect of the shift mode was quantified.

The operating points of the engine and CVT on their efficiency maps are shown in Figure 7.9. Both efficiency maps, of the engine and CVT, were obtained by measuring the power flow in and out of the components at steady state. As shown in Figure 7.9, use of the sports mode results in operation at higher engine speeds. In general, this results in both the engine and CVT operating at lower efficiency on their respective efficiency maps.

The fuel economies for both operations are shown in Table 7.2. Using the sports mode rather than the normal mode decreases fuel economy by 28.2%, for the Hot 505 test.

Table 7.2 Fuel economies according to shift mode

Operation	Normal mode	Sports mode	Difference
Fuel economy (mpg)	32.99	23.25	28.2%

In order to clarify the factors that dominate this fuel economy loss, the energy losses for each component were calculated. The results are shown in Figure 7.10. The additional fuel losses for the engine and CVT are;

- Engine: 81.3 grams
- CVT: 10.2 grams

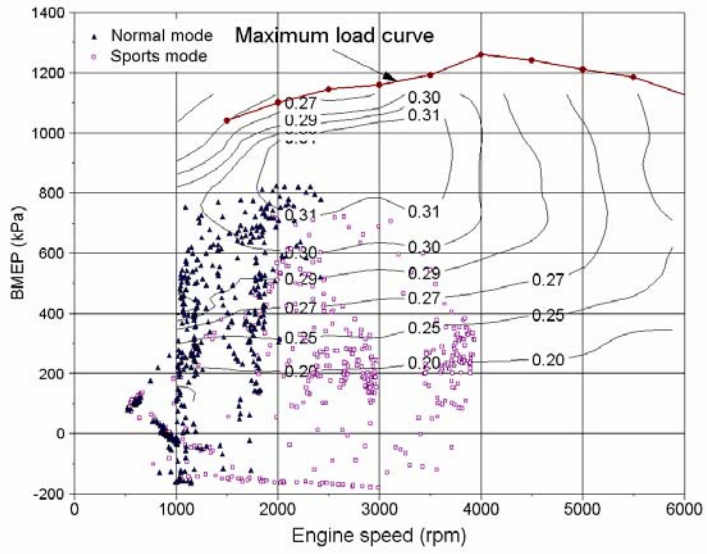

(a) On engine efficiency map

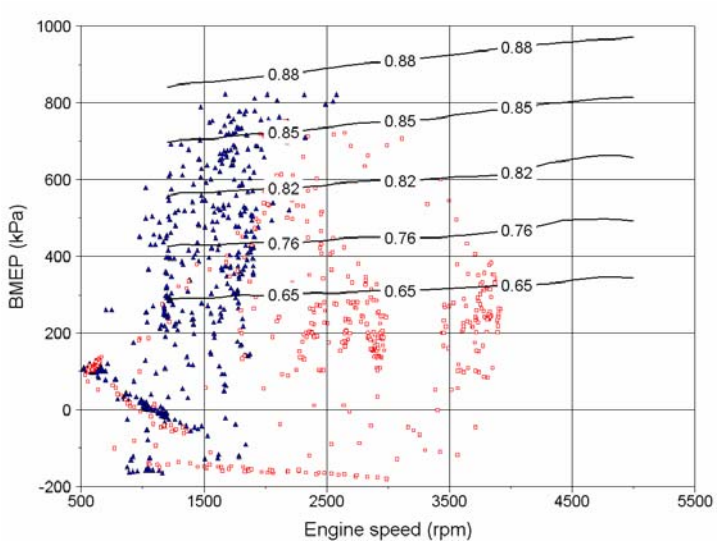

(b) On CVT efficiency map

Figure 7.9 Operating points according to shift modes

A portion of the increased fuel consumption by the engine is, in fact, due to the CVT. The increased fuel consumption by the engine is caused by the CVT in 2 ways.

- Change of engine operating points
- Increased energy requirement from decreased efficiency of the CVT

As the engine has a limited efficiency, the increase in energy requirement from the transmission necessarily increases the energy loss in the engine. That is, even if the engine operating points do not change, the engine energy loss would have increased.

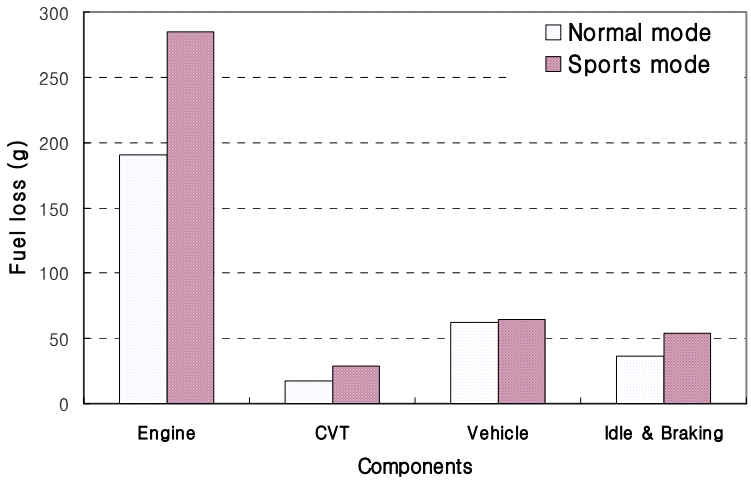

Figure 7.10 Energy losses at each component

Figure 7.11 shows the change of efficiencies of the engine and CVT. The efficiency of the engine decreases about 4 percentage points and that of the CVT decreases about 10 percentage points.

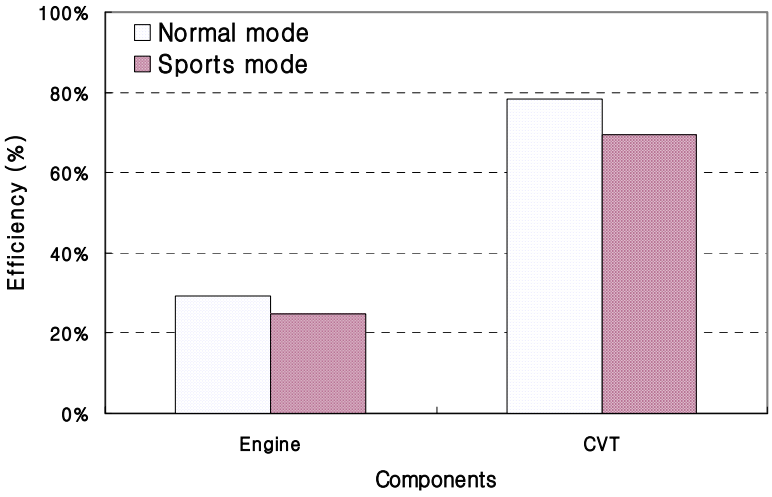

Figure 7.11 Change of efficiencies by shift modes

7.4 COMPARISON WITH SIMULATION

In the vehicle simulation, the most important parameters are energy flows between the major powertrain components. The fuel consumption and emissions make sense only if the input and output torque and speeds of the powertrain components are defined correctly. In this section, the measured fuel rates and power flows are compared with the simulation results.

PSAT and ADVISOR were used as the simulation tools for this purpose. Both of them are programmed in MATLAB/Simulink. PSAT uses a forward facing modeling approach and ADVISOR uses backward facing modeling. The backward facing calculation begins with a required speed trace that the vehicle must meet. The model calculates the necessary force at the wheels to move the vehicle as required. It then works backwards through differential, transmission, clutch and finally the engine. In contrast, the forward facing approach starts from the driver and determines the power requirement based on the difference between the actual speed and target speed. Then, this power transmits to the vehicle through the components such as the clutch, transmission, final drive and wheel.

The calculations of power through each component are based on the efficiency and performance of each component. Therefore, the required input includes the efficiency maps for each powertrain component: engine, CVT, and so on. In this research, those efficiency maps were generated by steady state mapping tests and used in this simulation. For example, the efficiency of the engine was obtained by measuring the torque and speed of the engine keeping the vehicle at constant speed. The basic model parameters for this simulation are shown in Table 7.3.

Figure 7.12 shows the measured results and simulation predictions simultaneously. From this figure, the simulated results agree well with the measured results.

Table 7.3 Description of basic model parameters

Component	Parameter	Specification	Source
Vehicle	Frontal area	2.5848 m^2	Specification
	Weight	1417.5 kg	Specification
	Drag coefficient	0.3362	Coast down test
	Rolling resistance coefficient	0.009843	
Engine	Max torque curve	In Figure 6.7 (a)	Specification
	BSFC Map	In Figure 6.7 (a)	Steady state test
CVT	Ratio range	0.428~2.396	Specification
	Efficiency map	In Figure 6.2 (b)	Steady state test

From the simulated power flows, the energy losses for each component were calculated, as shown in Figure 7.13(a). Comparing this result with the measured results in Figure 7.6, we can see that the simulation makes a good estimation for the energy loss of each component. As expected from Figure 7.12, the stabilization loss in the ADVISOR simulation is a little larger than measured and that in the PSAT simulation is a little less. The estimated loss contributions of the other components do not deviate more than 4%.

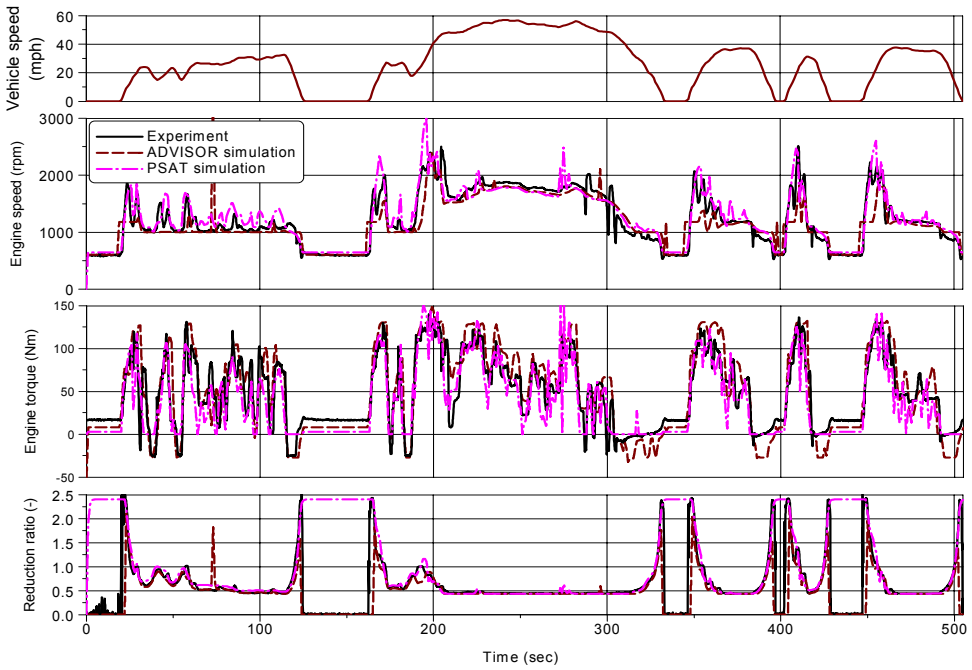

(a) Engine speed and torque

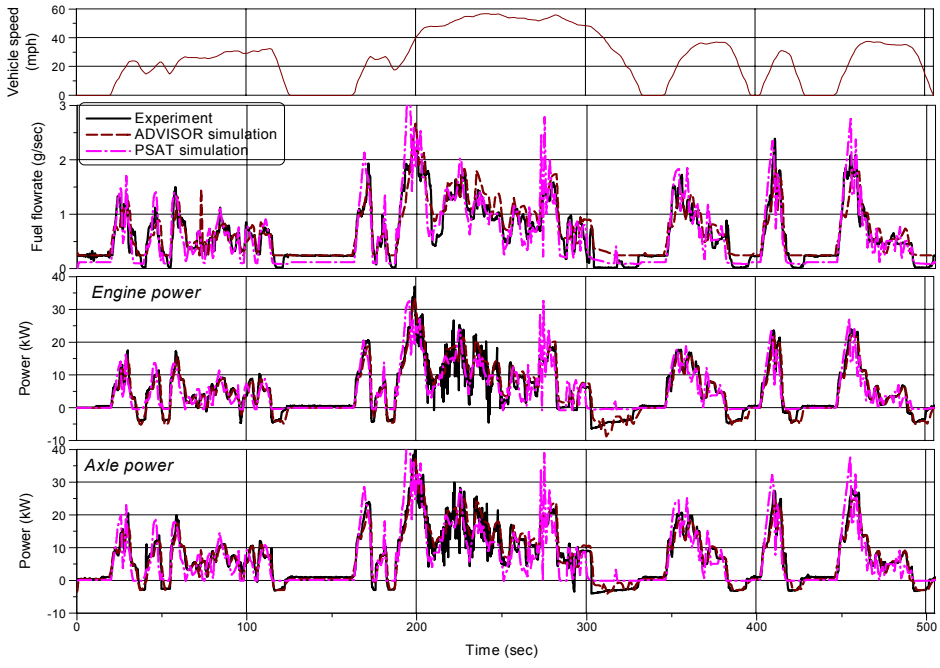

(b) Power through the engine and CVT

Figure 7.12 Comparison of measured power flows with simulated

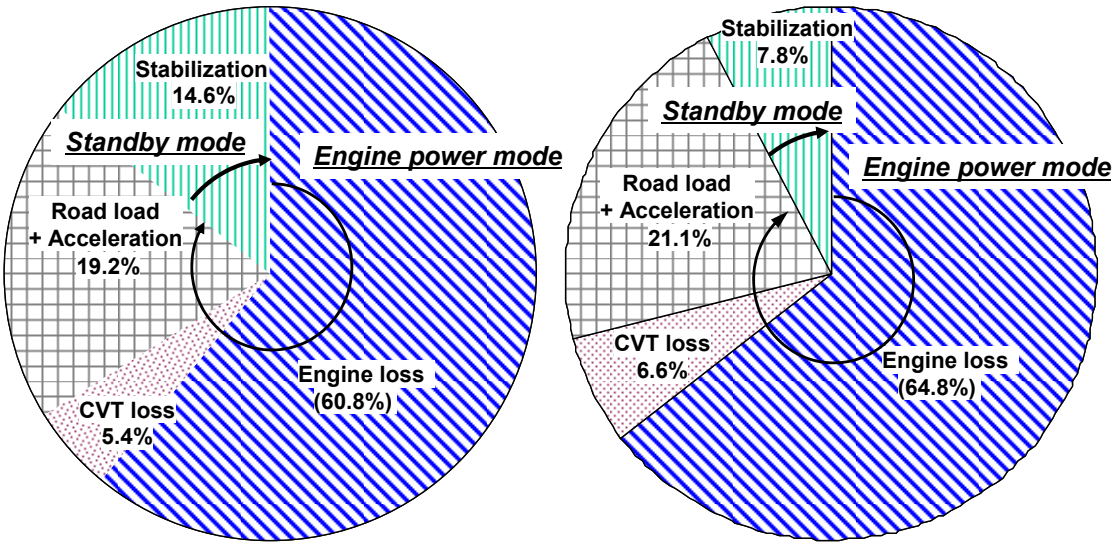

(a) ADVISOR (b) PSAT

Figure 7.13 Simulated energy loss distributions

The fuel economy and efficiencies for both the Hot 505 and Cold 505 are compared in Table 7.4. For the Hot 505, ADVISOR predicts the engine and CVT efficiencies within 2% of the measurements, but underpredicts the fuel economy by 10%. Half of this difference is due to the inability to account for the fuel cut during deceleration and the remaining part might be caused by other factors such as inaccuracies of modeling assumptions and/or of experimental measurements.

Table 7.4 Comparison of basic model parameters

Condition		Fuel economy (mpg)	Efficiency	
			Engine	CVT
Hot 505	Test	33.0	29.3%	78.4%
	Simulation(ADVISOR)	29.6	28.8%	77.3%
	Simulation(PSAT)	31.5	28.2%	76.3%
Cold 505	Test	24.3	25.0%	74.1%
	Simulation(ADVISOR)	27.5	26.8%	77.3%

The predictions of PSAT for the efficiencies are also within a few percent and that for the fuel economy seems to be also within the error bound. For the Cold 505, ADVISOR overpredicts the engine efficiency by 7% and overpredicts the fuel economy

by 13%. Even though ADVISOR includes a routine for estimating the starting and warm-up behavior from the steady state maps for fully warmed-up operation, it is obvious that this routine is not as accurate as might be desired. PSAT does not have the routine to account for the effect of cold start.

7.5 COMPARISON WITH PRIOR RESULTS

The results in this research are compared with the results from the PNGV study [5] in Figure 7.14. The present study is only for Phase I and Phase III whereas the PNGV study was for whole FTP cycle. The previous study was for a 1993 mid-size car, so there is a 7 year difference between the models for these studies.

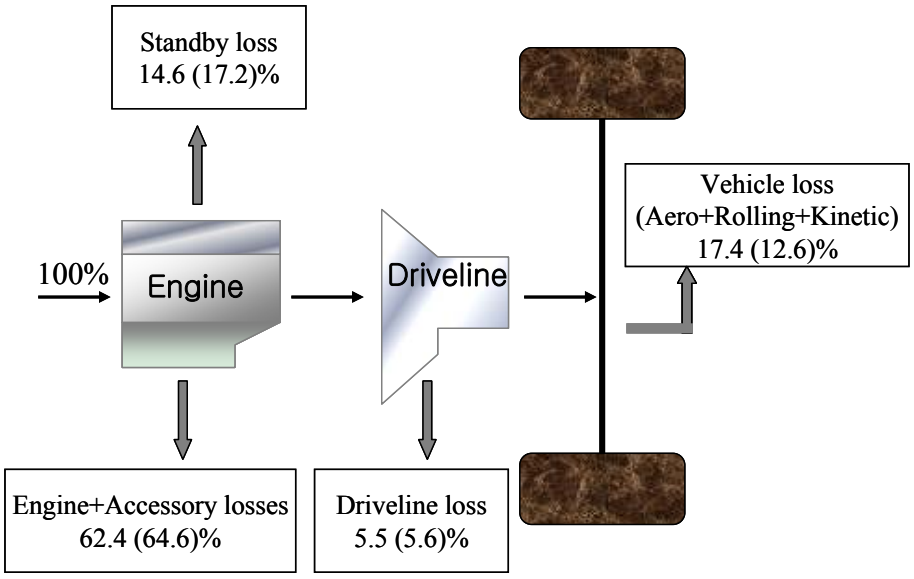

Note: Numbers in parentheses indicate the energy loss presented in [Anon., 1994]

Figure 7.14 Energy flow distribution

Regardless of the differences of the vehicle model and operating cycle, the energy distributions seem to agree well with each other. What is seen in this comparison is that the stand-by loss and engine + accessory losses decreased but the driveline loss is almost the same. As a result, the relative portion assigned to vehicle loss increased. The decrease in engine loss is probably caused by the use of the CVT. The CVT on the

present test vehicle could locate the engine operating points in the more efficient region. The reduction of stand-by loss is partially due to the deceleration fuel cut and partially due to the reduction of idle engine speed.

7.6 FUEL ECONOMY POTENTIAL OF A DISI ENGINE IN A CONVENTIONAL VEHICLE

The D-4 engine in the OPA is supposed to work in the lean combustion mode except for the cold start, braking and high load operation. The potential fuel economy improvement due to the DISI engine over a PFI engine was addressed by Seiffert [33] who concluded that the reduction of pumping work is the principal factor contributing to the improvement in fuel economy. Therefore, even though the engine is a DISI engine, its fuel economy can be assumed to be equivalent to that of a PFI engine if it is working in homogeneous stoichiometric mode instead of stratified lean mode. Fortunately, it was possible to manipulate the combustion of the D-4 engine in the stoichiometric mode.

By comparing the engine efficiency and fuel consumption in two different combustion modes, the benefit of the DISI engine was attempted to be evaluated. The OPA was tested in two different combustion modes over the Hot 505 cycle. The Hot 505 cycle was selected as the comparison cycle as it can represent the benefit of lean operation. The fuel economies for both combustion modes were obtained and are shown in Table 7.4. The fuel economy benefit that can be realized by lean operation is obtained as 1.76~1.89 mpg. The absolute experimental value of fuel economy is different from that of the simulation. However, the difference is almost the same. Thus, it can be concluded that the simulation is reliable to estimate the relative effect.

Table 7.5 Fuel economy for both combustion modes

Operation		Homogeneous charge stoichiometric mode	Stratified charge lean mode	Difference
Fuel economy (mpg)	Experiment	32.99	34.88*	1.89 mpg
	Simulation	31.15	32.91	1.76 mpg

*1st run of 3 FTPs

To analyze the factors on this difference in fuel economy caused by combustion modes, the energy loss distribution of each component obtained from both the experiment and simulation are shown in Figure 7.15.

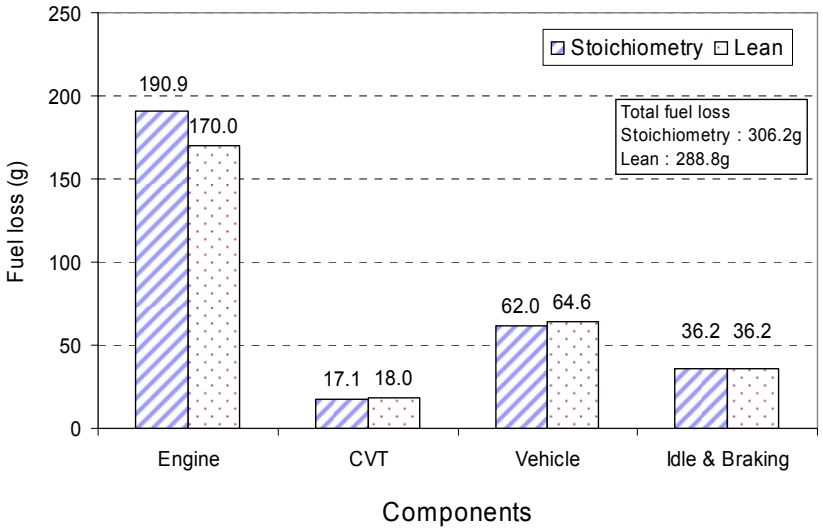

(a) Experimental results

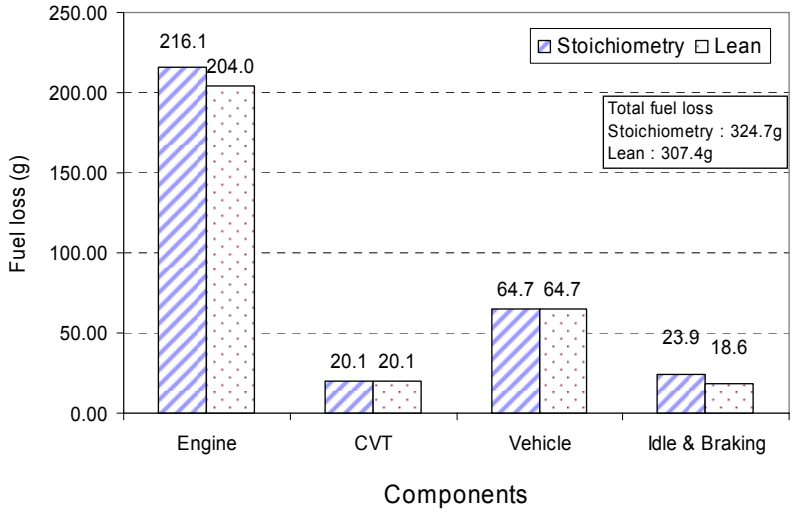

(b) Simulation results

Figure 7.15 Comparison of the energy loss and efficiency according to combustion mode

The other contributions are expected to be the same regardless of the combustion mode but the energy loss in the vehicle for the lean combustion mode was measured a

little more than that for the stoichiometric mode. In fact, these different combustion mode tests were performed with different chassis dynamometers. Lean mode testing was done using the chassis dynamometer of SwRI and stoichiometric mode testing was done at ANL. Even though the same dynamometer coefficients were used, it is not possible to set all other conditions the same. As the energy absorption for lean mode is larger than that for stoichiometric mode, the fuel economy benefit might be underestimated compared to the actual benefit. The difference in fuel economy of 1.89 mpg is mostly caused by the reduction in fuel consumption in the engine. The lost fuel in the engine is reduced from 190.9 g for stoichiometric mode to 170.0 g for the lean mode. The simulation results show similar results.

The effects of combustion modes on the overall engine efficiency and fuel economy are shown in Figure 7.16 and summarized in Table 7.6

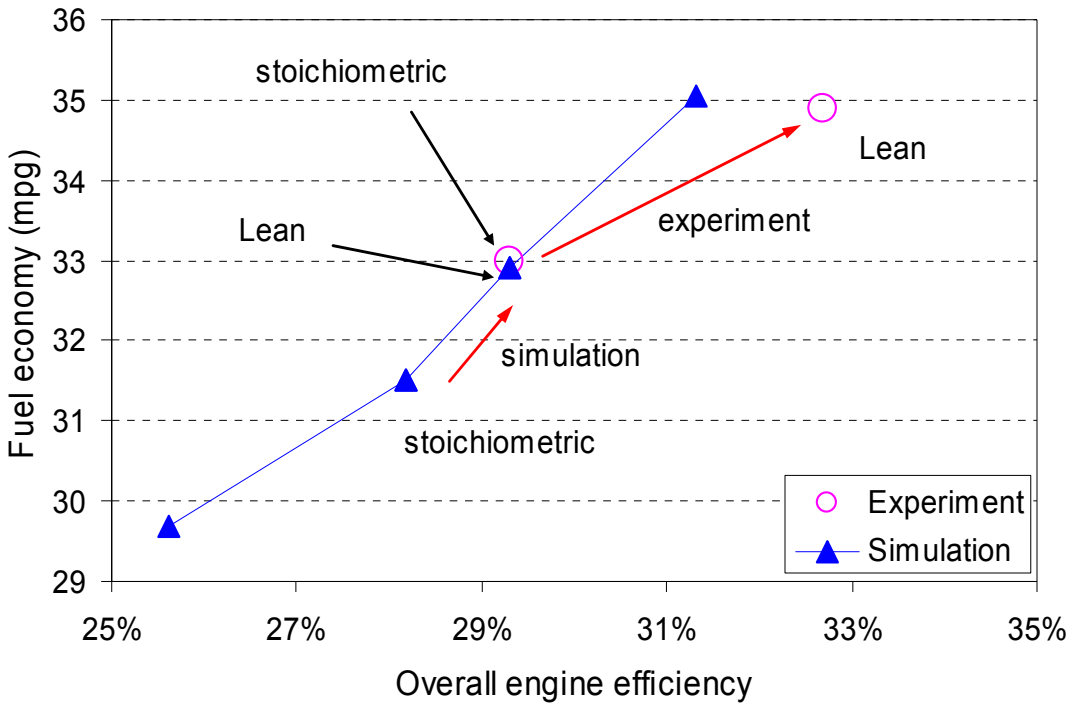

Figure 7.16 Effect of combustion mode on the overall engine efficiency and fuel economy

. The overall engine efficiency and fuel economy were obtained for both the experiment and simulation. The simulation results were obtained using PSAT with different engine specific fuel consumption maps as shown in Figure 6.7. The resulting benefit of fuel economy was 5.7% for both the experiment and simulation. As this result is only for Phase 3 of the FTP, the actual benefit in the FTP cycle which includes cold starts should be smaller than this value.

Table 7.6 Summary of the benefit of lean combustion during the Hot 505 cycle

	Overall engine efficiency	Fuel economy improvement
Experiment	29.3→32.7% 2.6% point	5.7%
Simulation	28.2→29.4% 1.2% point	5.7%

In Figure 6.8 of the previous chapter, the relative improvement of the lean combustion mode in BSFC was 5~25%. This improvement of steady state fuel consumption is relieved as the viewpoint goes from the engine to the vehicle. The engine operating points on the BSFC map are shown in Figure 7.17. It is shown that the engine operating points disperse not only at low load but also t high load where both operations are in stoichiometric combustion mode.

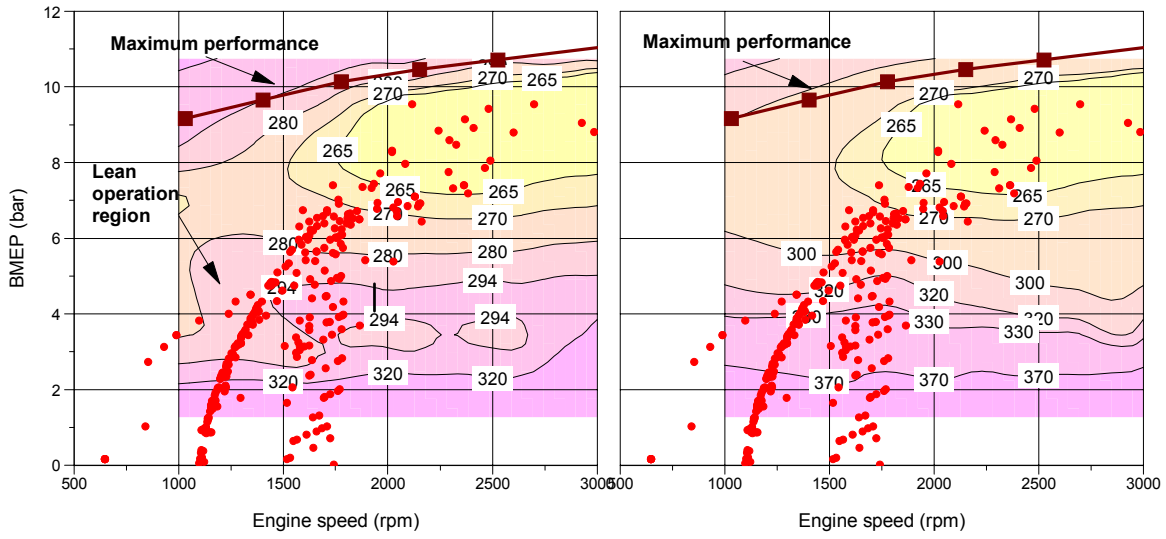

(a) On BSFC map in lean mode (b) On BSFC map in stoichiometric mode

Figure 7.17 Simulated engine operating points on BSFC map

The simulated fuel consumptions for stoichiometric and lean operation are shown in Figure 7.18. The relative difference and accumulated fuel consumption are shown in that figure, too. Even though we can see more than 20% of the relative improvement, the final difference in fuel consumption is about 5%.

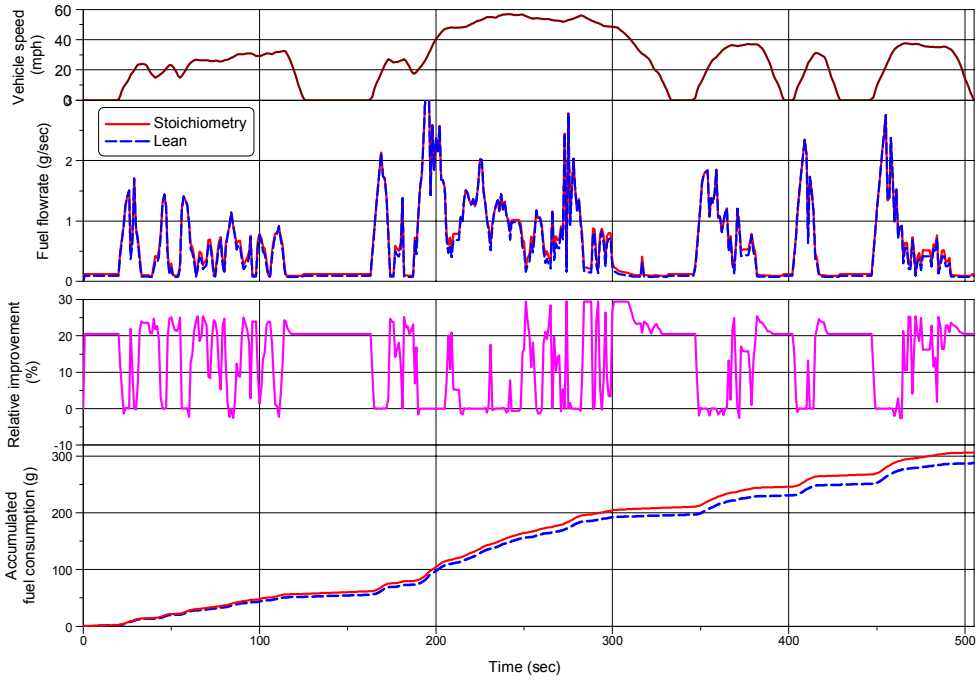

Figure 7.18 Simulated fuel consumption and relative improvement during the Hot 505 cycle

7.7 CHAPTER SUMMARY

In order to determine the factors that affect fuel economy quantitatively, the power flows through the major powertrain components were measured during operation over the FTP cycles. By operating the engine in two different combustion modes, lean and stoichiometric combustion, the effect of the lean combustion on the overall efficiency and the resulting fuel economy was evaluated. The measured results were compared with simulation results using PSAT and ADVISOR.

The energy losses were calculated from the measured power flows. The engine, the largest energy sink, consumes 62.3% of the total energy loss during the power mode

and additionally consumes 11.8% more during the idling and braking. The CVT consumes 5.6% and the vehicle consumes 20.2%. The overall efficiencies of the engine in stoichiometric combustion during the Hot and Cold 505 cycle were measured as 29.3% and 25%, respectively. The CVT efficiencies were 78.4% during the Hot 505 cycle and 74.1% during the Cold 505 cycle. The sports shift mode lower the engine efficiency by 4.6% points and the CVT efficiency 8.9% points.

The overall efficiency of the engine, which is 29.3% during the Hot 505 cycle, is improved to 32.7% with the change in combustion mode to lean combustion. The resulting fuel economy improvement was measured as 5.7%. Therefore, it can be concluded that the fuel economy benefit of a DISI engine over a PFI engine during Phase 3 of the FTP cycle is 5.7% due to the 3.4% improvement in the overall engine efficiency.

Both the PSAT and ADVISOR predictions for the power flows, speeds and torques of each component, agree well with the measured results. PSAT is found to be a reliable simulation tool to estimate the relative effect of the change in engine efficiency on the fuel economy.

CHAPTER 8: FUEL ECONOMY AND EMISSIONS OF DISI POWERED HYBRID ELECTRIC VEHICLE

A 2005 Chevrolet Equinox is selected as the vehicle for simulating a virtual hybrid powertrain with a DISI engine. The 2005 Equinox was chosen because the University of Texas has been accepted as a competitor in ChallengeX. ChallengeX is a three year competition sponsored by DOE and GM, beginning in fall 2004 and ending in spring 2007. Participating teams will design and develop a vehicle that will minimize energy consumption, emissions and greenhouse gases on a well-to-wheel basis while maintaining or exceeding the utility and performance of the stock vehicle. For the first year, every team has to focus on modeling and simulation of the stock vehicle and of the powertrain design which can accomplish the goals of the competition. The Equinox is the base vehicle on which the modified hybrid powertrain is installed. This research is involved as one of the attempts to design the hybrid powertrain. Therefore, the Equinox is also used as a base vehicle in the present research.

In this chapter, the modeling results of the stock vehicle are addressed and compared with the vehicle specifications. Then the hybrid system, using the DISI engine in the OPA, is modeled. By comparing the HEV with a DISI engine and that with a SI engine, the benefit of a DISI engine in an HEV application was evaluated. The steady state efficiency maps of the OPA engine in the lean and stoichiometric modes were used in the simulation.

8.1 STOCK VEHICLE MODELING

8.1.1 Equinox model

As a first step for the testing of a DISI engine in the HEV application through simulation, the PSAT model was validated by comparing the simulation results with the vehicle's technical specifications. The specifications of the Equinox that will be used in the input data for PSAT are shown in Table 8.1. The available specifications were not enough for a complete simulation. Thus, in the cases that the data for simulation were not available, equivalent data from the PSAT library were used instead of the actual Equinox data. The important parameters with relation to vehicle performance, such as the vehicle resistance and speed reduction ratios came from the actual specifications of the Equinox.

Table 8.1 Specifications of the Equinox

Component	Parameter		Specification
Vehicle	Frontal area		3.19 m^2
	Drag coefficient		0.417
	Rolling resistance coefficient		0.0084
Engine	Displacement		3.4L
	Maximum power		138 kW @ 5200 rpm
	Maximum torque		285 N-m @ 3800 rpm
Transmission	Type		5 speed automatic
	Gear ratios	1^{st}	4.68
		2^{nd}	2.94
		3^{rd}	1.92
		4^{th}	1.30
		5^{th}	1.00
Final drive	Reduction ratio		2.65
Tires	Nominal specification		P235/60R17

The frontal area of the vehicle was calculated based on the dimensions shown in the specifications. The drag coefficient and weights are also available in the specifications. The rolling resistance coefficient was not available so that of the Explorer

in the PSAT library was assumed to be same as that of the Equinox. The only available engine data were the maximum power and maximum torque, as shown in Table 8.1. The maximum torque curve and efficiency map were not available. The 4.0L SI engine for the Explorer was selected as its characteristics are similar to that of the engine in the Equinox. To make the power rating of the two engines equivalent to each other, the torque curve of the Explorer was scaled so that the maximum power is the same as that of Equinox. The maximum torque and power curves are shown in Figure 8.1(a). The efficiency of the Explorer engine was assumed to be same as that of the Equinox. The efficiency of the engine can be expressed in terms of both brake specific fuel consumption and brake thermal efficiency which is defined as the ratio of the brake power to the rate of input fuel energy. The brake thermal efficiency map is shown in Figure 8.1(b).

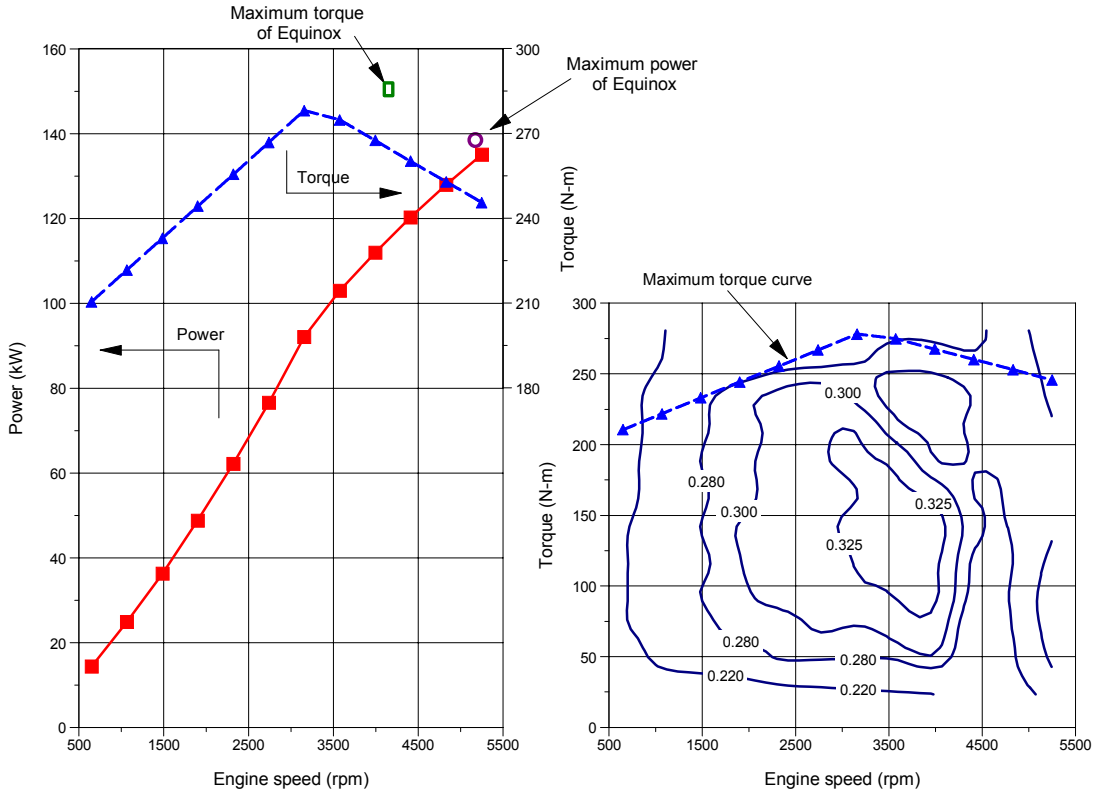

(a) Maximum performance (b) Efficiency map

Figure 8.1 Engine performance and efficiency used in simulation

For the transmission, the 5 speed automatic transmission data file for Explorer was used and the gear ratios at each step were substituted by Equinox data. The efficiency map for transmission is shown in Figure 8.2.

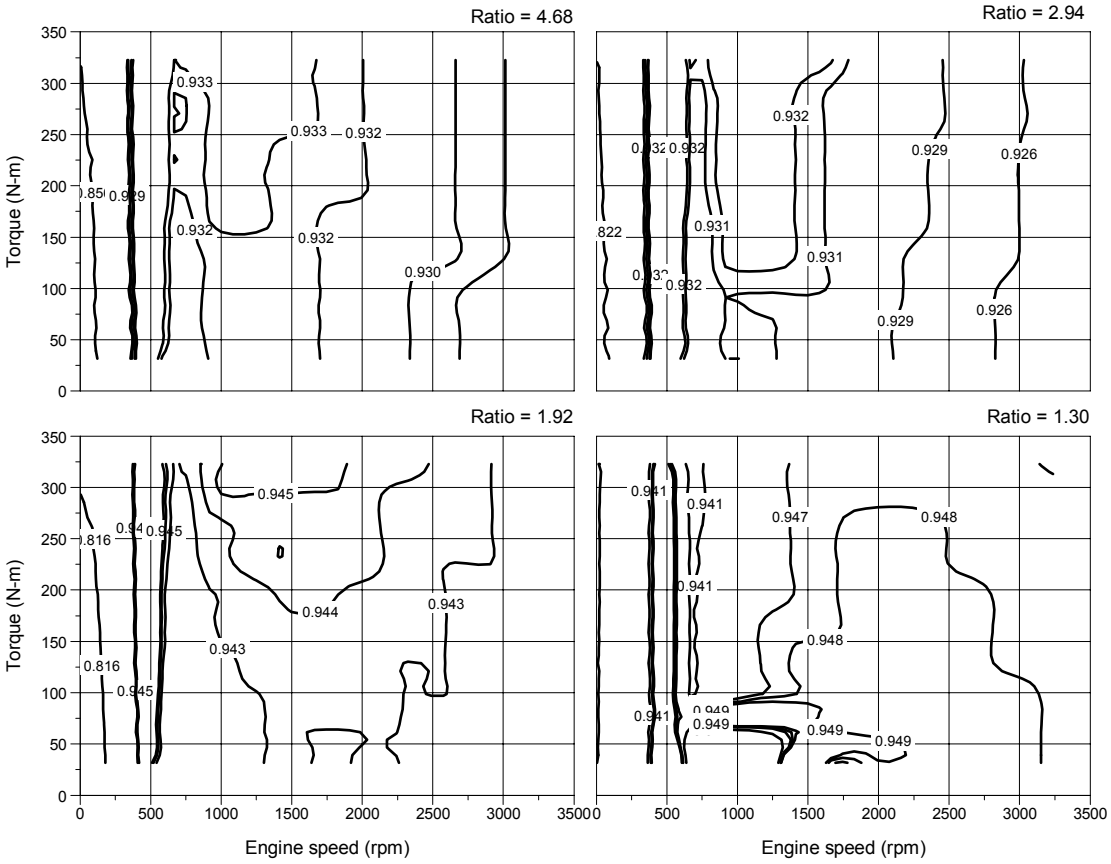

Figure 8.2 Transmission efficiencies used in the simulations

8.1.2 Simulation results

The EPA combined fuel economy, acceleration performance and gradeability were obtained from the PSAT simulations. Those results are compared with the vehicle technical specifications shown in the ChallengeX draft rules which are shows in Table 8.2. The trailering capacity defined in the ChallengeX rules is 3500 lbs. However, the ability of the vehicle with the maximum weight of the trailer is not clearly shown. The

author followed the PNGV performance guidelines and assumed that the gradeability of the vehicle with trailer (3500 lbs) must be the ability to climb a grade higher than 6.5%.

Table 8.2 Selected vehicle technical specifications in ChallengeX and PNGV performance guidelines

Vehicle technical specifications in ChallengeX rules		
Description	Base vehicle (V6)	Competition requirement
0-60 mph	8.9 sec	9.0 sec
50-70 mph	6.8 sec	6.8 sec
Vehicle mass	4000 lbs	4400 lbs
MPG combined EPA	23.3 mpgge	32.0 mpgge
Highway range	320 miles	200 miles
Passenger capacity	5 passenger	5 passenger
Emission cert. level	Tier 2, Bin 5	-
Trailering capacity	3500 lbs	2500 lbs
Starting time	< 2.0 sec	< 5.0 sec
PNGV guidelines		
Description		Requirement
0-60 mph		12 sec
0-85 mph		25 sec
40-60 mph		5.3 sec
Maximum speed		85 mph
Gradeability, forward & reverse		30% at GVW
Gradeability, forward		6.5% @55mph for 20 minutes (GVW with full accessory load)

The screenshots for a PSAT simulation are shown in Figure 8.3. The first screen is for the construction of the test vehicle. The configuration and data file for each component is set in this screen. The second one is for the test cycle. It determines the driving cycle or performance test on which the constructed vehicle is to be tested. It is possible to simulate for multiple driving cycles and multiple performance testing. The application of the SOC (State of Charge) correction algorithm is also determined here. The screenshot shown in Figure 8.4 is the result screen. The fuel economy and emissions data are shown. The acceleration performance can be known from this screen, too.

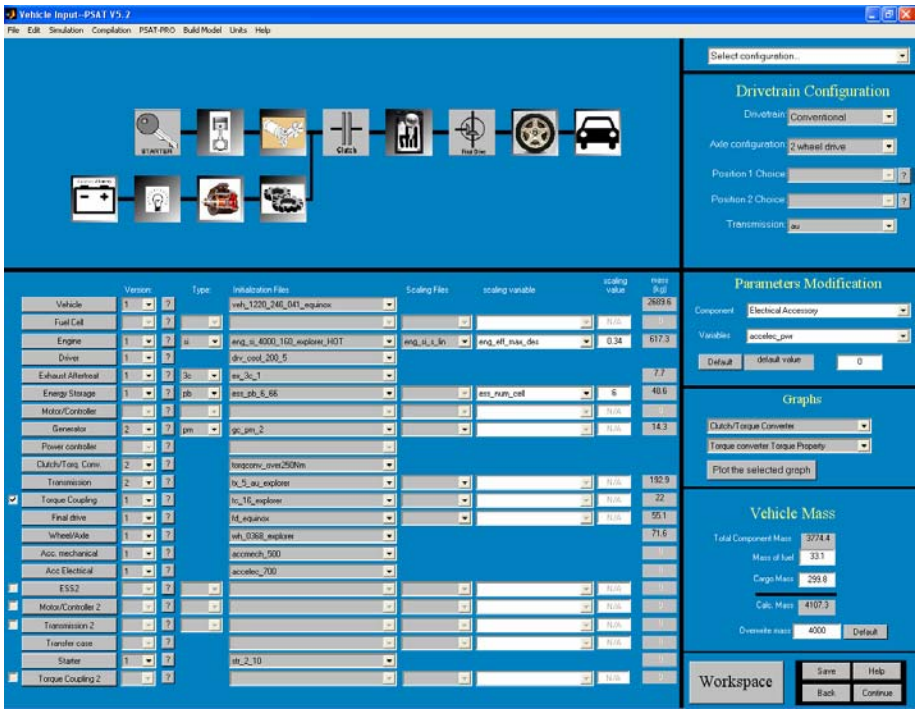

(a) Input data screen

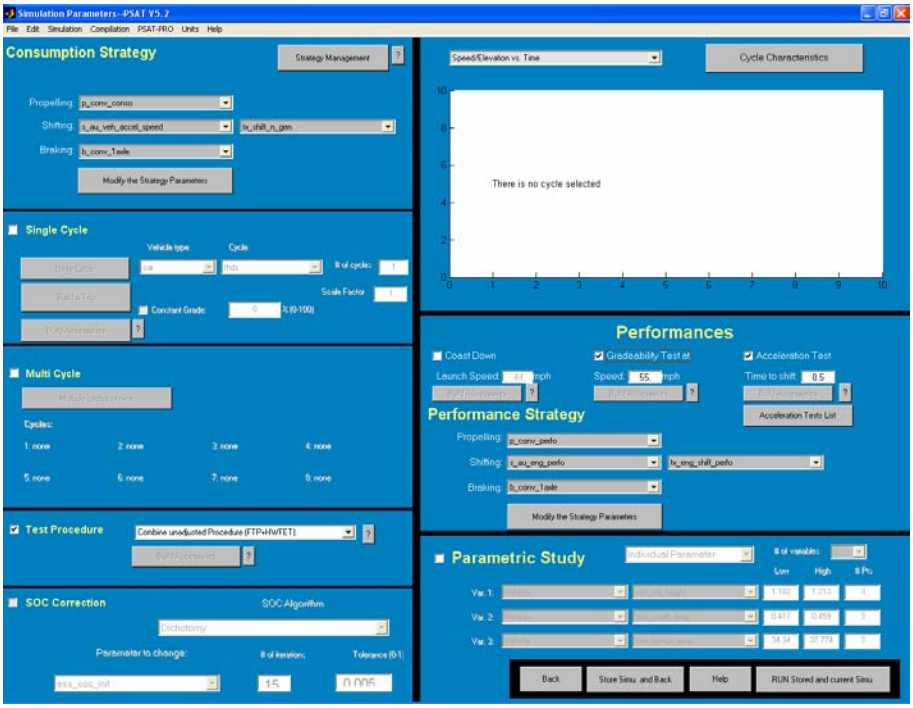

(b) Simulation condition screen

Figure 8.3 Screenshots for the simulation of conventional the Equinox

Figure 8.4 Screenshot of the simulation results

The simulation results and the technical specifications of the Equinox for comparison are shown together in Table 8.3. The EPA combined fuel economy estimated from PSAT is close to the technical specification. The acceleration performance, Z60 time (time from 0 to 60 mph), is longer than the specification even though the time from 50 to 70 mph is shorter. This is because the expert driver for acceleration performance testing usually uses a special technique to maximize the acceleration performance that is not taken into account in the simulation. It turns out that the vehicle can run on a road of 7.8% grade at 55 mph with a 3500 lb trailer.

Table 8.3 Comparison of simulation results with the vehicle technical specifications

Parameter		Specification	PSAT results
Fuel economy	EPA combined	23.3 mpg	24.56 mpg
Acceleration	0 – 60 mph	8.9 sec	10.2 sec
	50 – 70 mph	6.8 sec	6.36 sec
Trailering	3500 lbs trailer @ 55 mph	6.5 %	7.8 %

Except for minor discrepancies, the PSAT results seem to be reliable for the estimation of fuel economy and performances. These data will be used as the baseline data to determine the size of the components of the virtual HEV.

8.2 HEV MODELING

8.2.1 Component sizing

The conventional Equinox is a high performance vehicle satisfying a number of standards for acceleration performance, gradeability (hill-climbing ability), sustained high speed and driving range. It is necessary to find out the combination engine/battery/motor satisfying the performance guidelines. The starting point is the engine sizing to at least satisfy the gradeability requirement since the long duration of this requirement implies that the engine has the capability of gradeability by itself. The battery and motor are then to be sized to allow the vehicle to meet acceleration performance. The gradeability is not yet clearly defined in the ChallengeX rules. Instead, the trailering capacity is defined. Therefore, the author designed the virtual HEV which has the performance specifications shown in Table 8.4. The required Z60 time is 9.0 seconds in the given specifications. However, the simulated Z60 time can be reduced in the actual vehicle testing. The allowable Z60 time in simulation is assumed to be the same as that of the stock vehicle, 10.2 seconds.

Table 8.4 Criteria for component sizing

Component	Required performance	Specification
Engine	Gradeability @ 55 mph with GVW + trailer	More than 6.5% gradeability with 2500 lbs trailer
Motor/Battery	0-60 mph	9.0 (10.2) seconds

Various combinations of engine/battery/motor were simulated to find out the combination which can satisfy the performance requirement. At first, the engine of the OPA was tested to determine if it can satisfy the trailering capacity without changing the maximum power of the engine. Then the combination of motor and battery was selected

to meet the required acceleration performance. The combination found as results of the simulations are shown in Table 8.5 with the simulation results.

It turns out that the 112kW DISI engine in the OPA can satisfy the trailering capacity requirement by itself. The 30kW UQM motor with Ovonic battery were selected as their combination has the least power and capacity as well as the ability to satisfy the performance requirement.

Table 8.5 Combination of engine/motor/battery to satisfy performance guidelines

Specification				
Comp-onent	Manufacturer	Type	Maximum power/Capacity	File name in PSAT
Engine	Toyota	DISI	112 kW	Eng_si_2000_112_opa
Motor	Unique Mobility	PM Induction motor/inverter	30 kW	mc_pm_30
Battery	Ovonic	NiMH	28 A-hr	Ess_nimh_28_300_ovonic

Performance				
Parameter		Specification	PSAT results	
			Stock vehicle	Virtual HEV
Acceleration	0-60 mph	9.0 sec	10.2 sec	10.21 sec
	50-70 mph	6.8 sec	6.4 sec	5.7 sec
Trailering capacity	Gradeability @ 55 mph with 3500 lbs (stock vehicle) with 2500 lbs (virtual HEV)	6.5 %	7.8 %	6.5 %

8.2.2 HEV model for simulation

The base vehicle for simulation is the Equinox and the parallel 2-wheel drive configuration was selected as the HEV system to be simulated. The configurations and the specifications of the components used are shown in Table 8.6.

Table 8.6 Configurations and components used

Configuration
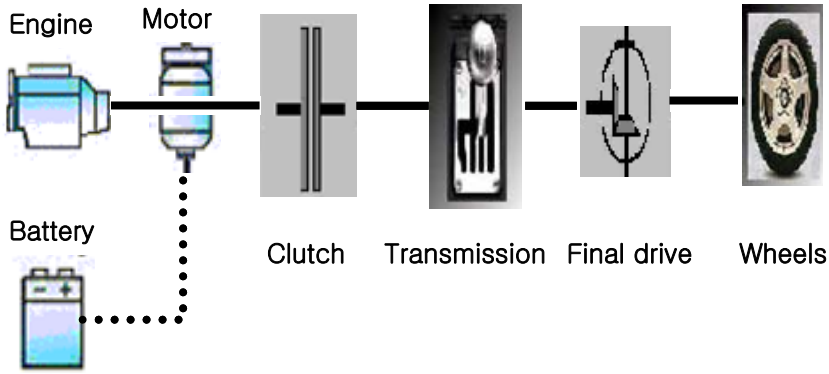

Components specifications		
Component	Parameter	Specification
Vehicle	Frontal area	3.19 m^2
	Drag coefficient	0.417
	Rolling resistance coefficient	0.0084
Engine	Displacement	1998 cc
	Type	Direct Injection Spark Ignition
	Maximum power	112 kW @ 6000 rpm
	Maximum torque	200 N-m @ 4000 rpm
	Efficiency map	Figure 6.7
	Emissions maps	Figure B.2 ~ B.3
Catalyst	Type	3 way + DeNOx catalyst
	Efficiency	Figure 8.6
Transmission	Type	5 speed manual transaxle
	Gear ratios	3.2 - 2.3 - 1.5 - 1.0 - 0.75
Final drive	Reduction ratio	3.24
Motor	Continuous maximum power	30 kW
	Continuous maximum torque	305 N-m
	Efficiency map	Figure 8.5
Battery	Capacity	28 A-hr

The efficiency map and the maximum torque curve of the motor used are shown in Figure 8.5. The efficiency of the catalyst is defined as a function of temperature. The catalyst efficiency was approximated based on the obtained conversion efficiency during the FTP cycle and shown in Figure 8.6.

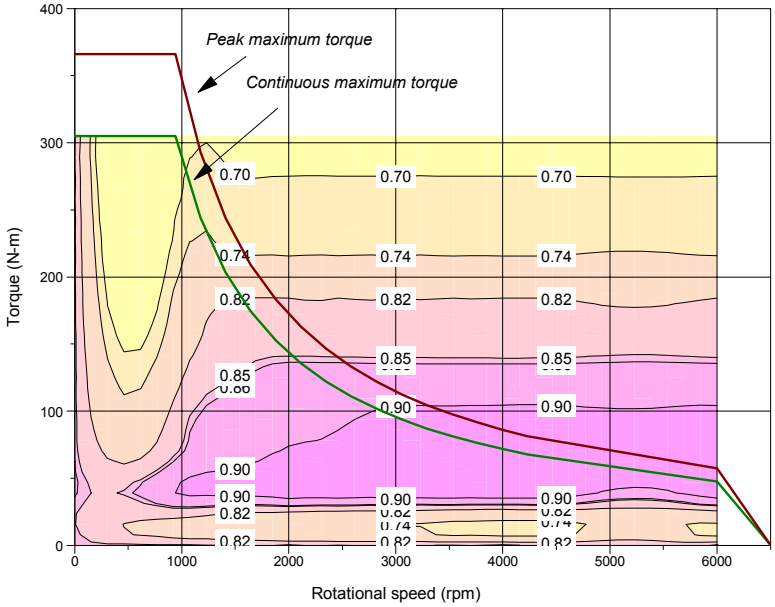

Figure 8.5 Characteristics of used motor

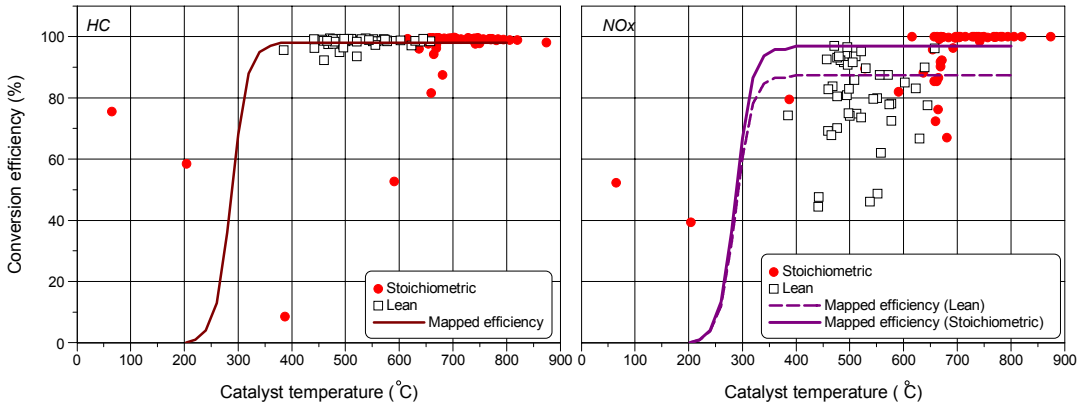

(a) HC (b) NOx

Figure 8.6 Catalyst efficiency curve

8.2.3 Simulation results

The hybridization results in an increase in vehicle weight. The gross vehicle weight of the Equinox is 4000 lbs and that of the hybridized Equinox is calculated based on the added components and found to be around 4400 lbs, which is the regulated weight defined in the ChallengeX rule. Therefore, the test weight of hybrid Equinox was set as 4400 lbs.

The fuel economy results from the PSAT simulations are summarized in Table 8.7. Even with the increased vehicle weight, the fuel economy is improved by more than 10 % due to the hybridization. The fuel economy improvement by adoption of a DISI engine instead of a conventional SI engine is found to be 4.2 % in terms of composite fuel economy.

Table 8.7 Fuel economy simulation results

		Conventional	HEV with SI engine	HEV with DISI engine
Vehicle weight		4000 lbs	4400 lbs	4400 lbs
Fuel economy (mpg)	FTP	22.37	25.44	26.93
	HWFET	27.92	30.39	30.99
	Composite	24.56	27.45	28.61
Improvement over conventional powertrain		-	11.8 %	16.5 %
Improvement over HEV with SI engine		-	-	4.2 %

To see in detail the contributing factors on the fuel economy improvement due to the hybridization, the energy loss at each component was calculated. In this calculation, only Phase 3 was considered. The fuel consumption of the conventional vehicle was 446.8 g and that of the HEV was 381.0 g. The difference of consumed fuel is 65.8 g and the corresponding energy difference is 2906 kJ. The calculated energy losses are shown in Figure 8.7. It is seen that there are three positive factors and one negative factor. The energy loss in the engine decreases as the engine size decreases. The reduced engine size makes the operating points closer to the most efficient region and increases the overall efficiency. The transmission loss decreases as the transmission changes from the automatic to the manual transmission. The energy loss for the vehicle increases because

the weight increases. Turning off the engine when power is not required (idle engine stop) is effective to decrease the fuel consumption during idle and braking.

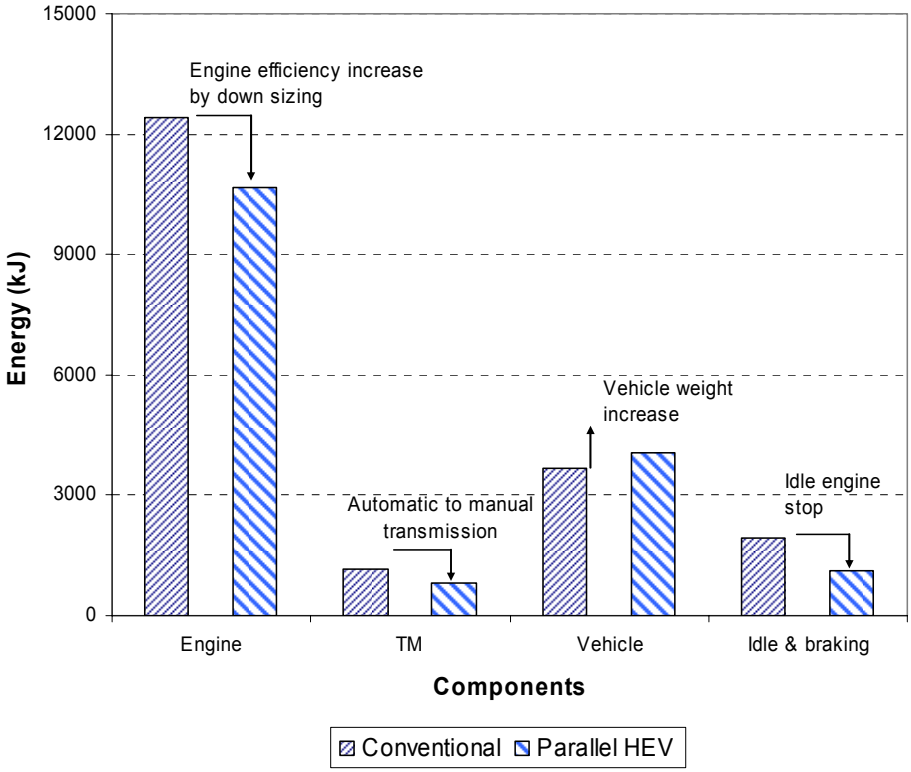

Figure 8.7 Energy losses for each component

The savings of fuel consumption for each factor are quantified and shown in Table 8.8. The savings in the engine including the savings for idle and braking is found to be the dominant factor on the fuel economy improvement due to the hybridization. The sum of these two factors is about 88% of the total savings.

Table 8.8 Contribution of each factor on the fuel economy improvement due to the hybridization

Components	Engine	Transmi-ssion	Vehicle	Idle & braking	Regenerated energy
Contributions	60.2%	11.7%	-12.9%	28.4%	12.6%

In Table 8.7, the fuel economy improvement from the DISI engine was found to be 4.2% in terms of composite fuel economy and that improvement during Phase 3 of the FTP was found to be 3.9%. This improvement is less than that of conventional vehicle mentioned in the previous chapter. In the previous chapter, the benefit of fuel economy of the OPA engine in the lean combustion mode over the stoichiometric mode was found to be 5.7% for both the experiment and simulation.

The overall engine efficiencies were calculated from the history of input and output power flows during the power mode and the following efficiencies were obtained.

- SI engine : 29.8%
- DISI engine : 30.3%

The difference in the overall efficiency of a DISI engine in a conventional vehicle (mentioned in the previous chapter: 1.2 percentage points) and that in an HEV is 0.5 percentage points. This is because the HEV engine operating points are primarily located in the high load region. In the HEV, the engine is down sized so the engine has to work in the high torque region at the same power requirement from the vehicle. Figure 8.8 shows the engine operating points on the BSFC map during the 505 cycle for both the DISI engine and SI engine in an HEV.

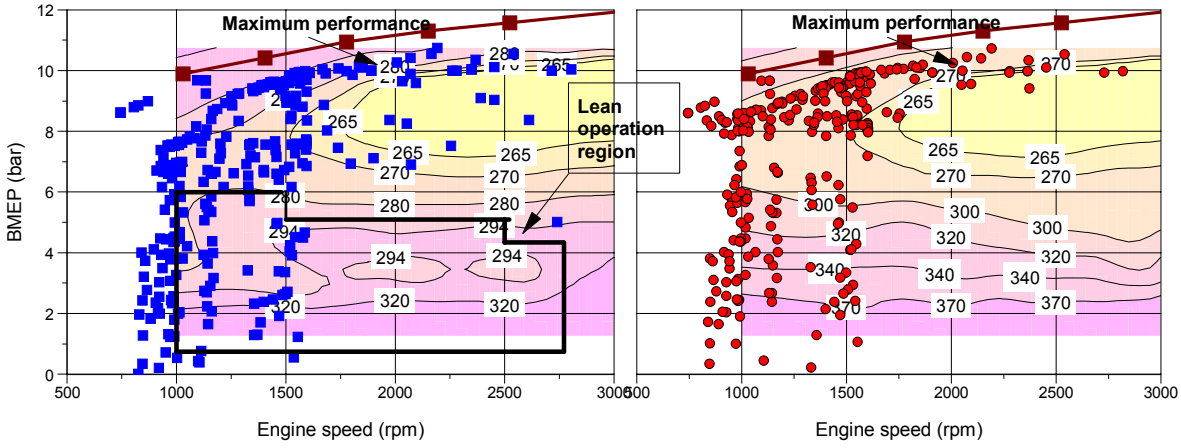

(a) DISI engine (b) SI engine

Figure 8.8 Engine operating points of an HEV

It is shown that the DISI engine operating points within the lean operation region are less than those in the case of the conventional vehicle shown in Figure 7.17. The dwell times in the lean combustion mode of the DISI engine for both the conventional and HEV are shown in Table 8.9. It is shown that the time in the lean combustion mode of the DISI engine for the HEV is less than one third of that for a conventional vehicle. As a result of that, the fuel economy improvement from use of a DISI engine in an HEV is not as high as might be anticipated because the down-sized DISI engine operates primarily in homogeneous charge mode.

Table 8.9 Dwell time in lean combustion mode of DISI engine during 505 cycle

	Engine power mode	In lean combustion mode	Ratio of lean combustion mode
Conventional	297 sec	189 sec	64 %
HEV	284 sec	56 sec	20 %

The emissions of two HEVs with different types of engines were calculated during the Hot 505 cycle and shown in Table 8.10. The HCs from the two HEVs are similar to each other. However, the NOx from the DISI engine is higher than that of the SI engine. This is mostly due to the worse efficiency of the lean NOx catalyst.

Table 8.10 Simulated emissions of HEVs with SI and DISI engines (g/mile)

	HC	NOx
SI engine	0.027	0.193
DISI engine	0.026	0.243

During the Hot 505 cycle, the use of a DISI engine in a parallel-type HEV application results in an improvement of fuel economy by 3.9% but 26% higher the NOx emissions and similar HC emissions.

8.3 CHAPTER SUMMARY

The fuel economy benefit of a DISI engine in an HEV application was evaluated for a virtual HEV which will be used in the ChallengeX competition. PSAT was used as

a simulation tool to calculate the fuel economy, emissions and performance for the given powertrain configuration and components.

The validity of the simulation was checked by comparing the simulated results with the vehicle specifications and test data. It is concluded that PSAT can predict the performance within an allowable error range. The sizes of the components were determined based on the performance requirements defined in the ChallengeX rules. The required maximum engine power was determined based on the gradeability with the specified maximum trailer. The 112kW engine in the OPA was found to be enough to satisfy that requirement without scaling of maximum power. Then the sizes of the motor/battery were determined so that the combination of engine/motor/battery can accomplish the specified acceleration performance of Z60 time. As results from the PSAT simulations, it was found that the combination of a 30kW PM induction motor and a 28A-h NiMH battery can satisfy the acceleration requirement.

The fuel economy improvement by hybridization was found to be a 12% increase in EPA composite fuel economy. The factors on the fuel economy improvement were analyzed and it was found that the fuel savings in the engine is a dominant factor responsible for 88% of the improvement.

The benefit of a DISI engine over a conventional SI engine in an HEV application is found to be 4.2% in terms of composite fuel economy and 3.9% for the Hot 505 cycle, which is less than that of 5.7% for a DISI engine in a conventional vehicle. The overall engine efficiency improvement of a DISI engine in an HEV application is 0.5 percentage points which is also less than that for a DISI engine in a conventional vehicle application. This is because the engine is working in the high load region due to the down-sized engine. This DISI engine operates primarily in homogeneous charge mode for high load, and thus does not offer a large fuel economy benefit. The HC emissions of both types of engines are similar to each other and the NOx emissions of HEV with a DISI engine is 26% higher than that with an SI engine.

CHAPTER 9: SUMMARY AND CONCLUSIONS

A Toyota OPA was selected as a test vehicle as it has the components of interest: a Direct Injection Spark Ignition (DISI) engine and a Continuously Variable Transmission (CVT). In order to estimate the benefit of the DISI engine and CVT, a 2001MY Toyota OPA was tested to collect the engine and CVT maps using in-situ measurement techniques. Three torque sensors were installed into the powertrain in the vehicle for that purpose; one is between the engine and transmission and the other two are installed on the drive axles. The overall efficiency of the engine and transmission was estimated using the measured torques and speeds during Phase 3 of the FTP cycle. The overall efficiencies of the engine at different operating modes including the lean and stoichiometric combustion modes were compared to each other. The overall efficiencies of the CVT are analyzed similarly. Finally, the measured steady state efficiency maps and emissions maps were used to predict the fuel economy and emissions of an HEV with the DISI engine and CVT.

9.1 CONCLUSIONS

1. Fuel economy and emissions of the OPA
   - 2^{nd} generation D4 – 30.5 mpg
   - FTP emissions
     - HC – 0.141 g/mile
     - NOx – 0.245 g/mile
     - CO – 1.114 g/mile
2. Toyota has made considerable improvements in tailpipe HC and NOx emissions with their second generation D-4 engine. For the HC emissions, the change in combustion system using their slit nozzle injector is the dominant factor. The dominant factor for the NOx emissions turns out to be the significantly improved catalyst efficiency.

3. Even with the improvement for the emissions reductions, the barriers to the U.S. market still remain high for the DISI engine. The tailpipe NMOG and NOx do not meet the LEV standards in the NLEV program.
4. Using the in-situ mapping technique, the map data for the engine and transmission was successfully obtained. This in-situ mapping is a promising tool.
5. The engine-out HC emissions in terms of BSHC for lean combustion are 2~3 times of that in the stoichiometric combustion mode. The engine-out NOx emissions are about one-half to one-sixth compared to that in the stoichiometric combustion mode.
6. Both the PSAT and ADVISOR predictions for the power flows, speeds and torques of each component agree well with the measured results.
7. It is concluded that the fuel economy benefit of a DISI engine over a PFI engine is 5.7% due to the 3.4 percentage points improvement in the overall engine efficiency.
8. The fuel economy benefit of a DISI engine over a PFI engine in an HEV application during Phase 3 of the FTP cycle is found to be 3.9%.
9. The fuel economy benefit of a DISI engine in an HEV application is found to be less than that for a DISI engine in a conventional vehicle application. This is because the engine is working in the high load region where the engine is in the stoichiometric combustion mode due to the downsized engine.
10. The tailpipe HC emission from a DISI engine in an HEV are about the same as those from a conventional SI engine in an HEV, but the tailpipe NOx emission are 26% higher.

9.2 RECOMMENDATIONS FOR FUTURE WORK

This dissertation research focused on the evaluation of the fuel economy benefit of the newly introduced DISI engine and CVT transmission using in-situ power flow

measurements. The power flow measurement technique is also applicable to compare the efficiency of the engine or transmission of two competing vehicles. The feasibility of the DISI engine in an HEV was tested using a simulation tool in a virtual vehicle. The simulation results are compared with the experimental results and the simulation approach is found to be reliable for the estimation of the fuel economy benefit. Therefore, the further direction can be either refinement or applications of this approach. Even though the application of the DISI engine in an HEV is found to be less effective than that in a conventional vehicle, there should be a way to maximize the benefit of the DISI engine in an HEV. Several topics for further research are addressed below.

9.2.1 Finding a way to maximize the benefit of a DISI engine in an HEV application

There are various configurations and control strategies in HEVs. In the present research, only the parallel 2 wheel drive HEV with the default control strategy in PSAT was simulated to examine the effect of the DISI engine. The other configuration, with a control strategy which takes into account the efficiency characteristics of the DISI engine, will be able to improve the fuel economy of an HEV with the DISI engine.

9.2.2 Refinement of engine torque measuring technique

The engine torque measurement in a vehicle is one of the most important techniques used in this dissertation research. This in-situ torque measurement technique has various applications in vehicle development. The problem of this method is time and cost of torque sensor installation. In the application to the OPA, it took four months to install the torque sensor between the engine and CVT. The finite length of the torque sensor increases the total length of the powertrain so the mounting has to be changed. Therefore, the best way to reduce the mechanical work is to use a zero clearance torque sensor which can eliminate the engine room work.

9.2.3 Correlation of engine efficiency with the vehicle's fuel economy

One of the questions of the engine designer is how the change in the BSFC map affects the actual vehicle fuel economy. The BSFC map is obtained from steady state engine dynamometer testing and the fuel economy comes from transient chassis dynamometer testing. As the fuel economy is the combined result of all powertrain components, it is not clear yet how the engine dynamometer test result is related to the vehicle test results. If the simulation tool is refined and validated by comparing the simulation results with the measured results, it would be possible to predict precisely the change in fuel economy given only the two BSFC maps.

APPENDIX A FTP TEST RESULTS

The following graphs are the measured engine data and emissions data during the FTP test. Except for the issues discussed in the main chapters, the other variables are presented here

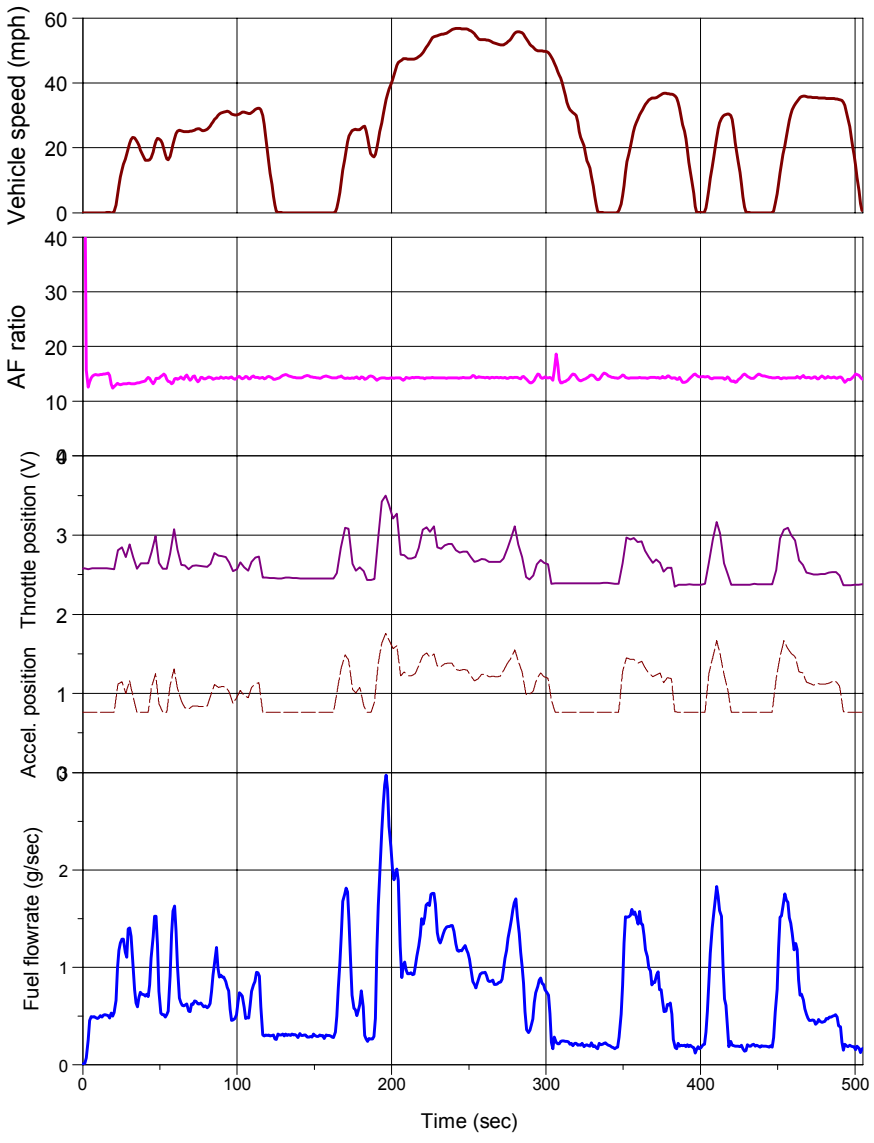

(a) Phase 1

Figure A.1 Engine operation during the FTP cycle

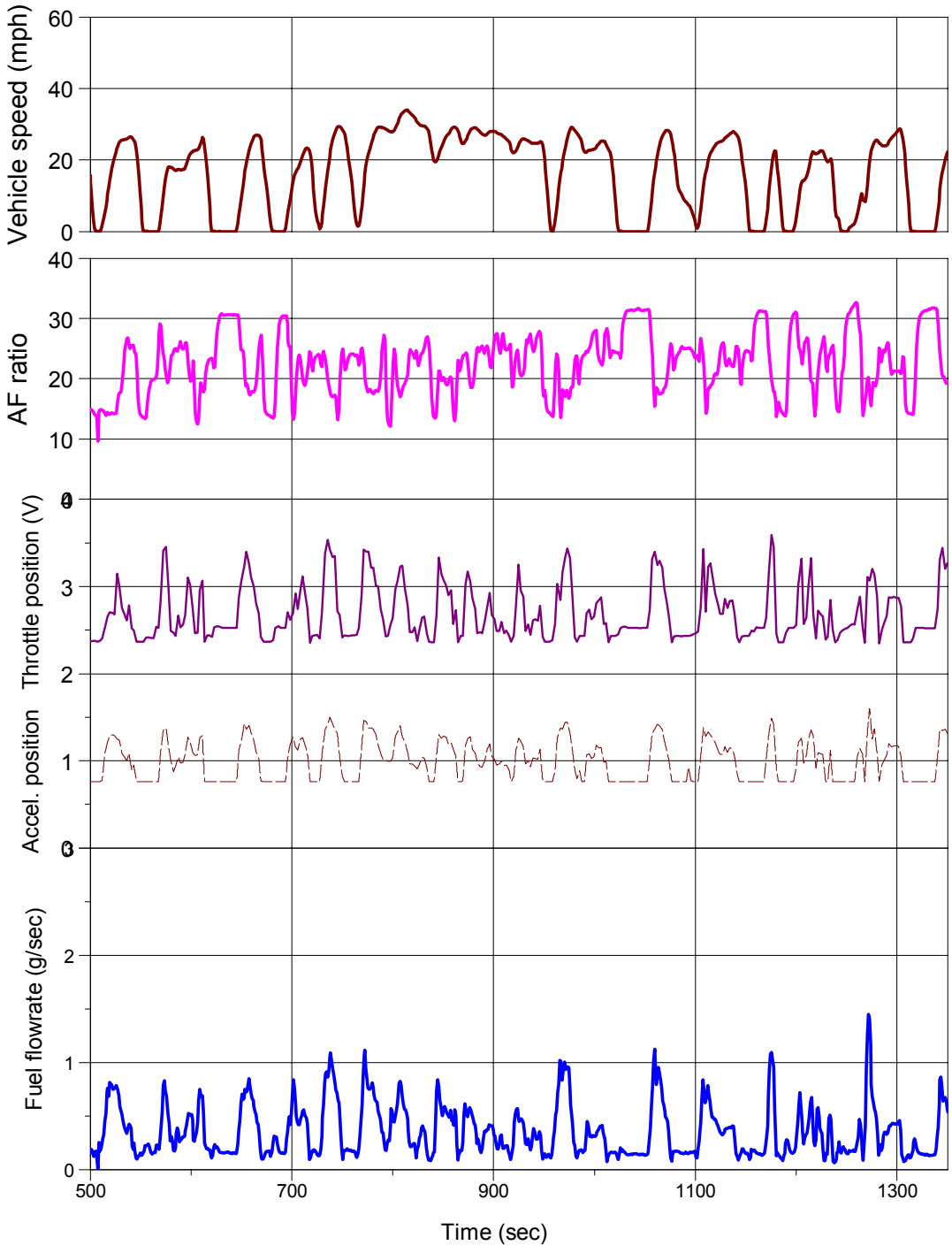

(b) Phase 2

Figure A.1 Engine operation during the FTP cycle

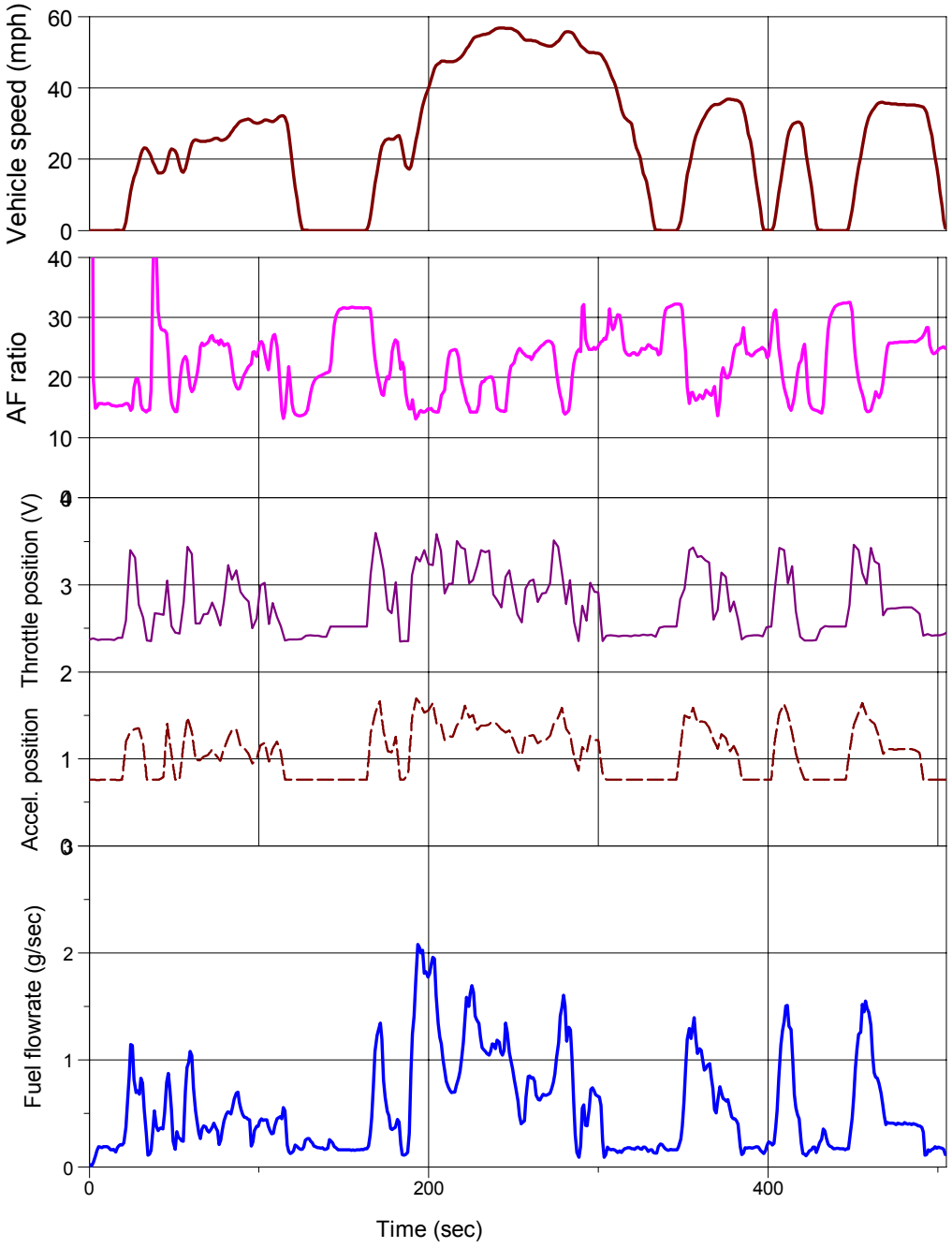

(c) Phase 3

Figure A.1 Engine operation during the FTP cycle

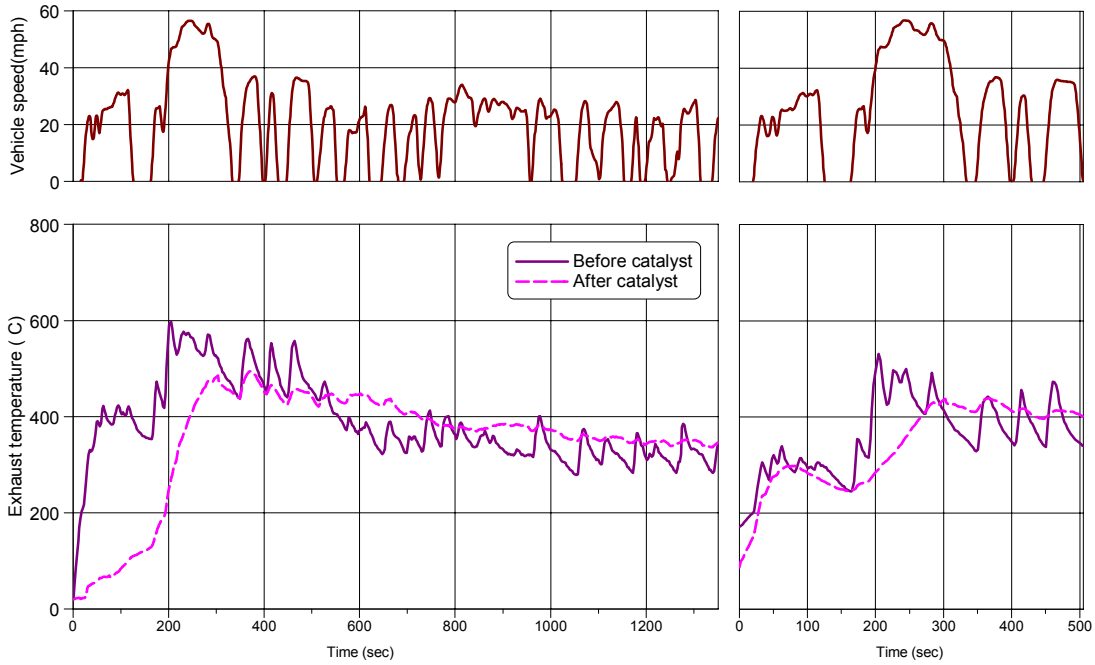

Figure A.2 Exhaust gas temperature during the FTP cycle

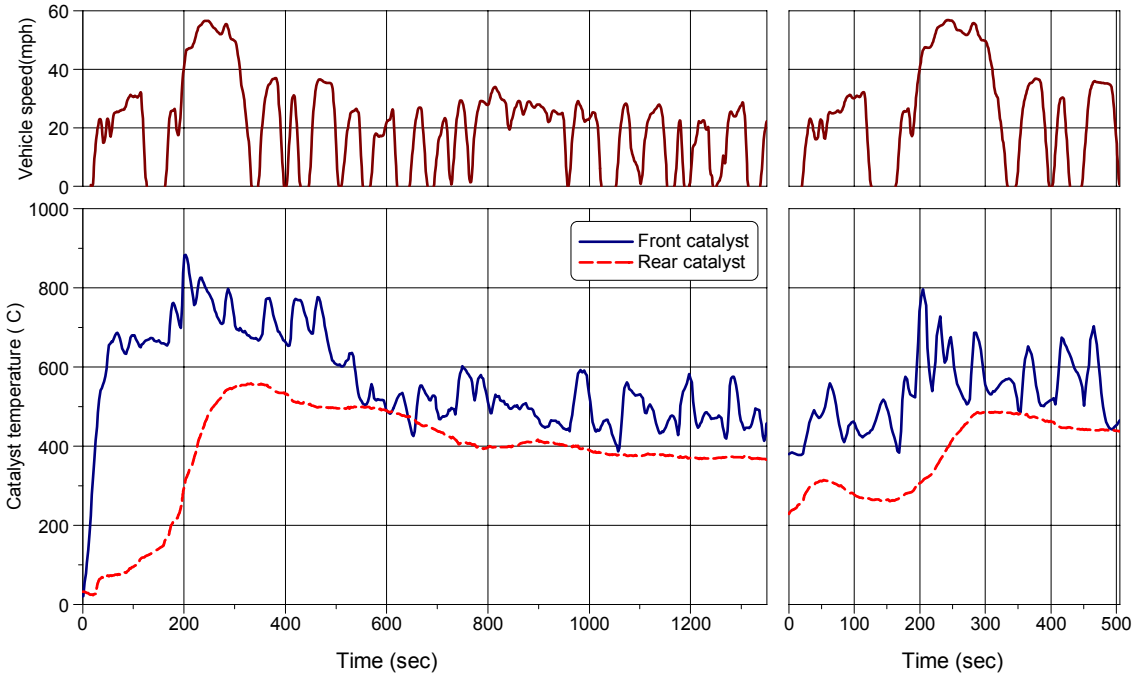

Figure A.3 Catalyst temperature during the FTP cycle

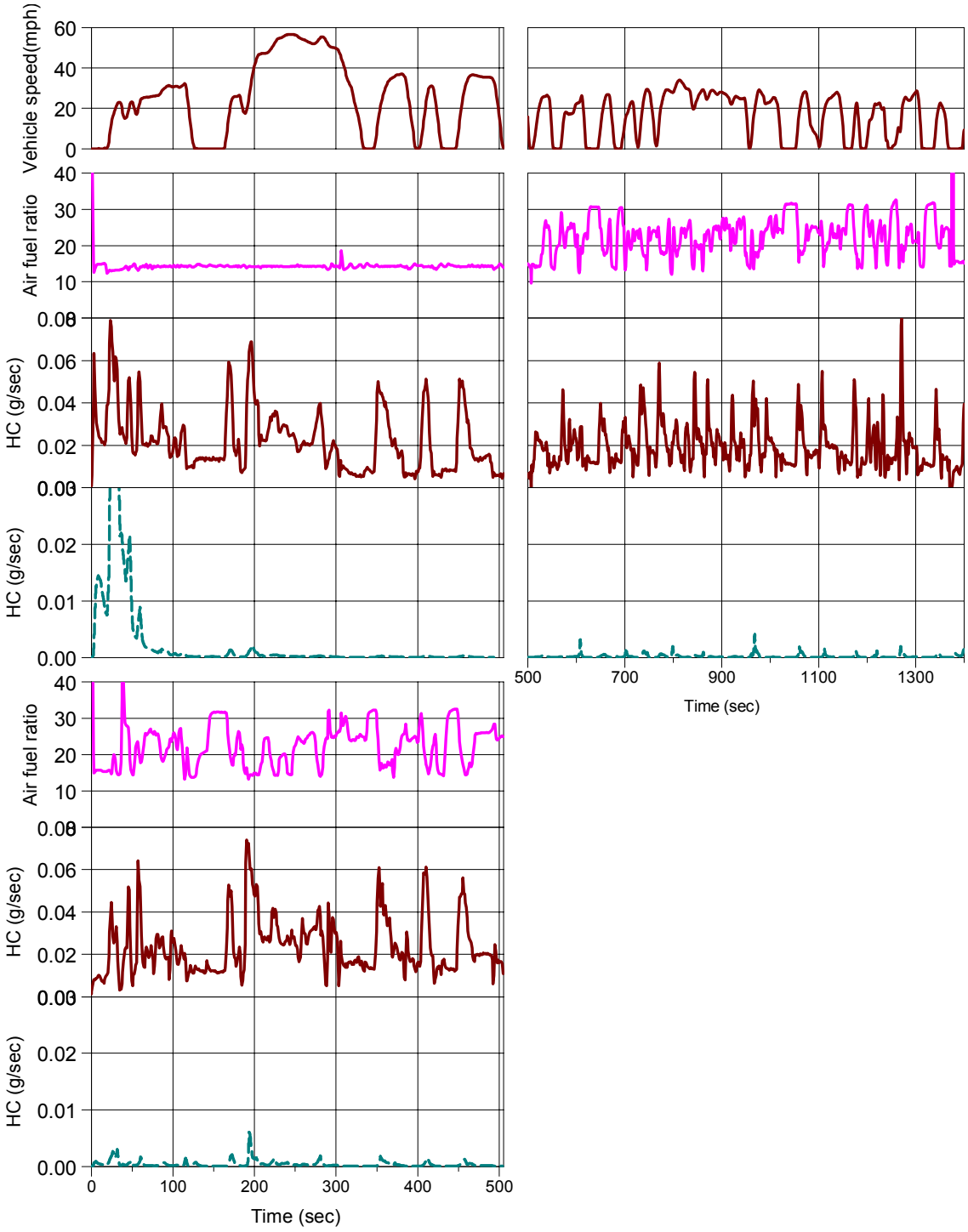

Figure A.4 Engine-out and Tailpipe THCs during the FTP cycle

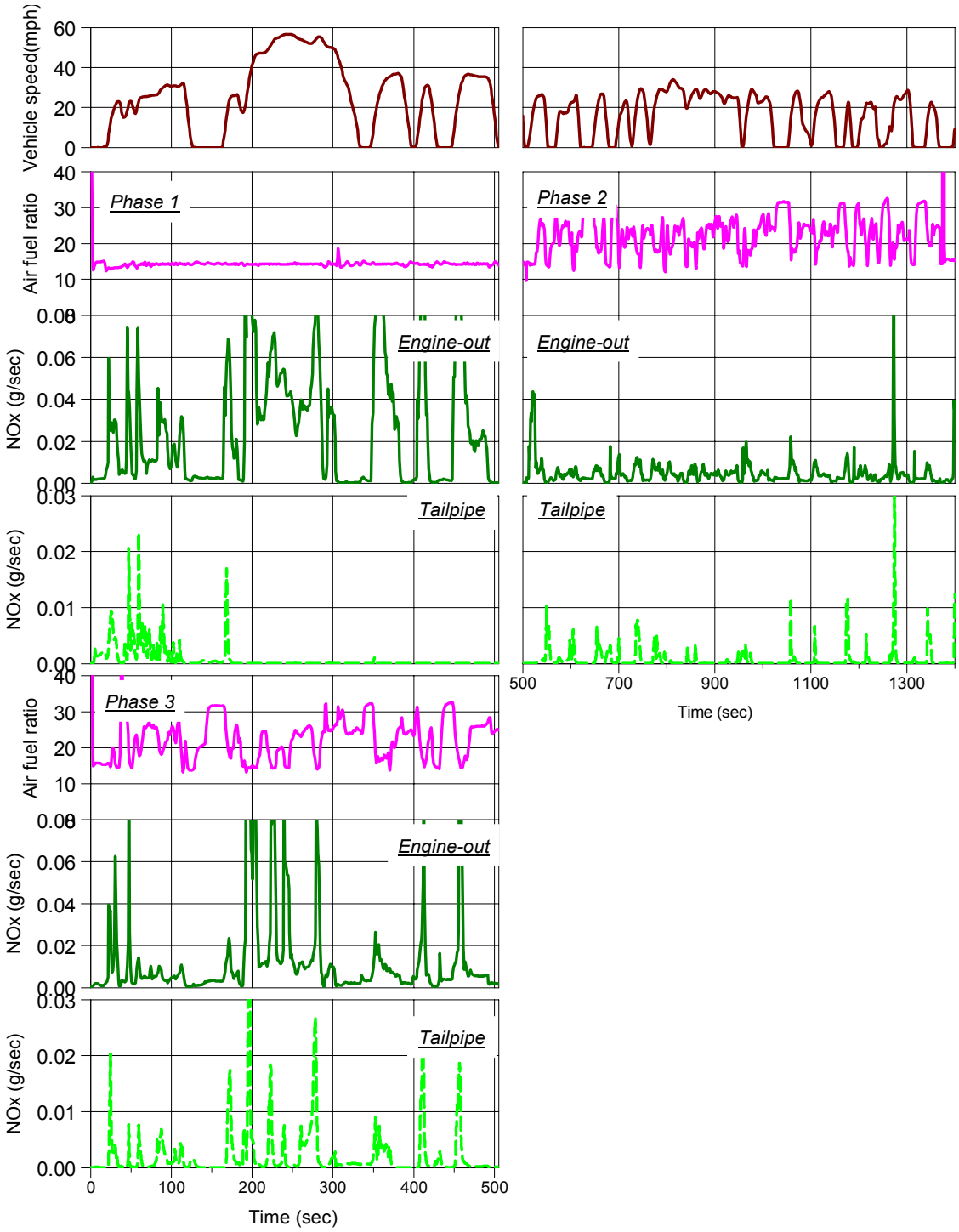

Figure A.5 Engine-out and Tailpipe NOx during the FTP cycle

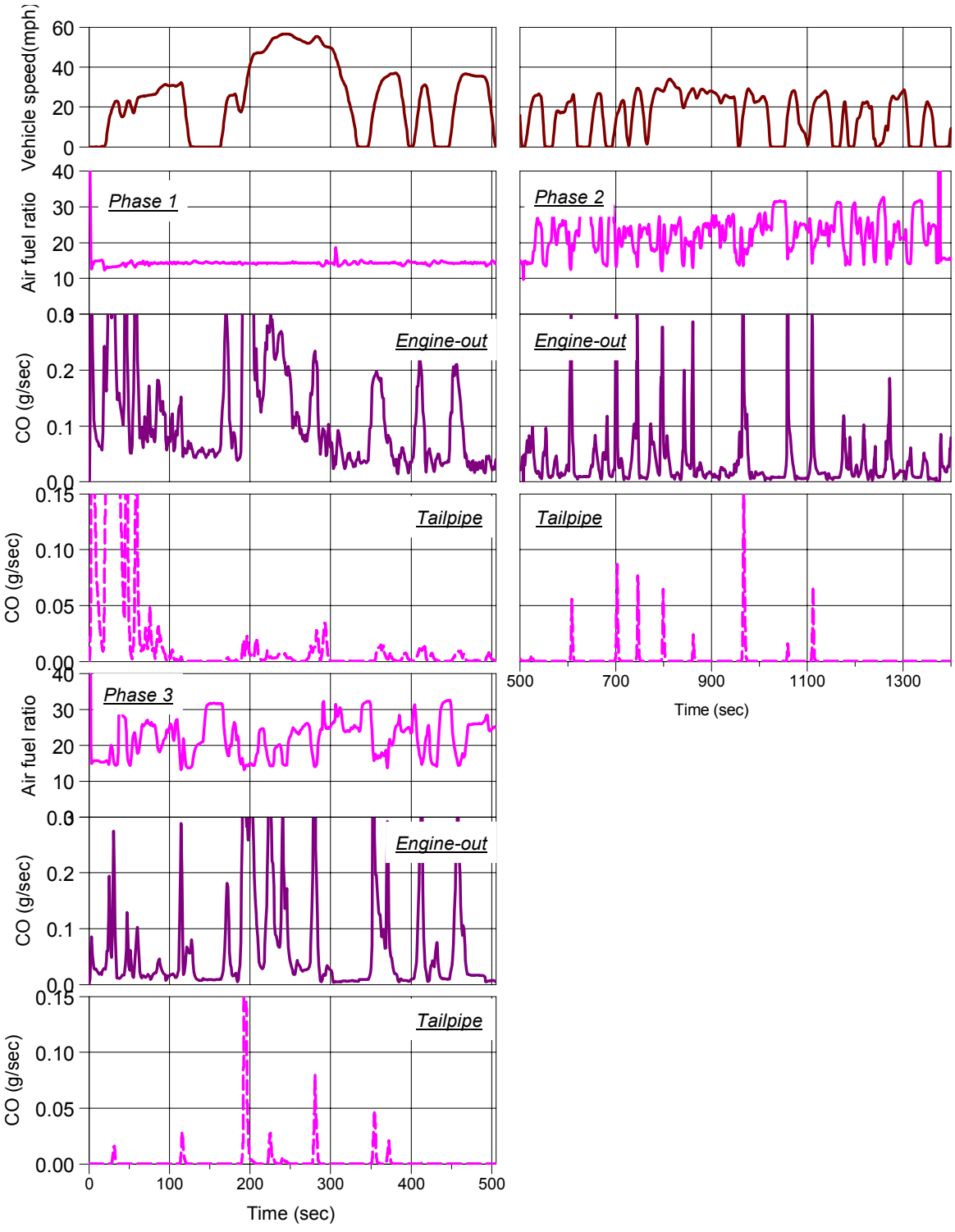

Figure A.6 Engine-out and Tailpipe CO during the FTP cycle

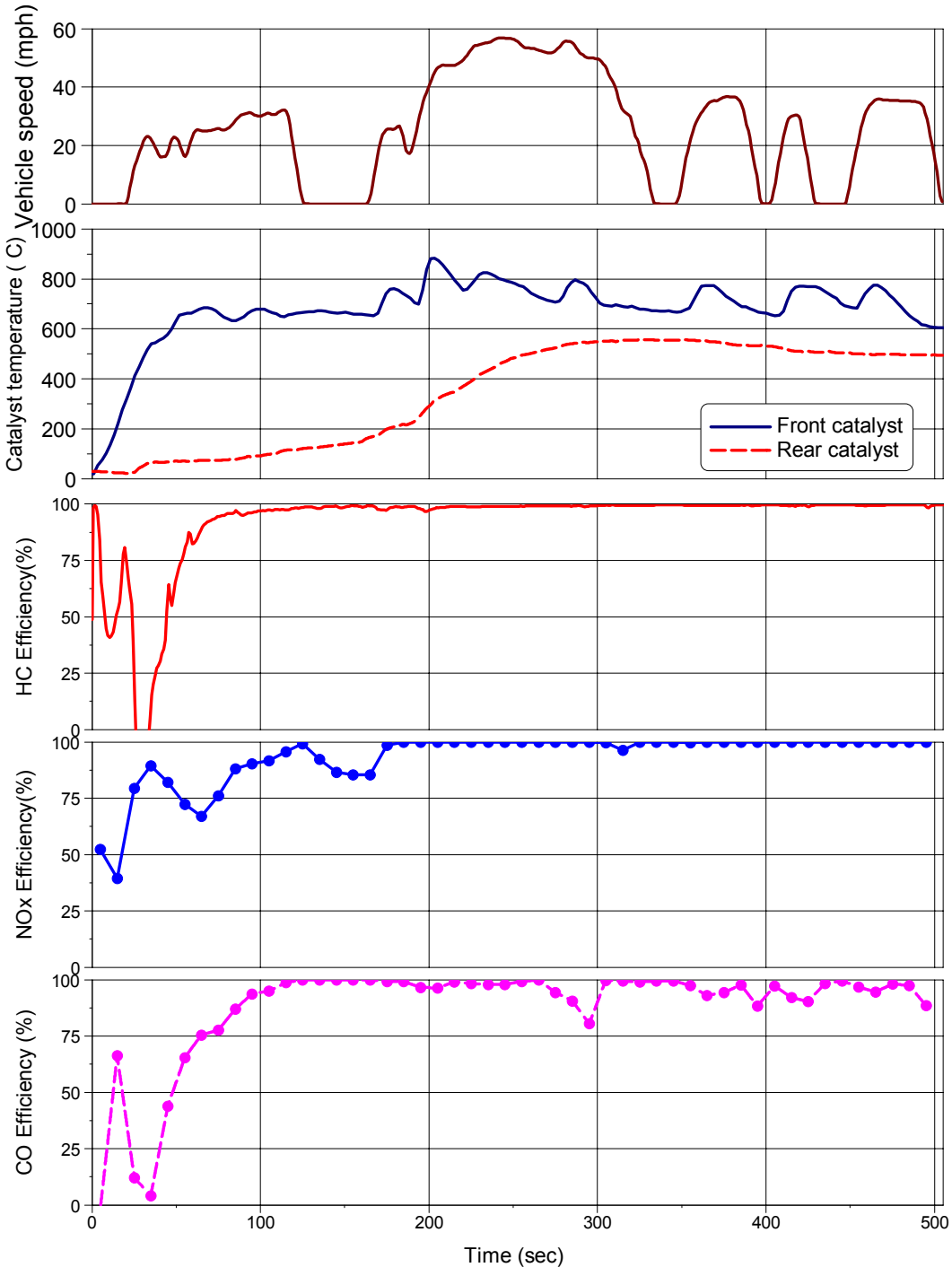

(a) Phase 1

Figure A.7 Catalyst efficiencies during the FTP cycle

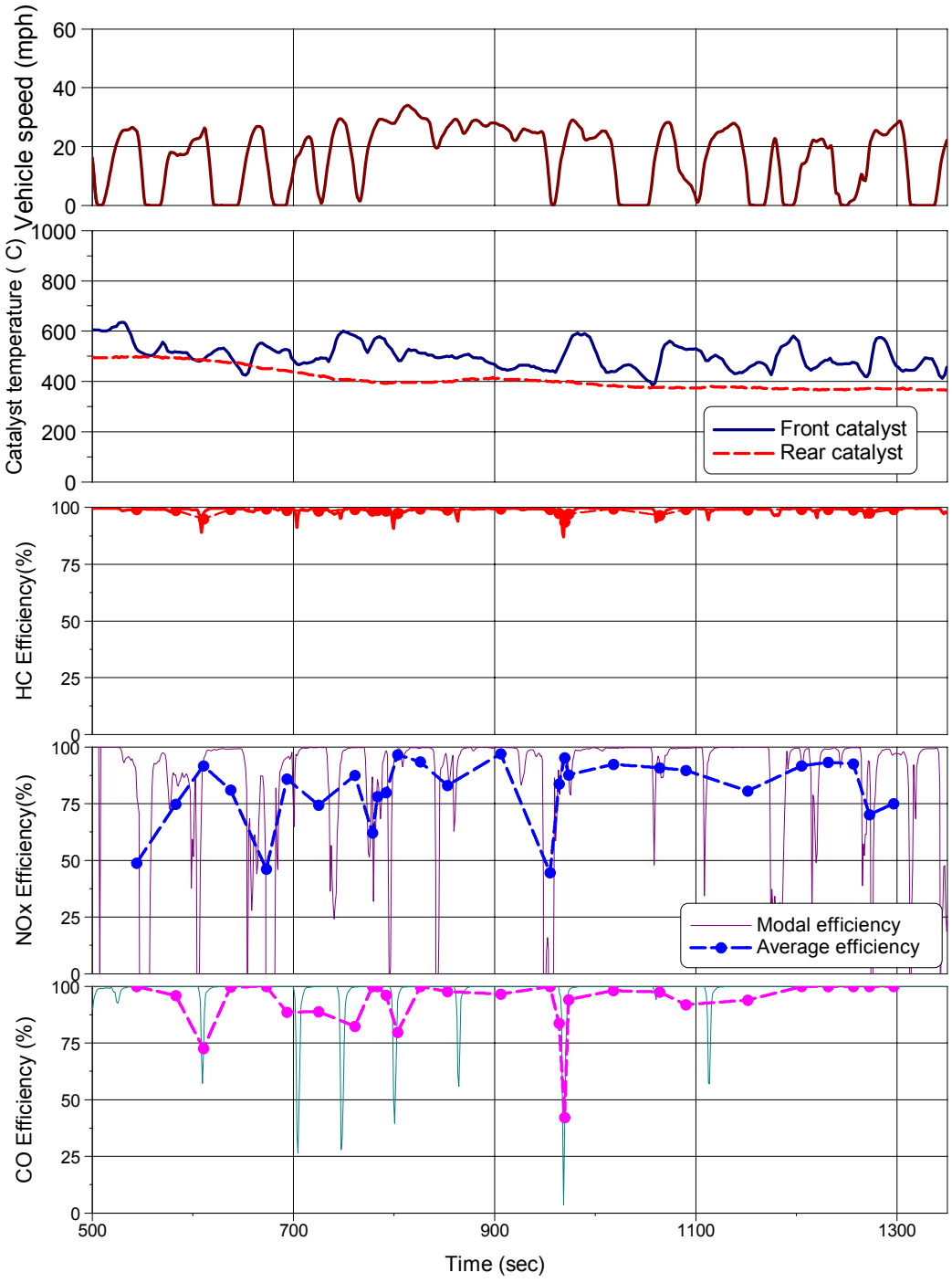

(b) Phase 2

Figure A.7 Catalyst efficiencies during the FTP cycle

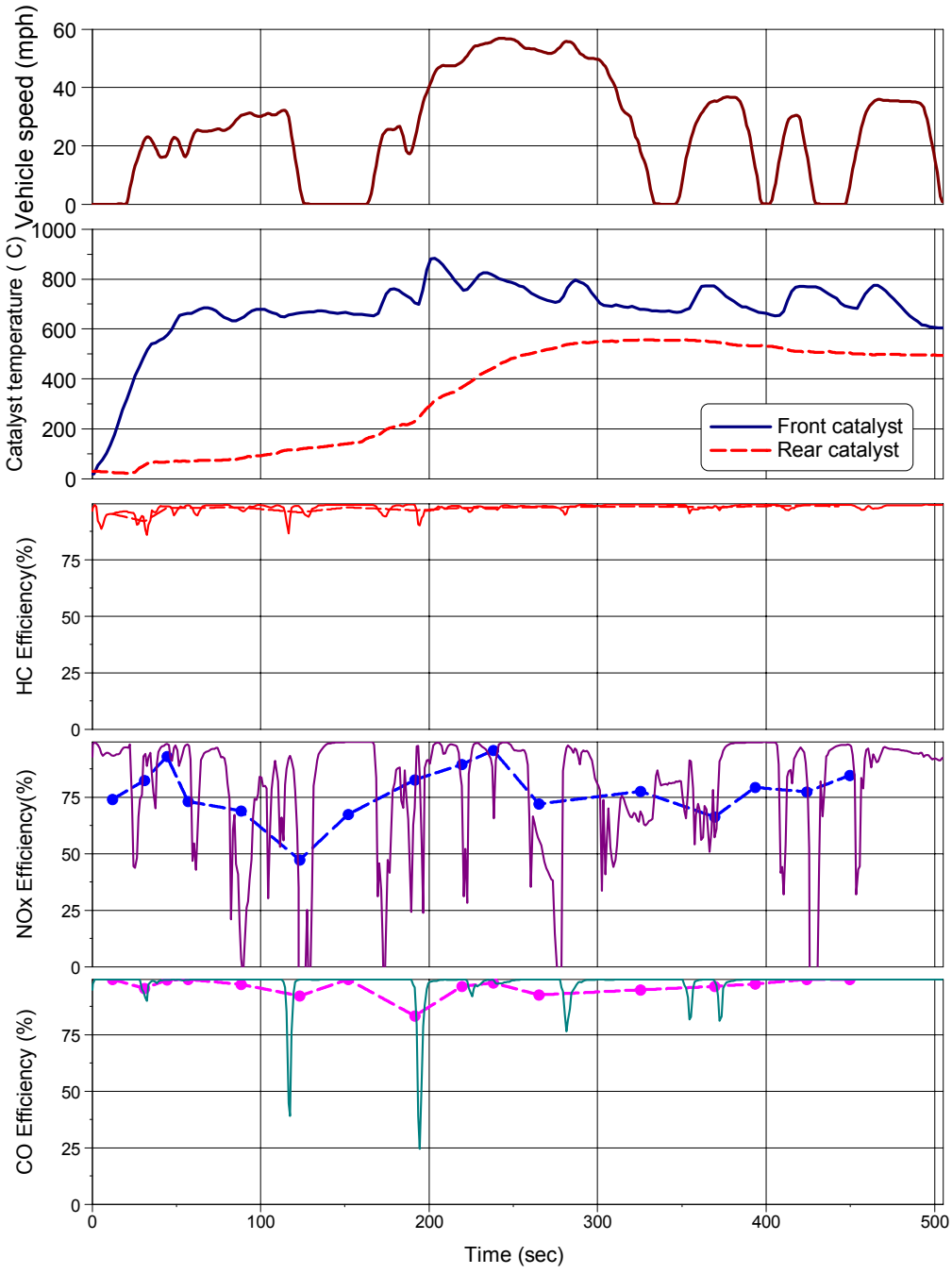

(c) Phase 3

Figure A.7 Catalyst efficiencies during the FTP cycle

APPENDIX B STEADY STATE TEST RESULTS

The following graphs are the measured engine and emissions data maps obtained during the steady state test. Except for the issues discussed in the main chapters, the other variables are presented here

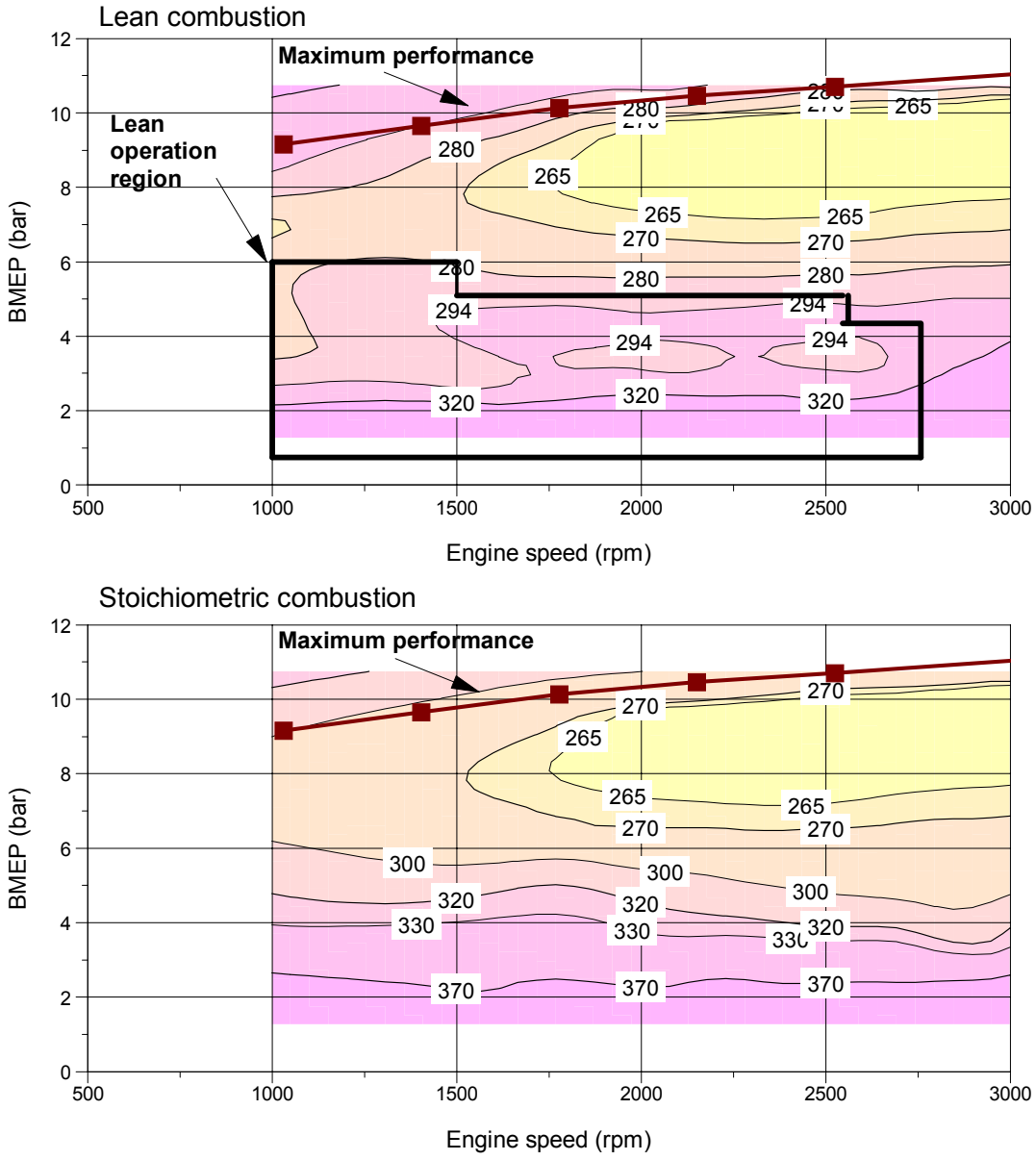

Figure B.1 Brake specific fuel consumption maps

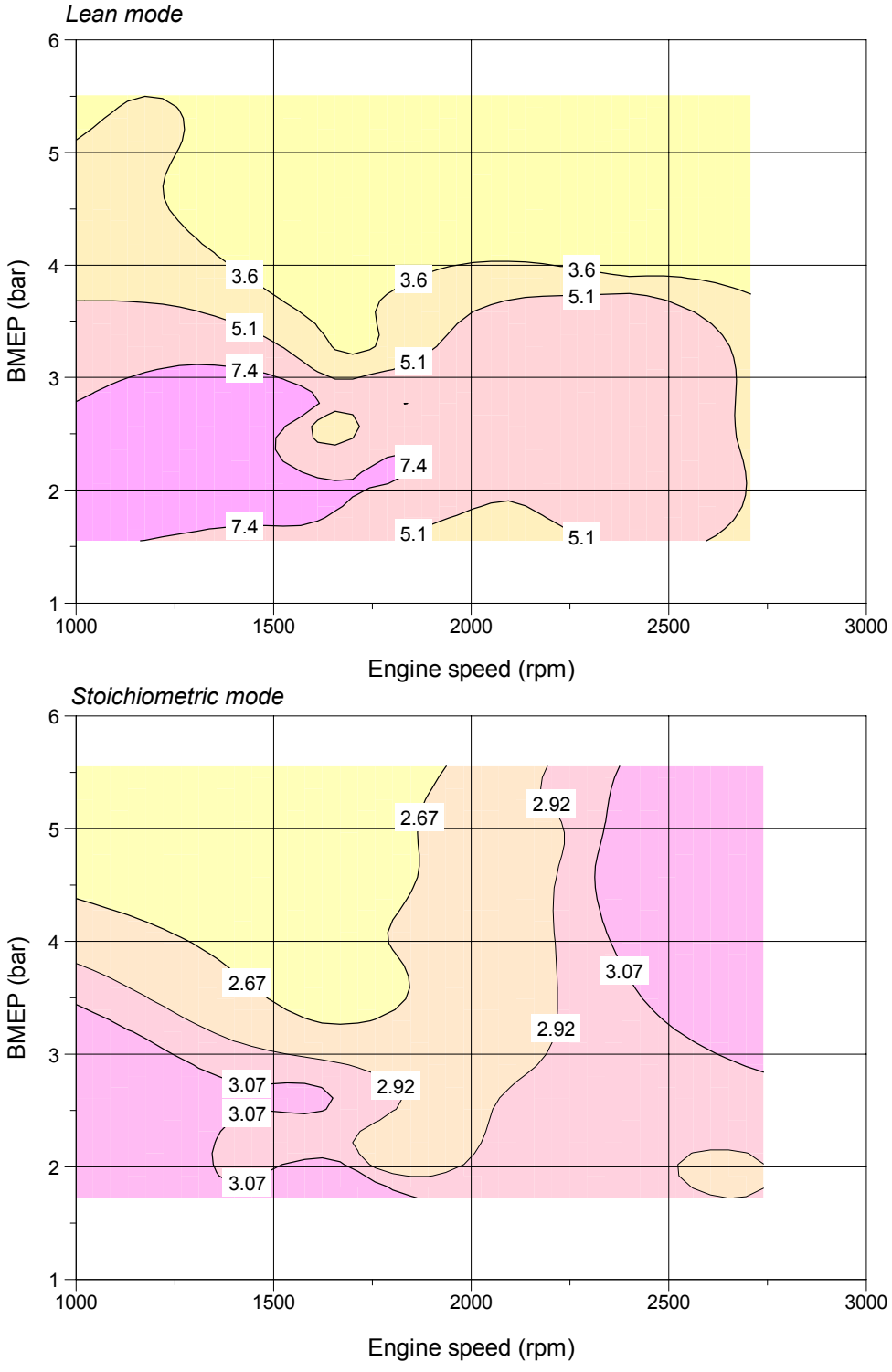

Figure B.2 Brake specific HC maps

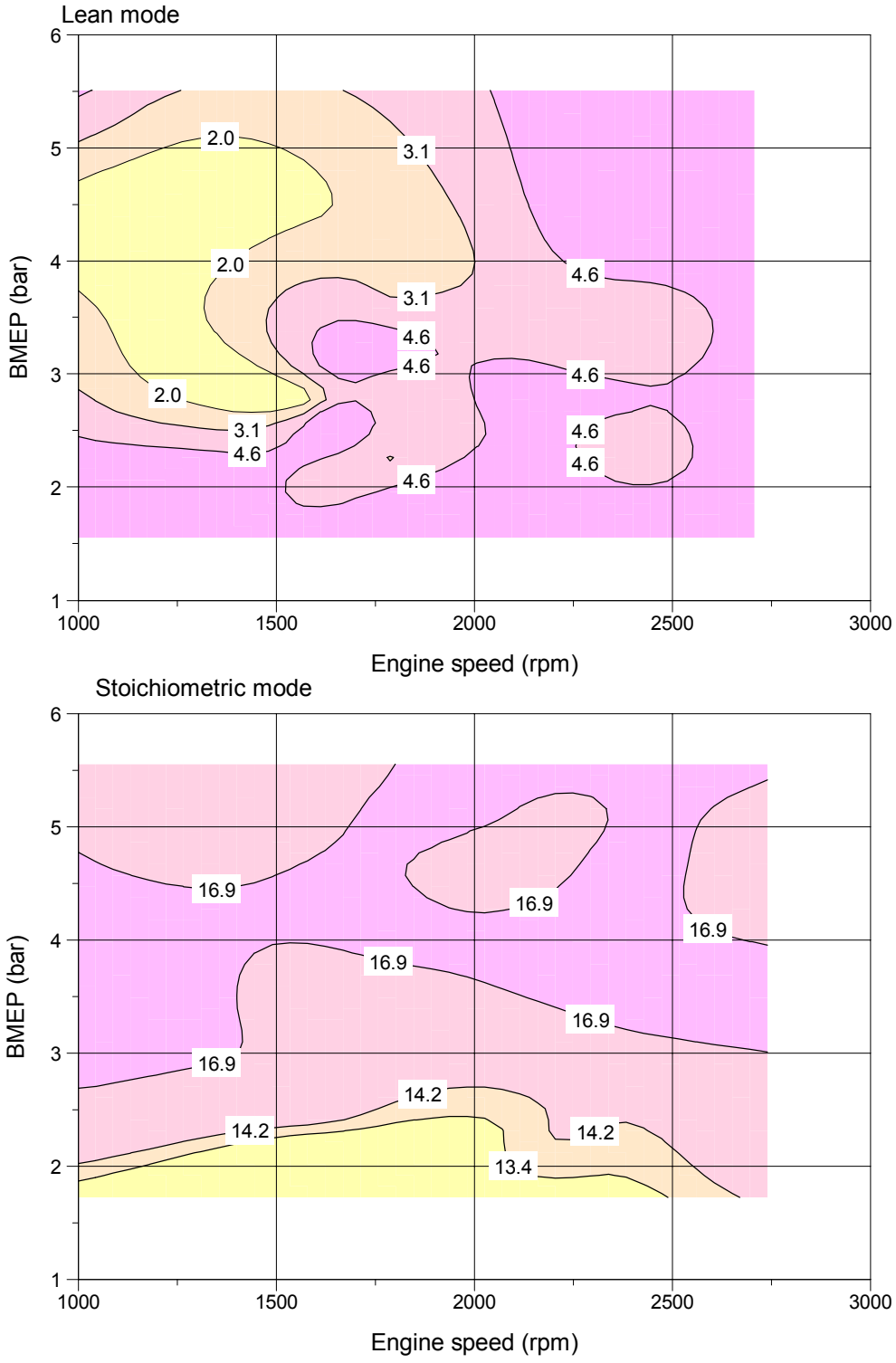

Figure B.3 Brake specific NOx maps

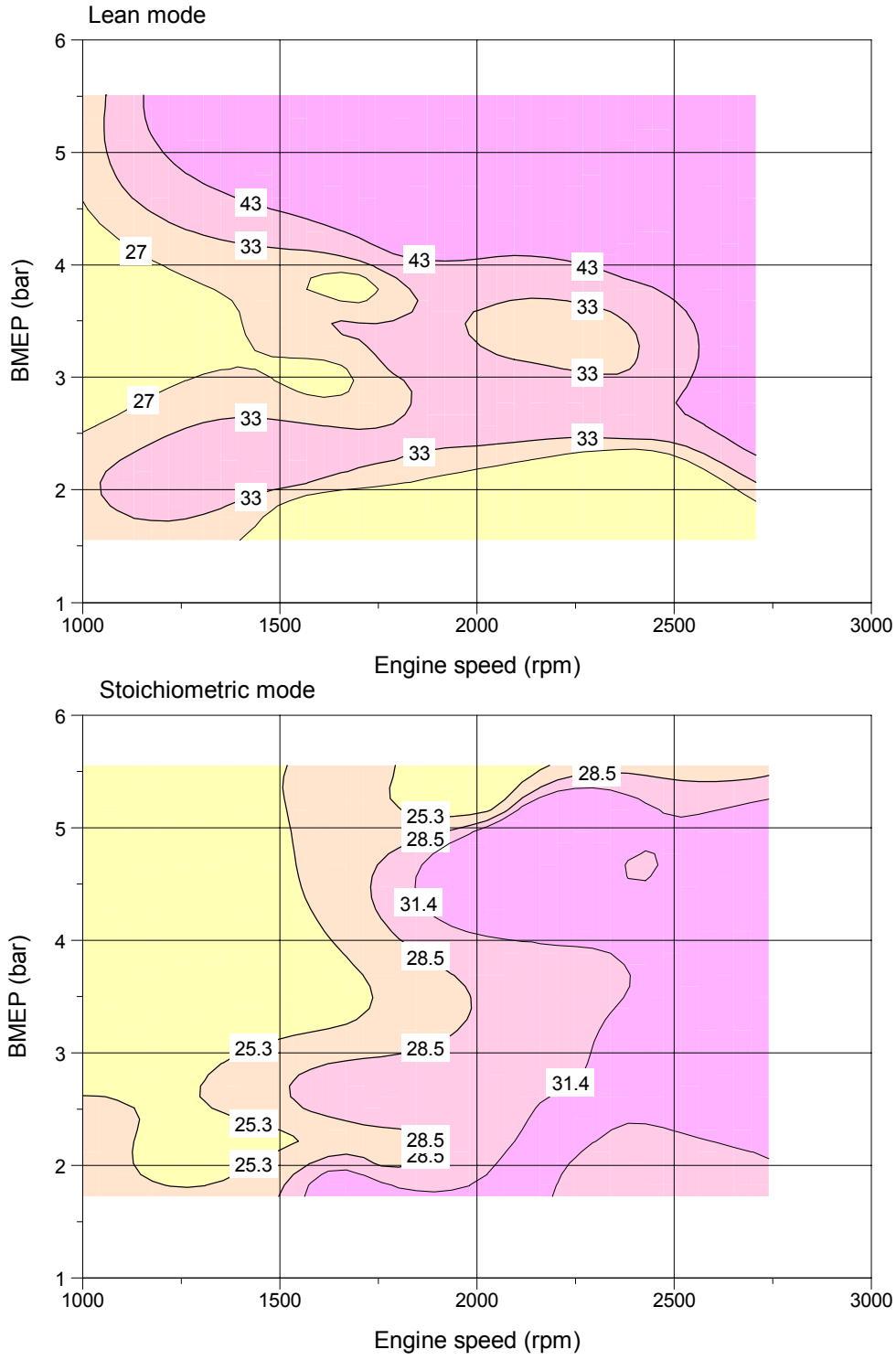

Figure B.4 Specific CO map

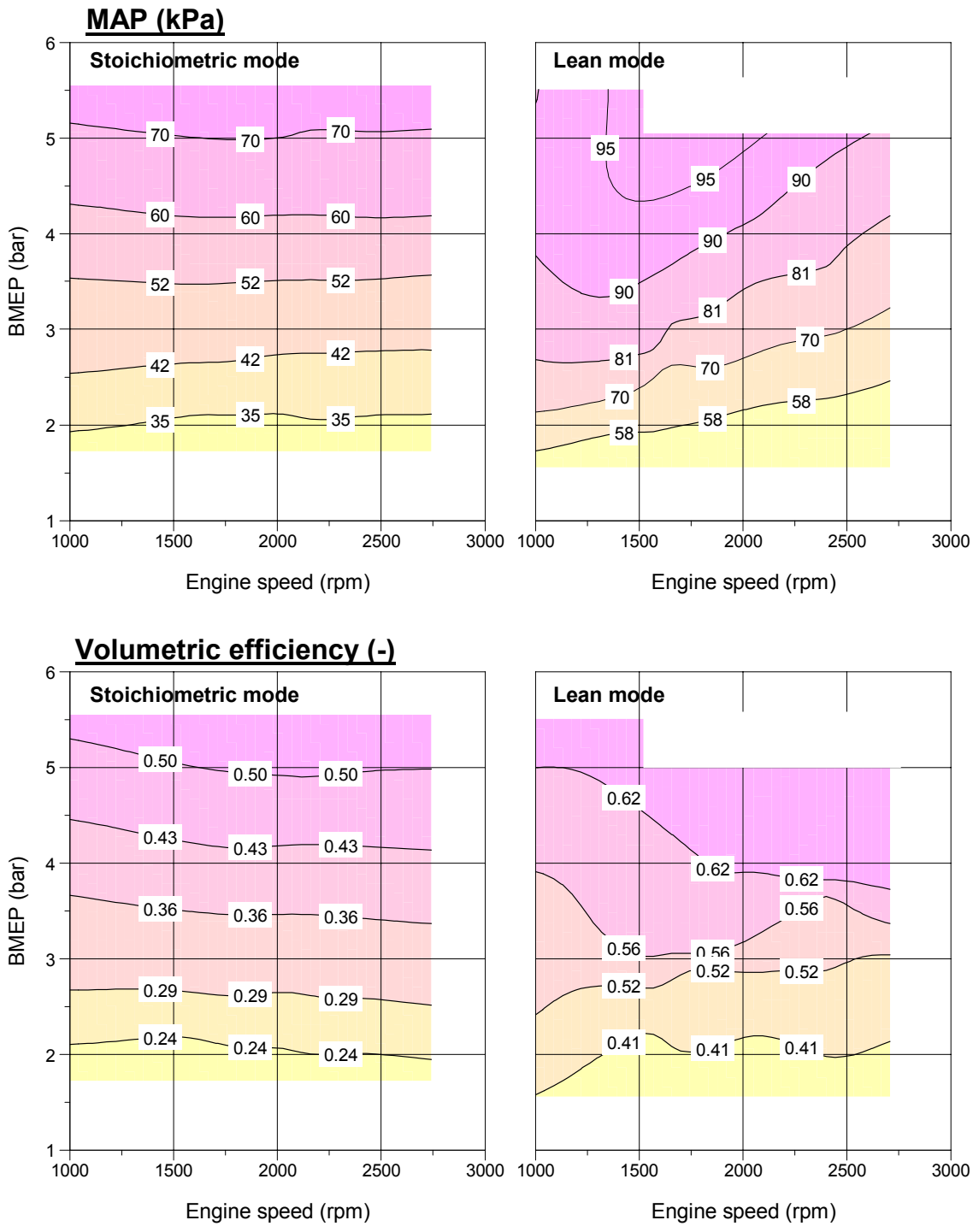

Figure B.5 MAP and volumetric efficiency

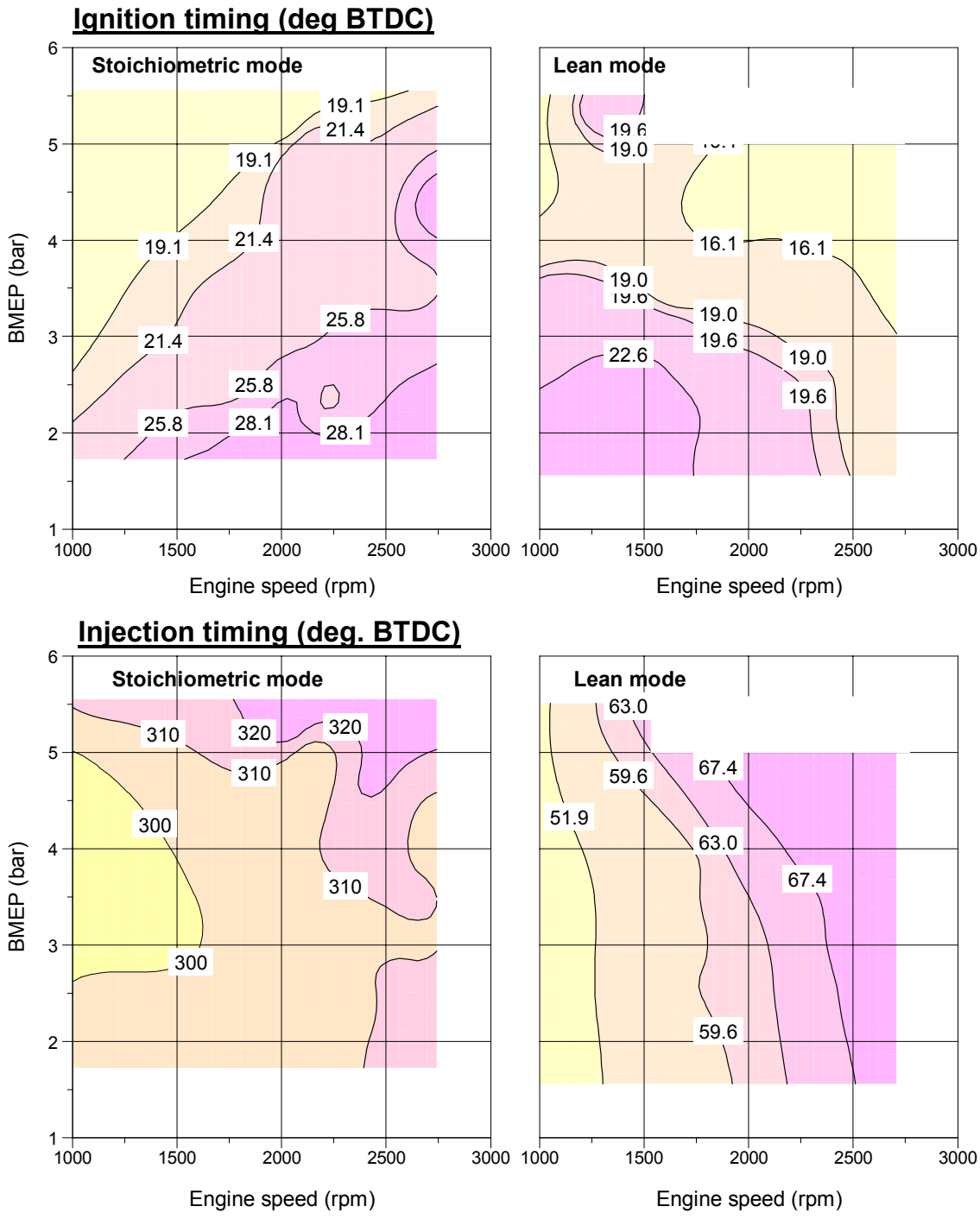

Figure B.6 Ignition timing and injection timing

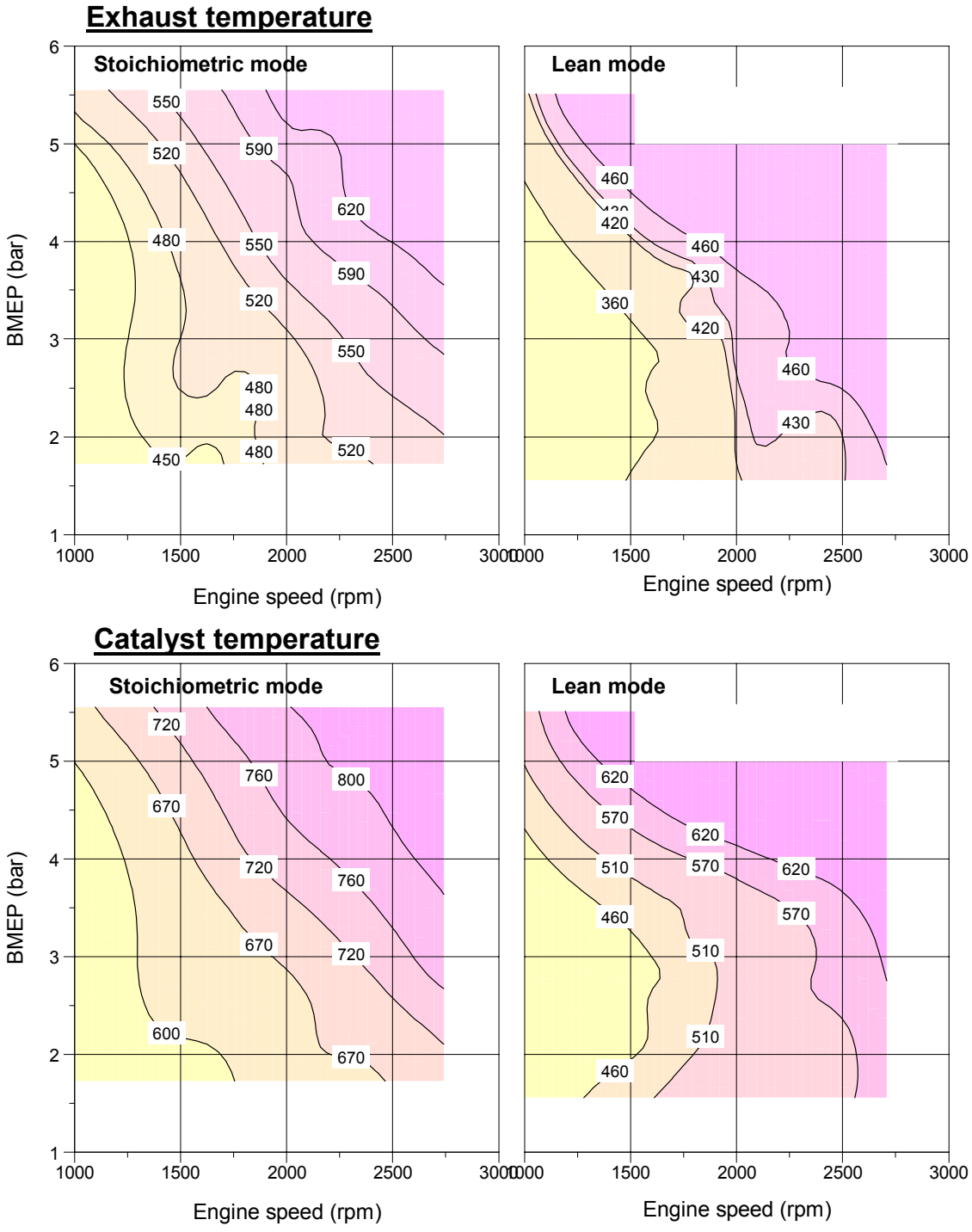

Figure B.7 Exhaust and catalyst temperatures

REFERENCE

1. Alkidas, A. and S. El Tahry (2003), "Contributors to the Fuel Economy Advantage of DISIE Engines Over PFI Engins", SAE Paper 2003-01-3101

2. Amann, C. (1997), "The Stretch for Better Passenger-Car Fuel Economy", SAE Paper 972658

3. An, F., F. Stodolsky, and D. Santini (1999), "Hybrid Options for Light-Duty Vehicles", SAE Paper 1999-01-2929.

4. Anderson, R., D. Brehob, J. Yang, J. Vallance, R. Whitaker, "A New Direct Injection Spark Ignition Combustion System for Low Emission" FISITA-96, No. P0201

5. Anon. (1994), "PNGV Program Plan", U.S. Dept. of Commerce, Washington, DC, and USCAR, Dearborn, MI (July 1994)

6. Brehob, D.D., J. Fleming, M. Haghgooie, R.A. Stein (1998), "Stratified charge Engine Fuel Economy and Emission Characteristics", SAE Paper 982704

7. Carney, D. (2004), "Internal Combustion Engineering", *SAE Automotive Engineering International*, 1997, No. 5, pp 39-46

8. Cole, R. C., R.B.Poola, and R. Sekar (1998), "Exhaust Emissions of a Vehicle with a Gasoline Direct-Injection Engine", SAE Paper 982605

9. Corsetti, A., G. O'Connell, K. Watkins (2002), "In-vehicle Torque Model Validation", SAE Paper 2002-01-1143

10. Davis, S.C. and S.G. Strang (1993), "Transportation energy data book: Edition 13", Report ORNL-6743, Oak Ridge National Laboratory,

11. Decicco, J. and M. Ross (1996),"Recent advances in automotive technology and cost-effectiveness of fuel economy improvement", Transportation Research Part D (2), 79-96

12. Duoba, M., H. Ng and R. Larsen (2000), "In-situ mapping and analysis of the Toyota Prius HEV engine", SAE Paper 2000-01-3096

13. Duoba, M., H. Ng and R. Larsen (2001) "Characterization and comparison of two hybrid electric vehicles (HEVs) – Honda Insight and Toyota Prius", SAE Paper 2001-01-1335

14. Fraidl, G., W. Piock, M. Wirth (1996), "Gasoline Direct Injection: Actual Trends and Future Strategies for Injection and Combustion System", SAE Paper 960465

15. Hachisuka, I., H. Hirata, Y. Ikeda, S. Matsumoto, "Deactivation Mechanism of NOx Storage-Reduction Catalyst and Improvement of Its Performance", SAE Paper 2000-01-1196

16. Harada, J., T. Tomita, H. Mizuno, Z. Mashiki, Y. Ito (1997), "Development of Direct Injection Gasoline Engine", SAE Paper 970540

17. Ikeda, Y. (1999), "Development of NOx storage Reduction Catalyst for Direct Injection Gasoline Engine", SAE Paper 991279

18. Kanda, M., T. Baika, S. Kato, M. Iwamuro, M. Koike, A. Saito(2000), "Application of a New combustion Concept to Direct Injection Gasoline Engine", SAE Paper 2000-01-0531

19. Karnopp, D., D. Margolis, R. Rosenberg (2000), System Dynamics 3rd ed., John Wiley & Sons, New York, ,

20. Karl, G., R. Kemmler, M. Bargende (1997), "Analysis of a Direct Injected Gasoline Engine", SAE Paper 970624

21. Kluger, M. A. and D. M. Long (1999), "An Overview of Current Automatic, Manual and Continuous Variable Transmission Efficiencies and their Projected Future Improvement", SAE Paper 1999-01-1259

22. Kluger, M. A. and Fussner, D. R. (1997). An overview of current CVT mechanisms, forces and efficiencies. SAE Technical Paper 970688.

23. Koike, M., A. Saito, T. Tomoda, Y. Yamamoto, "Research and Development of a New Direct Injection Gasoline Engine", SAE Paper 2000-01-0530

24. Krebs, R., E. Pott, T.P. Kreuzer, U. Gobel, K. Gluck (2002),"Exhaust Gas Aftertreatment of Volkswagen FSI Fuel Stratified Injection Engines", SAE Paper 2002-01-0346

25. Kume, T., Y. Iwamoto, K. Iida, M. Murakami, K. Akishino, H. Ando (1996), "Combustion Control Technologies for Direct Injection SI engine", SAE Paper 960600

26. Kuwahara, K., T. Watanabe, T. Shudo, H. Ando (1996), "A Study of Combustion Characteristics in a Direct Injection Gasoline Engine by High Speed Spectroscopic Measurement", Proceedings of the Internal Combustion Engine Symposium – Japan (in Japanese),1996, pp145-150

27. Lindhjem, C.E. (1997), "Conversion Factors for Hydrocarbon Emission Components," U.S. EPA Office of Mobile Sources Report No. NR-002

28. Markel, T., A. Brooker, T. Hendricks, V. Johnson, K. Kelly, B. Kramer, M. O'Keefe, S. Sprik, K. Wipke (2002), "ADVISOR: A system analysis tool for advanced vehicle modeling", Journal of Power Sources, Vol. 4801 pp 1-12

29. Matthews, R.D., C. Stovell, H. Ng, B. Larsen, and B.E. Johnson (1999), "Effects of Load on Emissions and NOx trap/catalyst Efficiency for Direct Injection Spark Ignition Engine", SAE Paper 1999-01-1528

30. Nishigaya, M., T. Tamura, H. Yasue, S. Kasuga and M. Sugaya (2001), "Development of Toyota's New Super CVT", SAE 2001-01-0872

31. Plotkin, S., D. Santini, A. Vyas, J. Anderson, M. Wang, J. He, and D. Bharathan (2001), "Hybrid Electric Vehicle Technology Assessment: Methodology, Analytical Issues, and Interim Results", Argonne National Laboratory Report, ANL/ESD/02-2.

32. Rousseau, A., P. Sharer F. Besnier (2004), "Feasibility of Reusable Vehicle Modeling: Application to Hybrid Vehicles", SAE Paper 2001-01-1618

33. Seiffert, U. (1996), "The Automobile in the Next Century", FISI Technical Paper, No. K0011

34. Shimotani, K., K. Oikawa, O. Horada, Y. Kagawa, "Characteristics of Gasoline In-Cylinder Direct Injection Engine", Proceedings of the Internal Combustion Engine Symposium – Japan (in Japanese), 1995, pp289-294

35. Stovell, C., R.D. Matthews (1999), "Emission and Fuel Economy of a 1998 Toyota with a Direct Injection Spark Ignition Engine," SAE Paper 1999-01-1527

36. Stovell, C., R.D. Matthews, B.E. Johnson, H. Ng and R. Larsen (1999), "Emissions and Fuel Economy of a 1998 Toyota with a Direct Injection Spark Ignition Engine", SAE Paper 1999-01-1527

37. Stovell, C. (2001) Emissions Study of a 1998 Toyota Direct Injection Spark Ignition Production Engine, Masters Thesis, University of Texas at Austin

38. Van den Brink, R. and B. Wee (2001), "Why has car-fleet specific fuel consumption not shown any decrease since 1990? Quantitative analysis of Dutch passenger car-fleet specific fuel consumption", Transportation Research Part D 6 75-93

39. Wojik, K., G.K.Fraidl (1996), "Engine and Vehicle Concepts for Low Consumption and Low Emission Passenger Cars", FISITA-96, Paper No. P1302

40. Yamaguchi, J., "OPA – Toyota's new-age vehicle", *SAE Automotive Engineering International*, 2000 Sep. pp 29-34

41. Zhao, F., M. C. Lai, D.L. Harrington (1999), "Automotive Spark Ignited Direct Injection Gasoline Engines", *Progress in Energy and Combustion Science* 25, pp437-562

42. Federal Highway Administration (1992), "Highway statistics 1991"

43. http://www.fueleconomy.gov/

44. https://www.psat.anl.gov/default.html

Vita

Byung-Soon Min was born May 26, 1966, in Incheon-shi, Republic of Korea, the son of Pyungja Shim and Kwanshik Min. Byungsoon Min graduated from Hwagok High School in February 1984 and entered Seoul National University in Seoul, Korea. He graduated in February 1988. He received the degree of Bachelor of Science from the department of Machine Design and Production Engineering in Seoul National University. He then entered the Graduate School of Seoul National University and graduated in February 1990 with the degree of Master of Science.

Byungsoon Min then began to work at Hyundai Motor Company as a powertrain test engineer. In September 2000, he entered University of Texas at Austin for his Ph.D. study in Mechanical Engineering. In May 2001, he was sent to Argonne National Laboratory to perform a research project as well as his dissertation project. He came to the University in September 2002 to finish his study.

After graduation, Byungsoon Min will be working in Hyundai Motor Company from September 2004.

Permanent Address: 402-402 Hyundai Apt. Okryun-dong, Yeonsu-gu, Incheon-shi,
Republic of Korea, 406-772

This thesis was typed by the author.